Masaryk university
Faculty of science

Study materials

Characterization of surfaces and thin films

Doc. Mgr. Lenka Zajíčková, Ph.D

Brno 2016

Contents

Literature

1. Ch. Kittel, Úvod do fyziky pevných látek, Academia, Praha 1985
2. L. Eckertová, Elektronika povrchu, SPN, Praha 1983
3. J. Hlávka, Za´klady fyziky povrchu pevných látek, SPN, Praha 1988 (skripta Univerzity J. E. Purkyně v Brně)
4. L. Eckertová (ed.), Metody analýzy povrchu - elektronová spektroskopie, Academia, Praha 1990
5. L. Frank, J. Král (ed.), Metody analýzy povrchu - iontové, sondové a speciální metody, Academia 2002
6. A. Zangwill, Physics at Surfaces, Cambridge University Press 1988
7. P. E. J. Flewitt, R. K. Wild, Physical Methods for Materials Characterisation (SE), IOP Publishing, Bristol 2003
8. J. A. Venables, Introduction to Surface and Thin Film Processes, Cambridge University Press, Cambridge 2000
9. W. Martienssen and H. Warlimont, Springer Handbook of Condensed Matter and Materials Data, Springer, Berlin 2005
10. V. Milata, Aplikovaná molekulová spektroskopia, STU, Bratislava 2008
11. P. Griffiths, J.A. De Haseth, Fourier Transform Infrared Spectrometry, Wiley-Interscience, New Jersey 2007
12. B.C. Smith, Fundamentals of Fourier Transform Infrared Spectroscopy, Second Edition, CRC Press, 2011
13. P.Y. Yu, Fundamentals of Semiconductors: Physics and Materials Properties (Graduate Texts in Physics), Springer, 2010
14. J.J Laserna, Modern Techniques in Raman Spectroscopy, Wiley, 1996
15. P.Larkin, Infrared and Raman Spectroscopy; Principles and Spectral Interpretation, Elsevier, 2011

16. E.Smith, Modern Raman Spectroscopy: A Practical Approach, Wiley, 2005

17. E.B. Wilson, Molecular Vibrations: The Theory of Infrared and Raman Vibrational Spectra (Dover Books on Chemistry), Dover Publications, 1980

18. R.F. Egerton, Electron Energy-Loss Spectroscopy in the Electron Microscope, Springer, 2011

Chapter 1

Structure of Condensed Matter

1.1 Amorphous and Crystalline Materials

Atoms can be aggregate through a number of different processes which determine, at least initially, whether this collection will take the form of gas, liquid or solid. The state usually changes as its temperature or pressure is modified. Melting is the process most often used to form an aggregate of atoms. When the temperature of a melt is lowered to a certain point, the liquid will form either a **crystalline** or **amorphous** solid.

Most crystals are solids, so the atoms, ions or molecules from which they are composed, with various types of long-range order, form 3-D structures. A more modern definition is that all material which show sharp diffraction peaks are crystalline. In this sense, aperiodic or quasicrystalline materials, as well as periodic materials, are crystals. A real crystal is never a perfect arrangement. Defects in the form of vacancies, dislocations, impurities, and other imperfections are often very important for the physical properties of the crystal. This aspect has been largely neglected in the classical crystallography but is becoming more and more a topic of modern crystallographic investigations.

The difference between crystalline and amorphous materials can be demonstrated as on an example of silicon oxide SiO_2, which can form both the forms. Silicon atoms are surrounded by three oxygen atoms, which is a short-range ordering. In crystalline polymorph, quartz, oxygen atoms are arranged in a hexagonal structure (see fig. 1.1).

1.1.1 Description of Crystal Structure

An ideal crystal is constructed by the infinite repetition of identical groups of atoms (a motif). A group is called the *basis*. The set of mathematical points to which the basis is attached is called the *lattice*. This principle is demonstrated for 2-D planar patterns in figure 1.2.

The lattice in three dimensions is defined by three *translation vectors* $\vec{a}_1$, $\vec{a}_2$, $\vec{a}_3$, such that the arrangement of atoms in the crystal looks the same when viewed from the point $\vec{r}$ as when viewed from every point $\vec{r}'$ translated by an integral multiple of $\vec{a}_{1,2,3}$

$$\vec{r}' = \vec{r} + u_1\vec{a}_1 + u_2\vec{a}_2 + u_3\vec{a}_3 \tag{1.1}$$

where u_1, u_2 and u_3 are arbitrary integers.

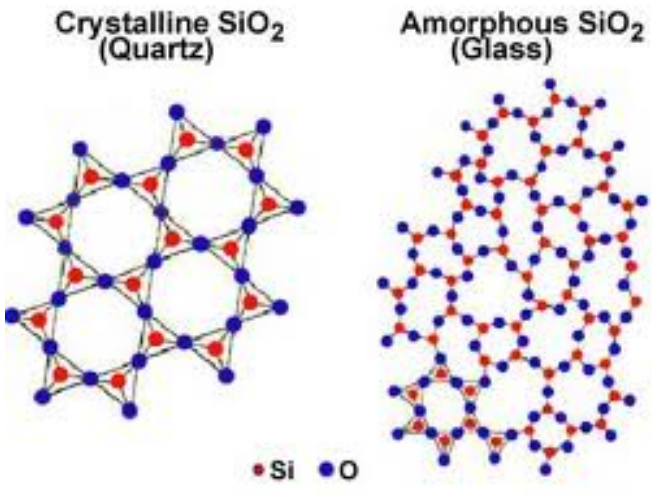

Figure 1.1: Schematic view of SiO_2: a) amorphous SiO_2 with short-range ordering b) crystalline SiO_2 with long-range ordering.

The lattice is said to be *primitive* if any two points from which the attomic arrangement looks the same always satisfy eq.(1.2) with a suitable choice of the integers u_i. This statement defines *primitive translation vectors* $\vec{a}_i$. An example of their possible selections for 2D lattice is shown in figure 1.3.

The parallelepiped defined by the primitive axes $\vec{a}_i$ is called a *primitive cell* (figure 1.5). A primitive cell is type of unit cell (or just cell). There is no cell of smaller volume than the primitive cell that can serve as a building block for the crystal structure. Its volume is calculated as $|\vec{a}_1.\vec{a}_2 \times \vec{a}_3|$.

Primitive translation vectors $\vec{a}_i$ are often used to define the *crystal axes* which form three adjacent edges of the primitive parallelepiped. Nonprimitive axes are used as crystal axes when they have a simple relation to the symmetry of the structure (figure 1.4).

1.1.2 Bravais lattices

In order to describe the crystal structure it is necessary to answeer three important questions:

1. *what lattice* we have (for a particular structure can be more than one),

2. *what translational vectors* $\vec{a}_1, \vec{a}_2, \vec{a}_3$ are we using to describe the lattice (more sets of translational vectors can be selected for a given lattice) and

3. *what is the basis* (which is choose after the lattice and translational vectors are selected).

Crystal lattice can be transformed into themselves by the lattice translation $\vec{T}$

$$\vec{T} = u_1\vec{a}_1 + u_2\vec{a}_2 + u_3\vec{a}_3 \tag{1.2}$$

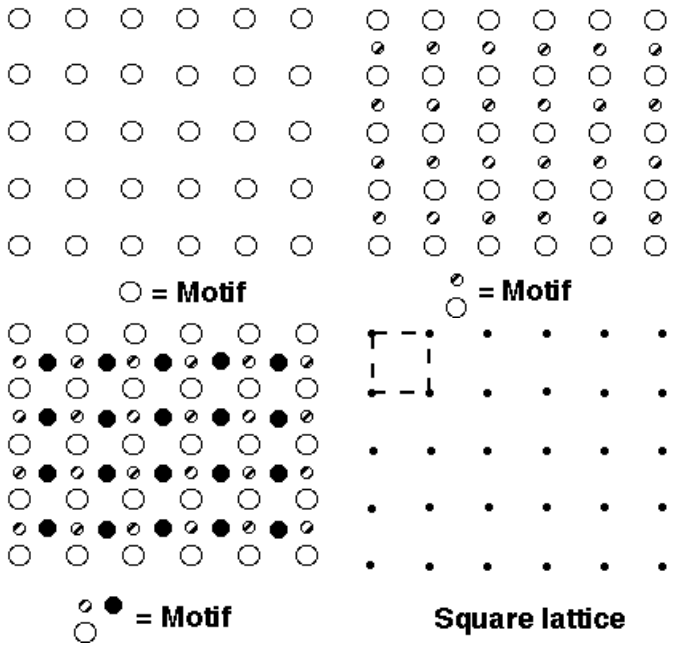

Figure 1.2: Application of the lattice and the basis (motif) for creation of 2D crystalline patterns.

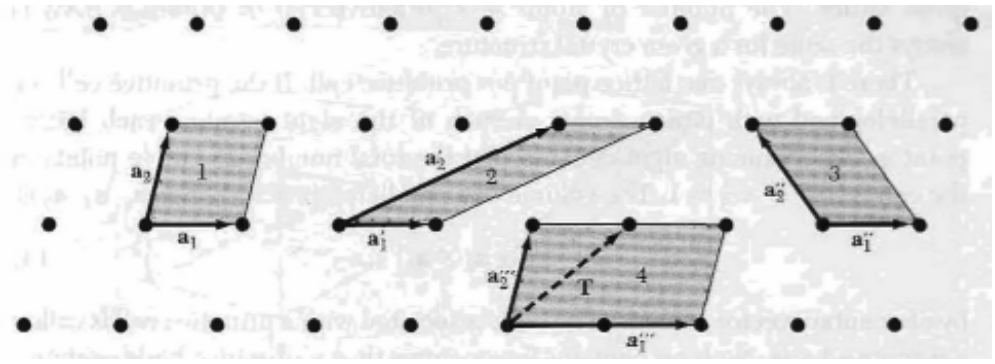

Figure 1.3: Lattice points in 2D. All pairs of vectors $\vec{a}_1$, $\vec{a}_2$ are translational vectors but $\vec{a}_1^{\,\prime\prime}$, $\vec{a}_2^{\,\prime\prime}$ are not primitive because the lattice translation $\vec{T}$ cannot be formed by integral combinations of $\vec{a}_1^{\,\prime\prime}$ and $\vec{a}_2^{\,\prime\prime}$.

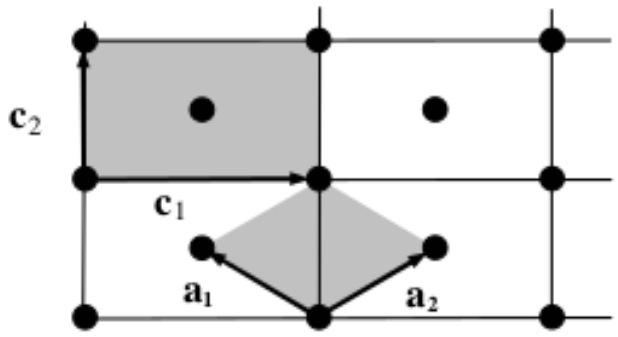

Figure 1.4: Lattice points for 2D centered rectangular Bravais lattice with the selection of primitive translation vectors $\vec{a}_1$ and $\vec{a}_2$ and nonprimitive translational vectors $\vec{c}_1$ and $\vec{c}_2$ that exhibits the rectangular symmetry more clearly.

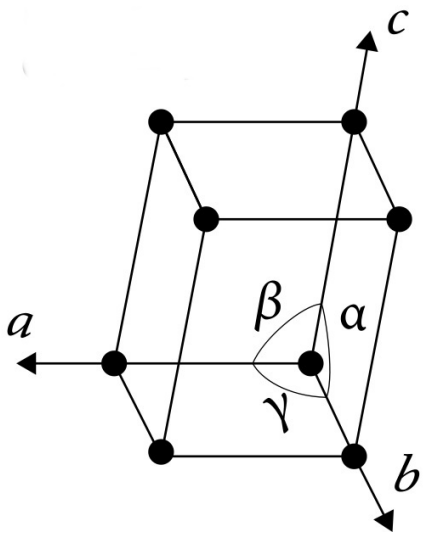

Figure 1.5: Translational vectors forming a parallelepiped in 3 dimensional scheme.

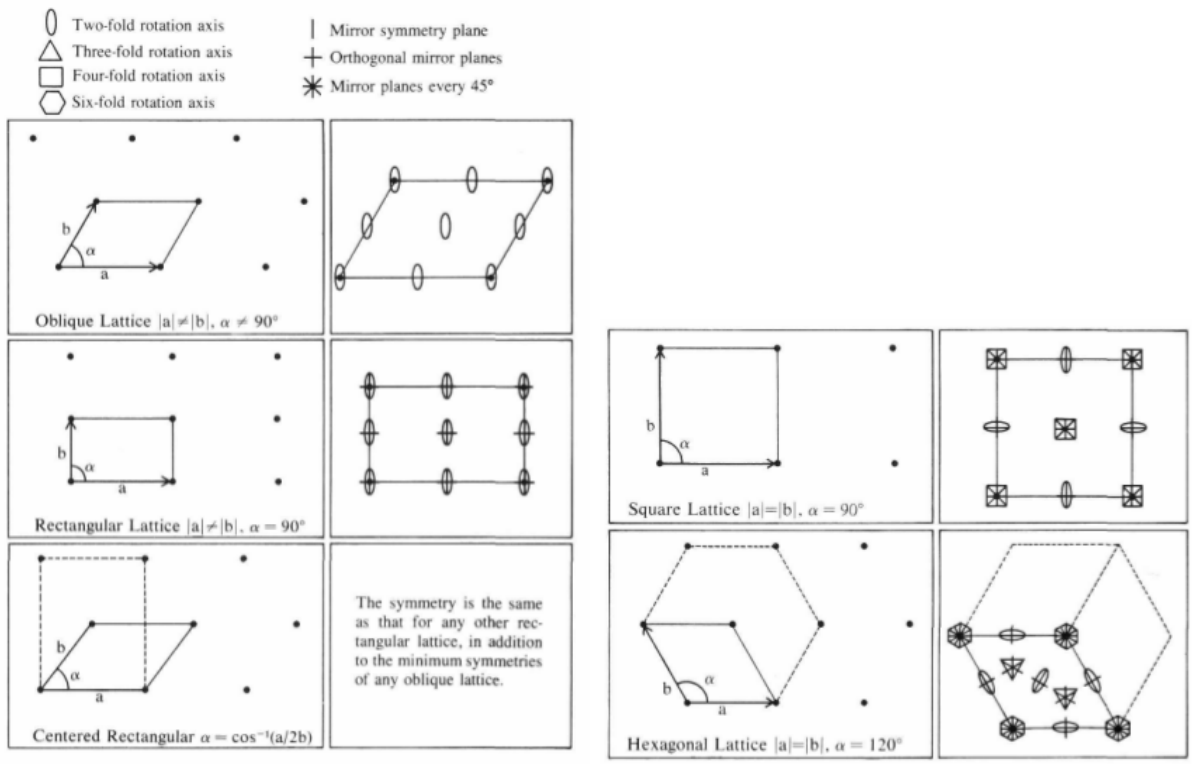

Figure 1.6: 2D Bravais lattices

and by various other symmetry point operations. A typical symmetry point operation is that of *rotation about an axis that passes through a lattice point.* Lattices can be found such that one-, two-, three-, four- and six-fold rotation axes carry the lattice into itself, corresponding to rotations by 2π, $2\pi/2$, $2\pi/3$, $2\pi/4$ and $2\pi/6$ radians and by integral multiples of these rotations. Another symmetry operations are *mirror reflections about a plane through a lattice point.* The collection of symmetry point operations which, applied about a lattice point, carry the latice into itself is called *lattice point group.*

In **two dimensions**, there is a general lattice known as oblique lattice and four special lattices. The oblique lattice is invariant only under rotation of π and 2π about any lattice point but special lattices can be invariant under rotation $2\pi/3$, $2\pi/4$ and $2\pi/6$ or under mirror reflection. *Bravais lattice* is the common phrase for a distinct lattice type and we say that in 2D there are *five* Bravais lattices: oblique, rectangular, centered rectangular (rhombic), hexagonal, and square (figure 1.6).

In **three dimensions**, there are 7 unique unit-cell shapes that can fill the space (triclinic, monoclinic, orthorhombic, tetragonal, rhombohedral, hexagonal and cubic). These are the 7 **crystal systems**. The Bravais lattices are obtained by combining one of the seven lattice systems with one of the lattice centerings. The lattice centerings are:

- simple - lattice points on the cell corners only.
- body-centered - one additional lattice point at the center of the cell.

- face-centered - one additional lattice point at center of each of the faces of the cell.
- base-centered - one additional lattice point at the center of each of one pair of the cell faces.

There are in total $7 \times 6 = 42$ combinations but it can be shown that several are equivalent to each other. Therefore, the number is reduced to **14 conventional Bravais lattices** described in table 1.1. The unit cells related to 14 Bravais lattices are shown in figure 1.7. From them only simple cubic (sc) is a primitive cell (figure 1.8).

Primitive translation vectors of the body-centered cubic (bcc) lattice (in units of lattice parameter a) are $\vec{a}_1 = (1/2, 1/2, -1/2)$; $\vec{a}_2 = (-1/2, 1/2, 1/2)$; $\vec{a}_3 = (1/2, -1/2, 1/2)$ (figure 1.9 left). The primitive cell is the rhombohedron. The packing ratio is 0.68, defined as the maximum volume which can be filled by touching hard spheres in atomic positions. Each atom has 8 nearest neighbors. The conventional unit cell is a cube based on vectors $\vec{a}_1 = (0, 0, 1)$; $\vec{a}_2 = (0, 1, 0)$; $\vec{a}_3 = (0, 0, 1)$. It is twice big compared to the primitive unit cell and has two atoms in it with coordinates $\vec{r}_1 = (0, 0, 0)$ and $\vec{r}_2 = (1/2, 1/2, 1/2)$ (figure 1.9 right). The bcc lattice have alkali metals such as Na, Li, K, Rb, Cs, magnetic metals such as Cr and Fe, and and refractory metals such as Nb, W, Mo, Ta.

Primitive translation vectors of the face-centered cubic (fcc) lattice (in units of lattice parameter a) are $\vec{a}_1 = (1/2, 1/2, 0)$; $\vec{a}_2 = (0, 1/2, 1/2)$; $\vec{a}_3 = (1/2, 0, 1/2)$. The primitive cell is the rhombohedron. The packing ratio is 0.74. Each atom has 12 nearest neighbors. The conventional unit cell is a cube based on vectors $\vec{a}_1 = (0, 0, 1)$; $\vec{a}_2 = (0, 1, 0)$; $\vec{a}_3 = (0, 0, 1)$. It is 4 times bigger than the primitive unit cell and has 4 atoms in it with coordinates $\vec{r}_1 = (0, 0, 0)$; $\vec{r}_2 = (1/2, 1/2, 0)$; $\vec{r}_3 = (0, 1/2, 1/2)$; $\vec{r}_4 = (1/2, 0, 1/2)$. The fcc lattice have noble metals such as Cu, Ag, Au, common metals such as Al, Pb, Ni and inert gas solids such as Ne, Ar, Kr, Xe.

1.1.3 Index systems for crystal directions and planes

Crystal directions

Any lattice vector can be written as that given by eq. (1.2). The direction is then specified by the three integers $[u_1\ u_2\ u_3]$. If the numbers u_1, u_2, u_3 have a common factor, this factor is removed. For example, [111] is used rather than [222], or [100], rather than [400]. When we speak about directions, we mean a hole set of parallel lines, which are equivalent due to transnational symmetry. Opposite orientation is denoted by the negative sign over a number. An example is in figure 1.11.

Crystal planes

The crystal plane is defined by three points in the plane provided they are not collinear. The orientation of a plane in a lattice is specified by *Miller indices*:

- Find the intercepts on the axes in terms of the lattice constants a_1, a_2 and a_3. The axes may be those of a primitive or nonprimitive cell.
- Take the reciprocals of these numbers and then reduce to three (usually smallest) integers having the same ratio (see figure 1.11).

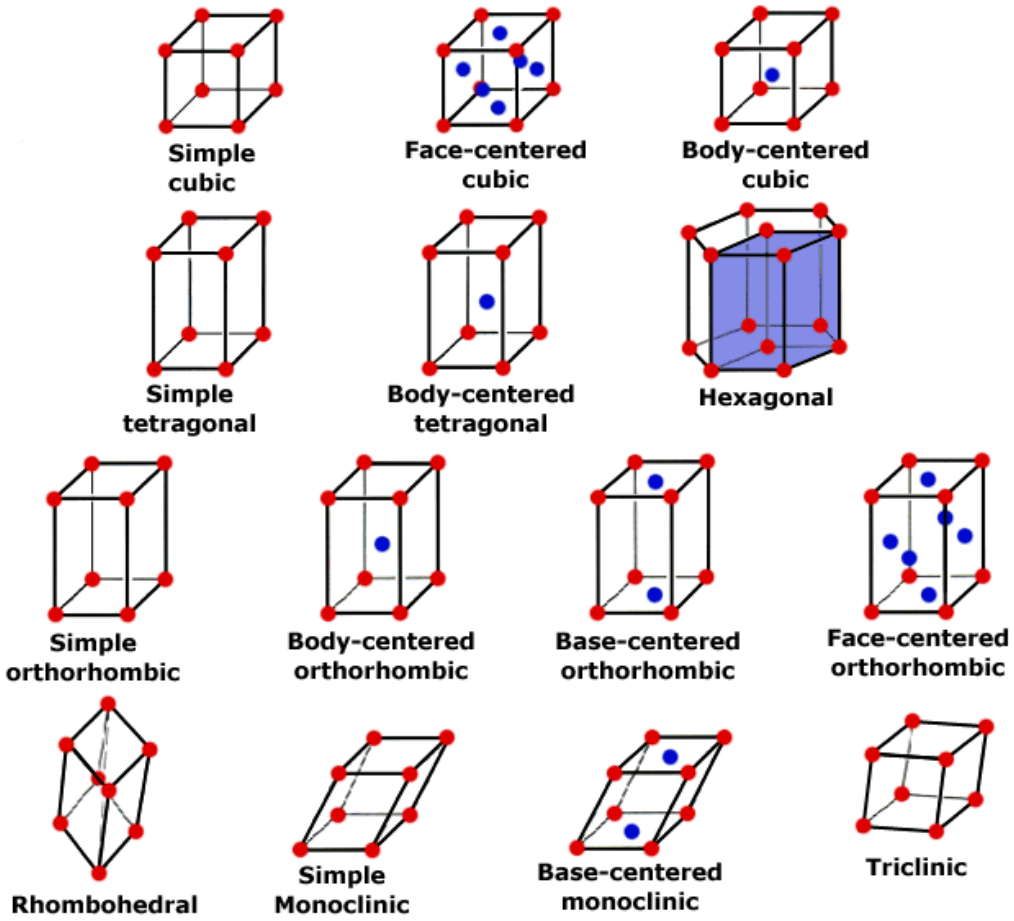

Figure 1.7: 3D Bravais lattices

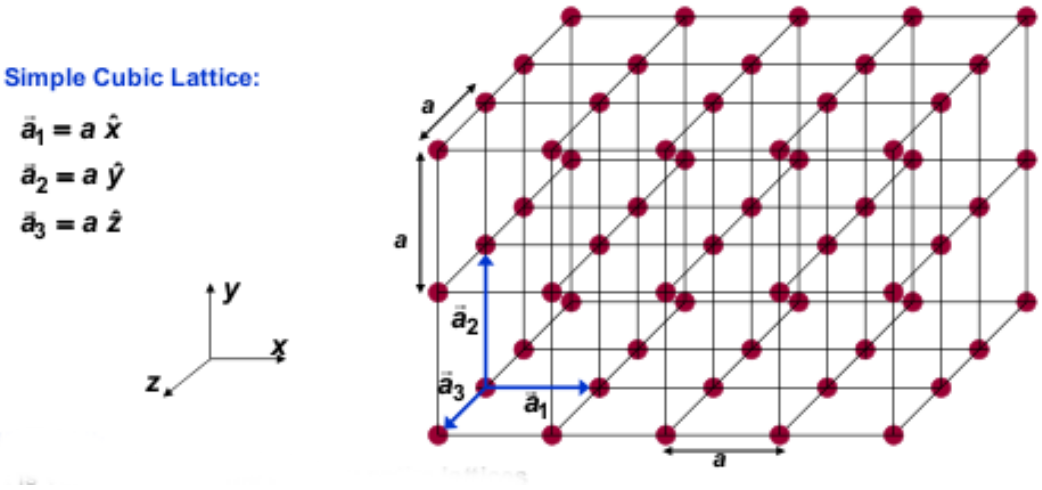

Figure 1.8: Simple cubic Bravais lattice - primitive cell.

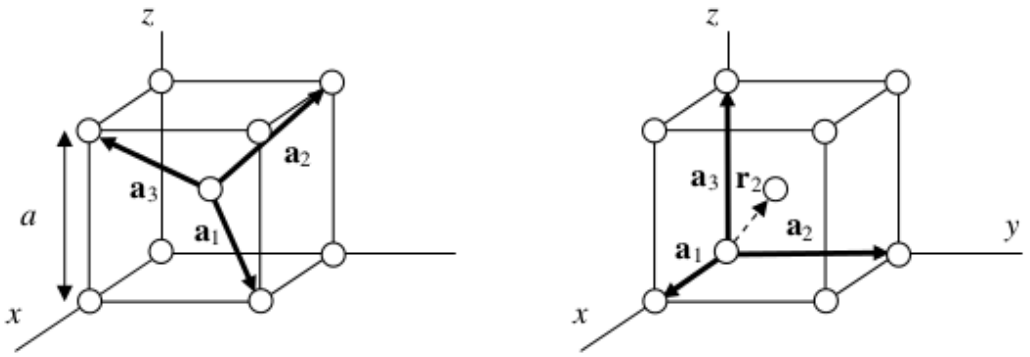

Figure 1.9: Body-centered Bravais lattice with depicted primitive translational vectors defining primitive cell (left) and conventional selection of cell expressing better the symmetry (right).

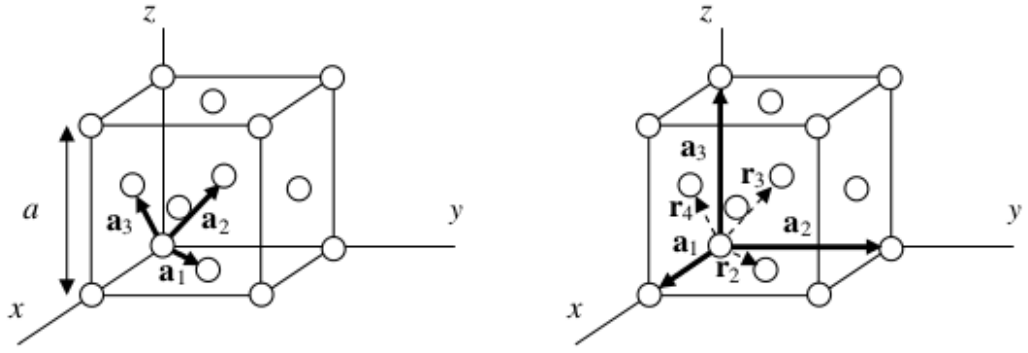

Figure 1.10: Face-centered Bravais lattice with depicted primitive translational vectors defining primitive cell (left) and conventional selection of cell expressing better the symmetry (right).

The result enclosed in parentheses (hkl) is called the index of plane. Examples for a cubic system are shown in figure 1.12.

Crystal System	Centering	Axial Distances (edge lengths)	Axial Angles	Examples
Cubic	simple body-centred face-centred	a = b = c	$\alpha = \beta = \gamma = 90^o$	NaCl, Zinc Blende, Cu
Tetragonal	simple body-centered	a = b $\neq$ c	$\alpha = \beta = \gamma = 90^o$	White tin, SnO_2, TiO_2, $CaSO_4$
Orthorhombic	simple body-centered face-centered base-centered	a $\neq$ b $\neq$ c	$\alpha = \beta = \gamma = 90^o$	Allotropes of sulfur, KNO_3, $BaSO_4$
Hexagonal	simple	a = b $\neq$ c	$\alpha = \beta = 90^o$,$\gamma = 120^o$	Graphite, ZnO, CdS
Rhombohedral (trigonal)	simple	a = b = c	$\alpha = \beta = \gamma \neq 90^o$	$CaCO_3$, HgS
Monoclinic	simple base-centered	$a \neq b \neq c$	$\alpha = \gamma = 90^o$, $\beta \neq 90^o$	Monoclinic Sulphur, $Na_2SO_4 * 10H_2O$
Triclinic	simple	$a \neq b \neq c$	$\alpha \neq \beta \neq \gamma \neq 90^o$	$K_2Cr_2O_7$, $CuSO_4$ $*5H_2O$, H_3BO_3

Table 1.1: Description of 14 Bravais lattices in 3D.

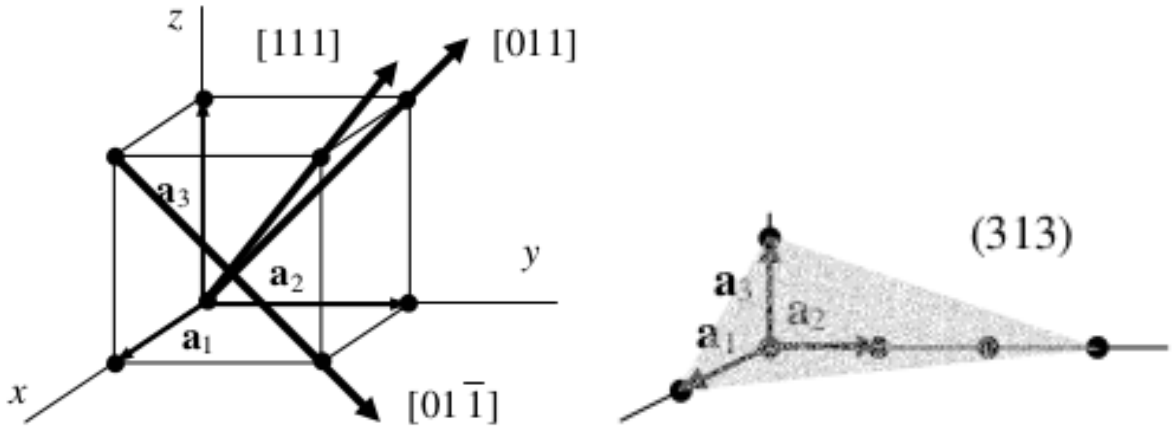

Figure 1.11: Example of crystal directions (left) and indexing of crystal plane (right).

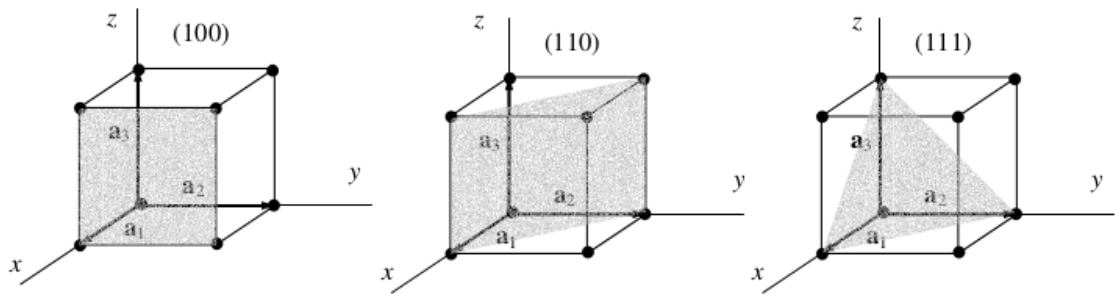

Figure 1.12: Example of crystal directions.

1.2 Bonds in Solids

Interatomic bonds in solids are following

- ionic
- covalent
- metalic
- Van der Waals

1.2.1 Ionic bonds

Ionic bonds are formed between particles which have a net electrical charge. Positive ions are called **cations**, since they are attracted to the negative cathode during electrolysis, negative ions are called **anions** and migrate to the anode on electrolysis. Ionic bond occurs when atoms with low ionization energy (lose electrons easily, i.e. they become positive ions) interact with the atoms with high electron affinity (easily accept electrons, i.e., become negative ions). They are held together by the Coulomb interaction between positive cations or negative anions. Large atoms or molecules have a low **ionization energy**, while small molecules tend to have higher ionization energies. Alkaline metals have low ionization energy. The **electron affinity** of an atom or molecule is the amount of energy released when an electron is added to a neutral atom or molecule to form a negative ion. Halogens have high electron affinity.

In ionically bonded crystals ions form a lattice in which each cation (anion) is surrounded by as many anions (cations) as possible, in a symmetric arrangement. It is thus not possible to distinguish electrically neutral molecules within the lattice. The most important contribution to

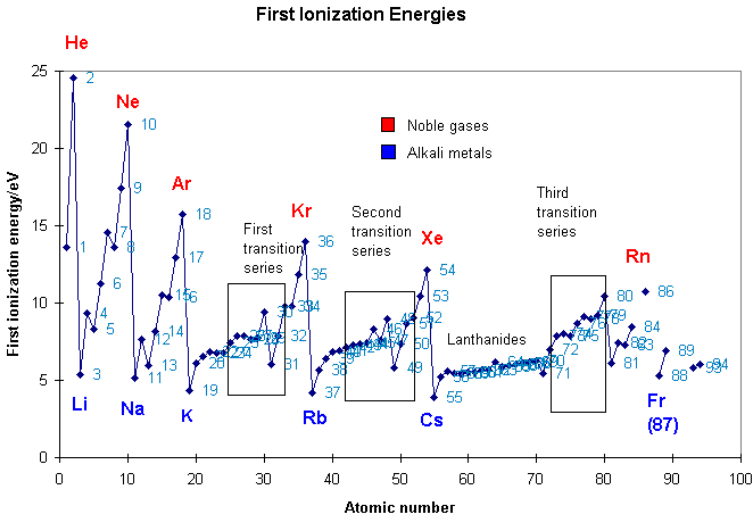

Figure 1.13: Ionization energy of atoms as a function of atomic number.

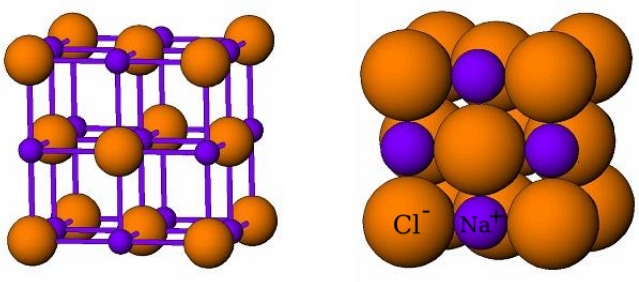

Figure 1.14: Model of the coordination of Na and Cl inll NaCl.

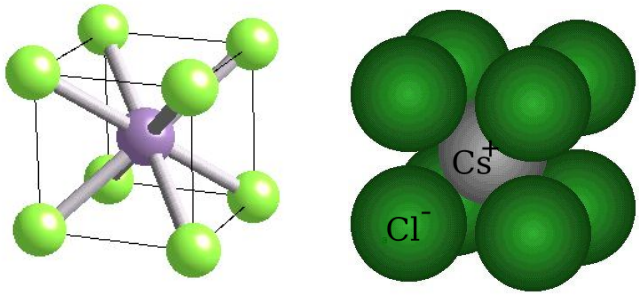

Figure 1.15: Model of the coordination of Cs and Cl inl CsCl.

the cohesive energy of crystals is due to the Coulomb interactions between ions. Because of their long range, one must take into account the attraction and repulsion between arbitrarily distant ions when calculating the energy of the system. There are two typical ionic crystals, NaCl and CsCl. In the sodium chloride (or rock-salt) crystal the sites of a regular cubic lattice are occupied by Na^+ and Cl^- ions alternately, in a 3D checkerboard pattern. In the CsCl crystal, Cs^+ ions make up a regular cubic lattice, and Cl^- ions occupy the center of each elementary cube.

The lattice constant a of the rock-salt crystal (NaCl) is customarily defined as the shortest distance between two similar ions along one of the lattice axes. The nearest neighbours of each Na^+ ion are then six Cl^- ions at a distance $d_1 = a/2$ because of the difference between atom size. In the case of CsCl the atoms have similar size and thus each atom of Cs is surrounded by 8 Cl ones. The cohesive energy is the crystal energy which is released when individual neutral atoms are created. Coulomb potential for ions. Let us consider Na^+ in NaCl. It is surrounded by six

Table 1.2: Electron affinity in eV.

Fluorine	3.45
Chlorine	3.61
Bromine	3.36
Iodine	3.06

Cl^- at the distance r:

$$V_1 = -\frac{6e^2}{4\pi\varepsilon_0 r}. \tag{1.3}$$

Another neighbour is 12 Na^+ each at the distance $\sqrt{2}r$:

$$V_2 = +\frac{12e^2}{4\pi\varepsilon_0\sqrt{2}r}. \tag{1.4}$$

When is summed for the entire crystal, we obtain:

$$\begin{aligned} V_{Coulomb} &= -\frac{e^2}{4\pi\varepsilon_0 r}\left(6 - \frac{12}{\sqrt{2}} + \ldots\right) \\ &= -1,748\frac{e^2}{4\pi\varepsilon_0 r} \\ &= -\alpha\frac{e^2}{4\pi\varepsilon_0 r}. \end{aligned} \tag{1.5}$$

The constant α is called **Madelung** crystal constant and has a values between 1.6 and 1.8 for simple crystals. The contribution of the repulsive force to the total potential energy can be written as:

$$V_{repulsive} = \frac{B}{r^n}. \tag{1.6}$$

Total potential energy in the crystal is:

$$\begin{aligned} V &= V_{Coulomb} + V_{repulsive} \\ &= -\frac{\alpha e^2}{4\pi\varepsilon_0 r} + \frac{B}{r^n}. \end{aligned} \tag{1.7}$$

In the steady case the separation of ions at a distance r_0 must be minimum V:

$$\left(\frac{dV}{dr}\right)_r = r_0 = 0, \tag{1.8}$$

so

$$B = \frac{\alpha e^2}{4\pi\varepsilon_0 n} r_0^{n-1} \tag{1.9}$$

and the total potential energy will be:

$$V = -\frac{\alpha e^2}{4\pi\varepsilon_0 r_0}\left(1 - \frac{1}{n}\right) \tag{1.10}$$

where n is approximately 9, $r_0 = 2.81$ in NaCl, thus $V = -1,27 \times 10^{-18}$ J $= -7,97$ eV. We must also calculate the energy required to transfer an electron between Na and Cl, which is the difference between the ionization energy 5.14 eV for Na and the electron affinity of -3.61 eV for Cl , i.e. 1.53 eV. Each atom is contributing with half of the value, so the overall cohesive energy per atom $E_{\text{cohesive}} = (-3,99 + 0,77)$ eV/atom $= -3,22$ eV/atom. Ionic compounds conduct electricity when molten or in solution, but not as a solid. They generally have a high melting point and tend to be soluble in water. Many ionic crystals are hard material due to the strength of their bonds.

1.2.2 Covalent bond

Covalent bond is formed when one or more electrons are shared by two atoms. The electron density reaches its maximum in the region between the two atoms. Covalent solids are held together by networks of directional covalent bonds between neighbouring atoms, where the wavefunctions of covalent bonds are constructed from pairs of atomic states.

If each bonding state is occupied by two electrons of opposite spins – i.e., each bond is saturated – then the electrons that participate in bonding are localized in space and cannot contribute to electrical conductivity. That is why covalent materials are usually insulators or semiconductors. This is the case for diamond and for two further elements of the carbon group: germanium and silicon, which have a diamond structure. Here each atom has four sp^3 hybrid states, and the bonds formed by them make up a tetrahedral network. The same structure is seen in semiconducting compounds formed by elements in groups 13 (IIIA) and 15 (VA) of the periodic table. As it was mentioned in the previous subsection, besides sp^3 wavefunctions, other hybrid states may also give rise to covalent bonding – however, their spatial directionality depends on which states are hybridized. The orientation of the bonds plays a crucial role in determining the crystal structure. The development of short–range order in the amorphous state of covalently bonded solids is also related to the directionality of the bonds. The cohesive energy of covalent crystals is given by the sum of the binding energies of individual bonds.

The binding energies of some typical covalent bonds are listed in table below. Much larger than their counterparts for molecular crystals, these values are comparable to the energies of ionic crystals.

1.2.3 Van der Waals bond

All atoms and molecules, even inert-gas atoms such as those of helium and argon, exhibit weak, short-range attractions for one another due to *van der Waals forces*. These forces were proposed a century ago by the Dutch physicist Johannes van der Waals to explain observed departures from the ideal-gas law. The explanation of the actual mechanism of the force, of course, is more recent.

Van der Waals forces are responsible for the condensation of gases into liquids and the freezing of liquids into solids in the absence of ionic, covalent, or metallic bonding mechanisms. Such familiar aspects of the behaviour of matter in bulk as friction, surface tension, viscosity, adhesion,

Table 1.3: Binding energy of some typical covalent bonds

Bond	eV	kJ/mol	Bond	eV	kJ/mol
H–H	4.48	432	C–H	4.28	413
N–N	1.65	159	C–N	3.16	305
P–P	2.08	201	N–H	4.03	389
C–C	3.58	346	Al–P	2.13	205
Si–Si	2.30	222	Si–C	3.17	306
Ge–Ge	1.95	188	Ga–As	1.63	157
O–O	1.47	142	Ga–P	1.78	172

cohesion, and so on, also arise from these forces. As we shall find, the van der Waals attraction between two molecules r apart is proportional to r^{-7}, so that it is significant only for molecules very close together.

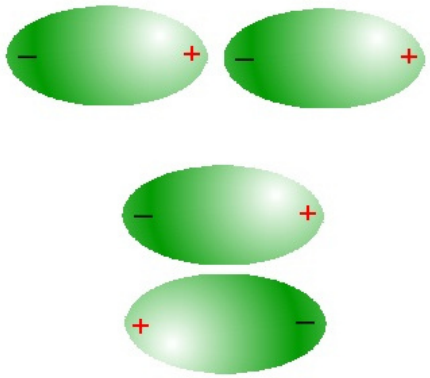

Figure 1.16: Polar-polar attraction

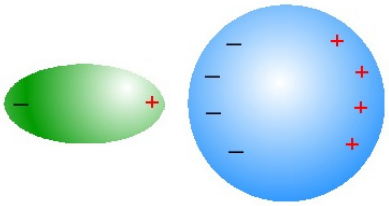

Figure 1.17: Polar-nonpolar attraction

Polar-polar attraction

We begin by noting that many molecules, called *polar molecules*, have permanent electric dipole moments. An example is the H_2O molecule (Fig. 1.19), in which the concentration of electrons around the oxygen atom makes that end of the molecule more negative than the end where the hydrogen atoms are. Such molecules tend to align themselves so that ends of opposite sign are adjacent, as in Fig. 1.16. In this orientation the molecules strongly attract each other.

Polar-nonpolar attraction

A polar molecule is also able to attract molecules which do not normally have a permament dipole moment. The process is illustrated in Fig. 1.17. The electrical field of the polar molecule causes a separation of charge in the other molecule, with the induced moment the same in direction as that of the polar molecule. The result is an attractive force. The effect is the same as that involved in the attraction of an unmagnetized piece of iron by a magnet.

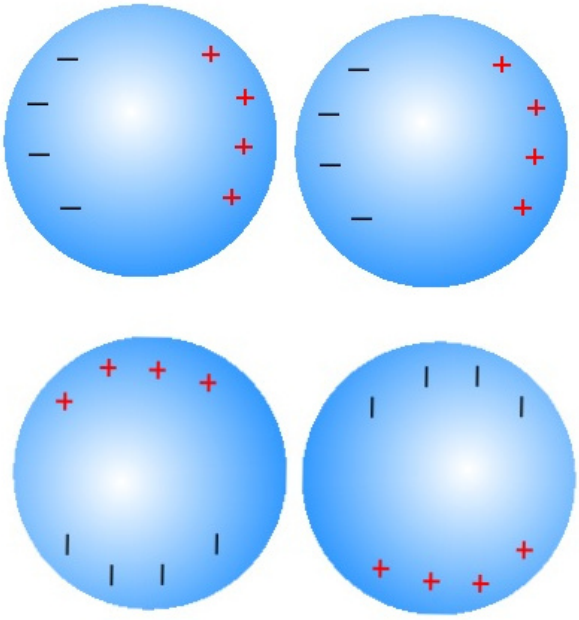

Figure 1.18: Nonpolar-nonpolar attraction

It is not difficult to determine the characteristics of the attractive force between a polar and a nonpolar molecule. The electric field $\vec{E}$ at a distance r from a dipole of moment $\vec{p}$ is given by

$$\vec{E} = \frac{1}{4\pi\varepsilon_0}[\frac{\vec{p}}{r^3} - \frac{3(\vec{pr})}{r^5}\vec{r}] \tag{1.11}$$

We recall from vector analyses that $\vec{pr} = pr\cos\theta$, where θ is the angle between $\vec{p}$ and $\vec{r}$. The field $\vec{E}$ induces in the other, normally nonpolar molecule an electric dipole moment $\vec{p}'$ proportional to $\vec{E}$ in magnitude and ideally in the same direction. Hence

$$\vec{p}' = \alpha\vec{E} \tag{1.12}$$

where α is a constant called the *polarizability* of the molecule. The energy of the induced dipole in the electrical field $\vec{E}$ is

$$\mathcal{E} = -\vec{p}'\vec{E} = -\frac{\alpha}{(4\pi\varepsilon_0)^2}(1+\cos^2\theta)\frac{p^2}{r^6} \tag{1.13}$$

The mutual energy of the molecules that arises from their interaction is thus negative, signifying that the force between them is attractive, and is proportional to r^{-6}. The force itself is equal to $d\mathcal{E}/dr$ and so proportional to r^{-7}, which means that it drops rapidly with increasing separation. Doubling the distance between two molecules reduces the attractive force between them to only 0.8 % of its original value.

Nonpolar-nonpolar attraction

More remarably, two nonpolar molecules can attract each other by the above mechanism. Even though the electron distribution in a nonpolar molecule is symmetric on the average, the electrons

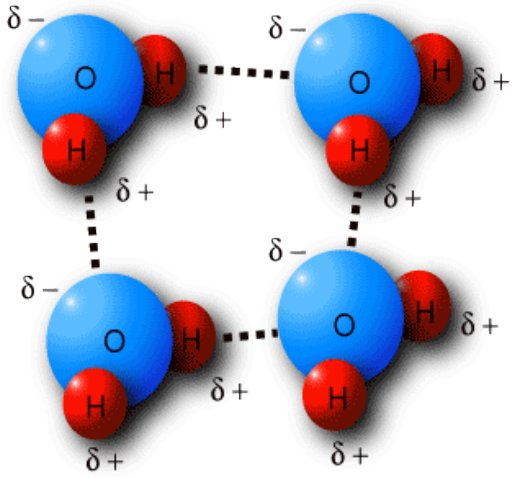

Figure 1.19: Water molecule

themselves are in the constant motion and at any given instant one part or another of the molecule has an excess of them. Instead of the fixed charge asymmetry of a polar molecule, a nonpolar molecule has a constantly shifting asymmetry. When two nonpolar molecules are close enough, their fluctuating charge distributions tend to shift together, adjacent ends always having oposite sign (Fig. 1.18) and so always causing an attractive force.

Hydrogen bond

An especially strong type of van der Waals bond called a *hydrogen bond* occurs between certain molecules containing hydrogen atoms. The electron distribution in such an atom is so distorted by the affinity of the "parent" atom for electrons that each hydrogen atom is essence has donated most of its negative charge to the parent atom, leaving behind a poorly shielded proton. The result is a molecule with a localized positive charge which can link up with the concentration of negative charge elsewhere in another molecule of the same kind. The key factor here is the small effective size of the poorly shielded proton, since electric forces vary as r^{-2}.

1.2.4 Metallic bond

A great part of the chemical elements have fewer electrons on the incomplete shells than what is necessary for having saturated covalent bonds between each pair of neighbouring atoms in the solid state. Electrons participating in unsaturated bonds are not localized. One may also say that the atoms lose these outermost (in general, s or p) electrons. While the positively charged ions left behind are arranged in a more or less regular pattern, the freed electrons fill the region among the ions almost evenly. This moving cloud of electrons gives rise to metallic bonding. In transition metals, where incomplete d-shells are also found under the outermost shell, further electrons may participate in metallic bonding. The same kind of bonding may appear in materials built up of molecules with incomplete shells.

The wavefunction of such an electron system cannot be written as the product of the wavefunctions of pairs of electrons forming bonds. It has to be chosen in such a way that it should show explicitly the antisymmetry with respect to the interchange of the coordinates of any two electrons. The analysis of such systems, the determination of electronic energies and states, and the study of those properties of solids that are due to electrons will be among our most important tasks. The determination of the total energy of metals is a difficult problem of solid-state physics. The cohesive energy per atom is usually 1–5 eV.

Electrons in metals

In particular, this problem is solved using the one electron approximation. However, it is necessary to introduce further approximations, such as

- approximation of free electrons - can correctly explain many properties of metals, such as specific heat, thermal conductivity, electrical conductance.
- approximation of weakly bound electrons - explain other important phenomena such as the difference between metals, insulators and metalloid, the relationship between conductivity and valence electrons in the metal

In both cases, we consider a system of electrons in a ideal gas of fermions (max 1 particle in a given state). Then the distribution of electron energies $n(\epsilon)$

$$n(\epsilon) = \frac{dn}{d\epsilon} = f_{\mathrm{FD}}\ g(\epsilon), \tag{1.14}$$

where $g(\epsilon)$ is the energy distribution of states and f_{FD} is the Fermi-Dirac distribution function for free electrons:

$$f_{\mathrm{FD}} = \frac{1}{exp(\frac{\epsilon-\mu}{kT}) + 1}. \tag{1.15}$$

The chemical potential μ can be determined from the normalization of the electron numbers N

$$N = \int_0^\infty f_{\mathrm{FD}}\ g(\epsilon)d\epsilon. \tag{1.16}$$

is a function of T. For particles with $m \neq 0$ so $\epsilon = \vec{p}^2/2m$

$$g(\epsilon)d\epsilon = g_0 \frac{\int_\epsilon^{\epsilon+d\epsilon} d\vec{q}d\vec{p}}{h^3}, \tag{1.17}$$

where g_0 contains information about the spin. If we take in account the two possible orientations of the electron we obtain

$$g(\epsilon)d\epsilon = \frac{4\pi L^3}{h^3}(2m)^{3/2}\epsilon^{1/2}d\epsilon \tag{1.18}$$

At $T = 0$ the f_{FD} is the highest energy to which states are filled $\epsilon = \mu = E_{\mathrm{F}}$; it corresponds also to the electrochemical potential of the system. The Fermi energy is only a very slow function of temperature, and for many effects not dependent directly on the rate of change of f_{FD} with

temperature. It can be shown that the temperature dependence of the Fermi energy can be expressed as

$$\mu = \mu_0 \left(1 - \frac{\pi^2}{12}\left(\frac{kT}{\mu_0}\right)^2 \dots\right), \tag{1.19}$$

where μ_0 is the chemical potential at absolute zero. The solution for Schrödinger equation in electric field for periodic ionic crystals shows the existence of a separate area of the energy bands. These areas are called **forbidden bands**.

1.2.5 Summary of Properties Associated with Interatomic Bonds

Property	Ionic	Covalent	Metallic	Van der Waals
	Non-directional; Structures of high coordination	Direcional; Structures of low coordination and low density	Non-directional; Structures of high coordination and high density	Analogous to metallic bonds
Mechanical	Strong, hard crystals	Strong, hard crystals	Variable crystals	Weak, soft crystals
Thermal	High melting point, low expansion coefficient	High melting point, low expansion coefficient	Range of melting points extended liquidus range	Low melting point large expansion coefficient
Electrical	Weak insulator, conduction by ion transport when liquid	Insulator in solid and liquid state	Conduction by electron transport	Insulator
Optical	Absorption and other properties mainly of the individual ions	High refractive index, absorption different in solid and gas	Opaque, with similar properties in liquid state	Properties of individual molecules

1.3 Types of Materials

1.3.1 Ceramics

The constitution of a ceramic is usually a combination of one or more metals with a non-metallic element, usually oxygen. As a result, the atoms in a ceramic crystal are linked by a combination of ionic and covalent bonds. The combination of oxygen atoms with the metal atoms provides a strong ionic bond because oxygen, with two vacancies in the outer electron shell, effectively borrows two electrons from the neighbouring metal atoms.

Table 1.4: Classification of materials based on nature and applications by Bever (1986)

Nature	Applications
Ceramics	Industrial Materials
Glasses	Electrical Materials
Metals and Alloys	Electronic Materials
Other Inorganic Materials	Superconducting Materials
Polymers	Magnetic Materials
Elastomers	Nuclear Materials
Fibres	Material for other Energy Applications
Composite Materials	Optical Materials
Wood	Biomedical Applications
Paper and Paperboard	Dental Materials
Other Biological Materials	Building Materials

(*) M. B. Bever ed., Encyclopedia of Materials, Science and Engineering, Vol. 1 ed. R. W. Cahn, Oxford (1986), Pergamon

If ceramic crystals were of perfectly organised structure and uniform microstructure, these materials would have mechanical properties that exceed those achieved. Indeed, failure of a ceramic is generally a consequence of a microstructural defect, or combination of defects, such as inclusions, pores, voids and distribution of irregular size grain.

1.3.2 Semiconductors

Many of the traditional semiconductor materials have crystal structures that are related to the simple diamond cubic lattice where each atom is tetrahedrally coordinated, but the local atomic environment is not identical for all atoms. Table below gives the values of basic physical parameters of some commonly encountered semiconductor materials. Most semiconductor compounds and alloys are designed to keep the average electron to atom ratio to a value of four. The simplest illustration is given by the range of AB-type semiconductor materials formed between Group III and Group V elements in the Periodic Table of Elements. These so-called III to V semiconductors include GaAs and have a sphalerite (zinc-blend) superlattice structure, whereas the Types II and VI and IV and VI compounds usually have crystal structures of the sphalerite and rock salt respectively. Here the lattice constants of these materials lie in the range 0.50 to 0.65 nm and are generally larger than for metallic elements. This makes it generally easier to obtain details of the crystalline defects. Moreover the binary semiconductor compounds have band gaps in the range 0 to 3 eV. Although covering the band gap range for applications to microelectronic devices it is not possible to prepare such devices from this limited range of materials. This is due to (i) difficulties in preparing suitable defect-free pure materials and (ii) the need to have precisely controlled band gaps to optimise the performance of particular devices. Hence the need to create materials by a combination of binary semiconductor compounds to give ternary and even quaternary semi-conductors (Pollock et al, 1982).

Table 1.5: Crystal structure and basic electrical properties of some important semi-conductor elements and compounds.

Element	Crystal structure	Lattice spacing (nm)	Band-gap width (at 300K) (eV)
IV elemental and compounds			
Si	D	0.5431	1.12
Ge	D	0.5646	0.66
C (diamond)	D	0.3566	5.47
SiC	S	0.4359	2.36
SiC	W	0.3073	3.23
SiGe	W	0.5431	0.67/1.11

D is diamond cubic, S is zinc-blend, W is wurtzite and R is the rocksalt lattice.

1.3.3 Superconductors

Superconductors are characterized by anomalous temperature dependence of the electrical resistivity. Below a critical temperature T_0, their resistivity drops by more than a factor of 10^{10}. In superconductors the magnetic flux density $B = \mu_r B_a$ induced by an externally applied field H_a is zero, like in ideal diamagnets with $\mu_r = 0$ (Meissner–Ochsenfeld effect). If H_a exceeds a critical value H_c the superconductor becomes normal conducting. But the magnetic induction B decreases from B_a at the free surface to $B = 0$ in the interior through a layer of finite thickness characterized by the Landau penetration depth λ. Superconducting substances of fundamental as well as practical interest may be divided into 3 main groups:

1. Metallic superconductors;

2. Superconducting oxides;

3. Superconducting carbides, nitrides and borides.

1.3.4 Glasses

Glass is a class of materials that does not crystallise when cooled from the molten state and, therefore, does not have long range periodicity within the atomic structure. A pure oxide glass consists of a random three-dimensional network of atoms where each oxygen atom is bonded to two atoms of metals, such as boron and each metal atom is bonded with three oxygen atoms. However, there are many type of glasses and in the case of silica glass, each metal atom is bonded with four oxygen atoms producing a more complex atomic configuration. The addition of fluxing atoms such as sodium reduces the number of bond cross links.

The major constituents of glasses are in two separated regions of the Periodic Table, Group VI (O, Si, Se and Te) and Groups I and II (used primarily as fluxes).

1.3.5 Metals and Alloys

Metals and alloys are opaque, lustrous and relatively heavy, easily fabricated and shaped, have good mechanical strength and high thermal and electrical conductivity. All these properties are a consequence of the metallic bonds. In general, they form one of the face centred cubic (fcc), body centred cubic (bcc) or hexagonal close packed (hcp) structures.

The overall mechanical properties of metals and alloys are controlled by the crystal lattice defects, such as dislocations and vacancies. Mechanical and chemical properties can be modified by the addition of alloying elements in varying proportion.

1.3.6 Polymers

Polymers are by definition materials composed of long-chain molecules, typically 10 to 20 nm, that have been developed as a consequence of the linking of many smaller molecules, monomers. The combination of tensile strength and flexibility make these materials attractive.

If the molecular chains are packed side by side, the molecules form an array with a crystalline structure. Natural polymers have complex microstructure comprising a mixture of crystalline and amorphous material. In the case of polymeric materials, the interatomic bonds between molecular chains are the weak van der Waals forces, but in the crystalline structures, the chains are closer together over comparatively large distances so that the contribution of intermolecular forces has the effect of producing a more rigid material. To develop stronger, more rigid, polymers:

1. production of a crystalline structure (polyethylene, nylon),

2. formation of a strong covalent bond between the molecular chains by cross linking (vulcanising raw rubber by heating with the controlled addition of sulphur atoms).

1.3.7 Composite Materials

A composite material was originally considered to be a combination of two materials but now this class of material is regarded as any combination which has particular physical and mechanical properties. The concept of composite materials has led to the design and manufacture of a new range of structural materials that are generally lighter, stiffer and stronger than anything previously manufactured.

- natural composites: wood - cellulose fibres provide tensile strength and flexibility and lignin provides the matrix for binding and adds the property of stiffness; bone - strong, but soft, protein collagen and the hard, brittle mineral apatite,

- synthetic composites: combining individual properties such as strong fibres of a material (for example carbon) in a soft matrix (such as an epoxy resin).

Element	Crystal structure	Lattice spacing (nm)	Band-gap width (at 300K) (eV)
III-V compounds			
GaAs	S	0.5653	1.42
GaP	S	0.5451	2.26
GaSb	S	0.6096	0.72
GaN	W	0.3186	3.4
InAs	S	0.6058	0.36
InP	S	0.5869	1.35
InSb	S	0.6479	0.17
InN	W	0.3536	0.65
InGaAs	S	0.5699	0.36/1.43
InGaP	W	0.3536	0.65
BAs	S	0.4777	1.5/3.47
BP	S	0.4537	2.0
BN	S	0.3615	5.5/6.4
AlAs	S	0.5661	2.16
AlSb	S	0.6136	1.58
AlP	S	0.5463	2.5
AlN	S/W	0.436	6.2
AlGaAs	S	0.5653	1.42/2.16
AlGaN	S	0.316	3.44/6.28
AlGaP	S	0.5537	2.26/2.45
II-VI compounds			
CdS	S/W	0.5832	2.42
CdSe	S	0.605	1.7
CdTe	S	0.6482	1.56
CdZnTe	S	0.6442	1.4/2.2
HgCdTe	S	0.648	0/1.5
HgZnTe	S	0.6459	0/2.25
HgTe	S	0.644	0
ZnS	S/W	0.542	3.68
ZnSe	S	0.5669	2.7
ZnTe	S	0.6089	2.2
ZnO	S/W	0.352	3.3
Chalcopyrite			
$CuInSe_2$	S	0.5782	1.04
CuCl	S	0.541	3.4
Cu_2S	W	0.4142	1.2
IV-VI compounds			
PbS	R	0.594	0.41
PbSe	R	0.612	0.27
PbTe	R	0.646	0.31
SmTe	R	0.632	0.18

D is diamond cubic, S is zinc-blend, W is wurtzite and R is the rocksalt lattice.

Chapter 2

Physics at surfaces

2.1 Introduction

The physical surface is obviously something different than the mathematical surface (an infinitely thin layer at the interface between solid and vacuum or gas). When we speak about the physics at surfaces, we usually mean a surface layer from a substance whose properties are different than those of volumes.

It is not possible to determine the thickness of the surface layer. It is different for different substances and it also varies depending on the properties that we consider, but is only a few atomic layers.

At the surface there are physical properties modifications and new phenomena, because the surface atoms are surrounded by asymmetric atoms.

- surface tension,
- surface space charge,
- work function,
- phase conditions,
- surface oscillations - the oscillations amplitude for surface atoms is higher for surface atoms than for the atoms in volume,
- lattice relaxation (atoms are slightly shifted from the equilibrium position),
- reconstruction (creation of new regular structures),
- adsorption.

2.2 Thermodynamics of Clean Surfaces

It introduces the concepts of surface free energy and surface stress. The essential features of bulk thermodynamics can be stated very succinctly (Callen, 1985). In equilibrium, a one-component

system is characterized completely by internal energy, U, which is a unique function of entropy, volume and particle number of the system:

$$U = U(S, V, N), \tag{2.1}$$

$$dU = |\frac{\partial U}{\partial S}|_{V,N} dS + |\frac{\partial U}{\partial V}|_{S,N} dV + |\frac{\partial U}{\partial N}|_{S,V} dN, \tag{2.2}$$

$$dU = TdS - PdV + \mu dN. \tag{2.3}$$

These equations define the temperature, pressure and chemical potential of the bulk. The extensive property of the internal energy,

$$U(\lambda S, \lambda V, \lambda N) = \lambda U(S, V, N), \tag{2.4}$$

together with the combined first and second laws of entropy, lead to the Euler equation,

$$U = TS - PV + \mu N. \tag{2.5}$$

Differentiating the Euler equation and using the entropy, we arrive at a relation among the intensive variables, the Gibbs-Duhem equation:

$$SdT - VdP + Nd\mu = 0 \tag{2.6}$$

2.2.1 Surface tension and surface stress

We create a surface of area A from the infinite solid by *cleavage* process. Since the bulk doe not spontaneously cleave, the total energy of the system must increase by amount proportional to A. The constant of proportionality, γ, is called *surface tension*:

$$U = TS - PV + \mu N + \gamma A. \tag{2.7}$$

In equilibrium at any finite temperature and pressure, the semi-infinite solid coexists with its vapor. A plot of the particle density as a function of distance normal to the surface is shown in the figure below.

Gibbs recognized that is convenient to be able to ascribe definite amounts of the extensive variables to a given area of surface. Accordingly, the vertical lines in the figure indicate a portion of space into a bulk solid volume, a bilk vapor volume and a transition, or surface, volume. The remaining extensive quantities can be partitioned likewise:

$$S = S_1 + S_2 + S_3, \tag{2.8}$$

$$V = V_1 + V_2 + V_3,$$

$$N = N_1 + N_2 + N_3.$$

In this formulae, the bulk quantities are defined by

$$i = 1, 2 \begin{cases} S_i = s_i V_i; \\ N_i = \rho_i V_i. \end{cases}$$

where ρ_i and s_i characterize the uniform bulk phases. Once the surface volume is chosen, the other surface quantities are defined as *excesses*. Note that changes in the surface excess quantities are completely determined by changes in the bulk quantities:

$$\begin{aligned} \Delta S_s &= -\Delta S_1 - \Delta S_2, \\ \Delta V_s &= -\Delta V_1 - \Delta V_2, \\ \Delta N_s &= -\Delta N_1 - \Delta N_2. \end{aligned} \tag{2.9}$$

Evidently, there is nothing unique about the particular choice of the boundary positions illustrated in the figure. Nevertheless, it will emerge that one always can be choose a subset of the surface excesses that are perfectly well-defined quantities with values that are *independent* of any such conventional choices. Now consider the effect of small variations in the area of the system, e.g., by *stretching*. We assume that the energy change associated with this process is described adequately by linear elasticity theory (Landau & Lifshitz, 1970). Accordingly, the entropy should be replaced by

$$dU = |\frac{\partial U}{\partial S}|_{V,N,A} dS + \frac{\partial U}{\partial V}|_{S,N,A} dV + \frac{\partial U}{\partial N}|_{S,V,A} dN + A \sum_{i,j} |\frac{\partial U}{\partial \epsilon_{i.j}}|_{S,V,N} d\epsilon_{i.j}$$

$$dU = TdS - PdV + \mu dN + A \sum_{i,j} \sigma_{i,j} d\epsilon_{i.j}$$

where $\sigma_{i,j}$ and $\epsilon_{i.j}$ are the surface stress and strain tensor.

2.3 Electronic Structure of Clean Surfaces

2.3.1 Hartree-Fock Approximation

The wave function describing the set of I electrons has the general form

$$\Psi(\vec{r}_1, S_{z1}, \vec{r}_2, S_{z2}, \ldots, \vec{r}_i, S_{zi}, \ldots \vec{r}_N, S_{zN})$$

where $\vec{r}_i$ is the position of electron number i, and S_{zi} its spin in a chosen z-direction, with measurable values $\frac{1}{2}\hbar$ and $-\frac{1}{2}\hbar$. Of course, what answer you get for the wave function will also depend on where the nuclei are, but in this section, the nuclei are supposed to be at given positions, so to reduce the clutter, the dependence of the electron wave function on the nuclear positions will not be explicitly shown.

Hartree-Fock approximates the wave function in terms of a set of single-electron functions, each a product of a spatial function and a spin state where $\updownarrow$ stands for either spin-up, $\uparrow$, or

spin-down, $\downarrow$. (By definition, function $\uparrow(S_z)$ equals one if the spin S_z is $\frac{1}{2}\hbar$, and zero if it is $-\frac{1}{2}\hbar$, while function $\downarrow(S_z)$ equals zero if S_z is $\frac{1}{2}\hbar$ and one if it is $-\frac{1}{2}\hbar$.) These single-electron functions are called "orbitals" or "spin orbitals." The reason is that you tend to think of them as describing a single electron being in orbit around the nuclei with a particular spin. Wrong, of course: the electrons do not have reasonably defined positions on these scales. But you do tend to think of them that way anyway.

The spin orbitals are taken to be an orthonormal set. Note that any two spin orbitals are automatically orthogonal if they have opposite spins: spin states are orthonormal so $\langle\uparrow|\downarrow\rangle = 0$. If they have the same spin, their spatial orbitals will need to be orthogonal.

Single-electron functions can be combined into multi-electron functions by forming products of them of the form

where n_1 is the number of the single-electron function used for electron 1, n_2 the number of the single-electron function used for electron 2, and so on, and $a_{n_1,n_2,\ldots,n_I}$ is a suitable numerical constant. Such a product wave function is called a "Hartree product."

2.3.2 Electron states at surfaces

Electronic surface states were first postulated by Tamm based on a crude one dimensional model. The solid was represented as a one-dimensional potential well with a periodic potential in the form of positive delta-functions. The general solutions for that potential are plane waves. Shockley considered a more realistic, yet still one-dimensional potential and Bloch-wave solutions . Shockley showed that the surface states found by Tamm were due to an incompleteness of the potential at the surface, i.e. due to a surface potential that was altered compared to the bulk. In the later literature, the distinction between surface states caused by a changed potential vs. surface states caused by the finiteness of the lattice was frequently made by referring to "**Tamm-states**" and "**Shockley states**", respectively. Some authors also refer to Tamm-states and Shockley-states in the sense that the former should be localized, tight-binding type surface states and the latter free-electron type surface states, a distinction that has little foundation in the original work of Tamm and Shockley. Early experimental evidence for the existence of surface states came from the electric properties of space charge layers at semiconductor surfaces. A high density of surface states pins the Fermi-level at the surface to a fixed position with respect to the valence and conduction band edges.

2.4 Work function

The work function is the energy, typically a few electronvolts, required to move an electron from the Fermi Level, E_F, to the vacuum level, E_0, as shown in figure below

The **work function**, ϕ, depends on the crystal face hkl and rough surfaces typically have lower ϕ. **Electron affinity**, χ, and **ionization potential** Φ would be the same for a metal, and equal to ϕ. The electron affinity χ is the difference between the vacuum level E_0, and the bottom of the conduction band E_C, as shown in figure above. The ionization potential Φ is E_0-E_V, where E_V is the top of the valence band. These terms are not specific to surfaces: they are also used for

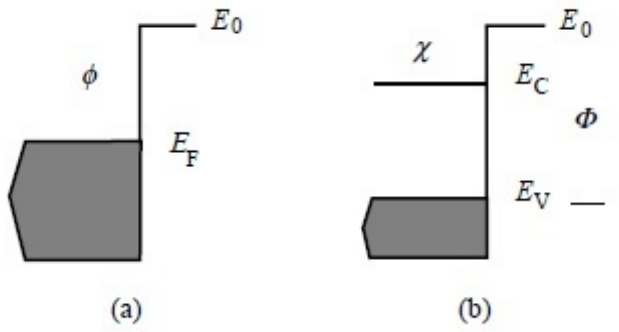

Figure 2.1: Schematic diagrams of (a) the work function ϕ; (b) the electron affinity χ and ionization potential Φ, both in relation to the vacuum level E_0, the Fermi energy E_F, and conduction and valence band edges E_C and E_V.

atoms and molecules generally, as the energy level which (a) the next electron goes into, and (b) the last electron comes from.

2.4.1 Contact potential

When two metals are electrically isolated from each other, an arbitrary potential difference may exist between them. However, when two different metals are brought into contact, electrons will flow from the metal with a lower work function to the metal with the higher work function until the electrochemical potential of the electrons in the bulk of both phases are equal. The actual numbers of electrons that passes between the two phases is small, and the occupancy of the Fermi levels is practically unaffected. In the case of semiconductors, the space charge give rise to a **contact potential difference** between the two sides of the junction. The presence of the contact potential difference makes possible the smooth transition of the Fermi level from its position near the acceptor level on the p side to its position near the donor level on the n side. This is the reason why the contact potential difference if often called *band bending*. It leads to a reduction in the electron affinity. Some materials (e.g. Cs/p-type GaAs) can even be activated to negative electron affinity, and such materials form a potent source of electrons, which can also be spin-polarized as a result of the band structure.

2.4.2 Work function in semiconductors and dielectrics

The work function is the minimum energy that must be given to an electron to liberate it from the surface of a particular substance. In the **photoelectric effect**, electron excitation is achieved by absorption of a photon. If the photon's energy is greater than the substance's work function, photoelectric emission occurs and the electron is liberated from the surface. Excess photon energy results in a liberated electron with non-zero kinetic energy. The work function is also important in the theory of **thermionic emission**. Here the electron gains its energy from heat rather than photons. According to the Richardson-Dushman equation the emitted electron current density.

2.4.3 Work function measuring techniques

A related method for determining the zero-electric-field condition between two parallel plates is by measuring directly the tendency for charge to flow as a result of *changing* the work function of one of the surfaces such as might occur during adsorption. In this static method, called **static capacitor**, the tendency for charge to flow through the external circuit is detected electronically and used to establish very quickly the correct value for the compensating potential.
In the **vibrating capacitor method** (Kelvin-Zisman) the contact potential difference between two metal connected electrically is just equal to the difference in their respective work functions. The contact potential difference arises from the transfer of electrons from the metal of lower work function to the second mater until their Fermi levels line up. If the two metals are arranged as two plates of a capacitor, then in the absence of an applied electric field, an electric field appears in the region between plates. By the application of a compensating potential, the field between the plates can be reduced to zero. In other words, the applied potential necessary to reduce the electric field is just equal to the contact potential difference.

2.4.4 Change of work function with temperature

For metals the work function has a linear relation with the temperature change:

$$\phi(T) = \phi(T_0) + \alpha(T - T_0), \tag{2.10}$$

where α has values between 10^{-4}–10^{-5} eV/K. For semiconductors and insulators the chemical potential varies strongly with temperature:

$$\phi(T) = E_{\mathrm{af}} + \frac{E_{\mathrm{g}}}{2} + \frac{kT}{2} \ln \frac{N_{\mathrm{c}}}{N_{\mathrm{v}}}, \tag{2.11}$$

where E_{g} is the band gap, E_{af} is the electron affinity, N_{c} a N_{v} are the densities of the conduction and valence band.
For n-type semiconductors at lower ionisations:

$$\phi(T) = E_{\mathrm{af}} + \frac{\Delta E_{\mathrm{D}}}{2} + \frac{kT}{2} \ln \frac{N_{\mathrm{c}}}{N_{\mathrm{D}}}, \tag{2.12}$$

where ΔE_{D} is the activation energy and N_{D} is the density of the donor states. At high temperatures it is change to:

$$\phi(T) = E_{\mathrm{af}} + \frac{kT}{2} \ln \frac{N_{\mathrm{c}}}{N_{\mathrm{D}}}. \tag{2.13}$$

In the case of p-type semiconductors:

$$\phi(T) = E_{\mathrm{af}} + E_{\mathrm{g}} - \frac{\Delta E_{\mathrm{A}}}{2} - \frac{kT}{2} \ln \frac{N_{\mathrm{v}}}{N_{\mathrm{A}}} \tag{2.14}$$

and

$$\phi(T) = E_{\mathrm{af}} + E_{\mathrm{g}} - \frac{kT}{2} \ln \frac{N_{\mathrm{v}}}{N_{\mathrm{A}}}. \tag{2.15}$$

2.4.5 Change of work function with electrical field

The work function is actually the binding energy of an electron to a metal surface. Neglecting the external electric field, this is work:

$$\phi = \frac{e^2}{(4\pi\varepsilon_0)4\alpha^2} \tag{2.16}$$

against the attractive image force (between the electron and its mirror image inside metal)

$$\phi = \frac{e^2}{(4\pi\varepsilon_0)(2r)^2} \tag{2.17}$$

Here, α is a typical interatomic distance in metal. In the presence of an external electric field E, extracting electrons from cathode, the total electric field applied to the electron can be expressed as a function of it‘s distance from the metal surface:

$$F_0 = \frac{e^2}{16\pi\varepsilon_0 x^2} - eE \tag{2.18}$$

As can be seen, the extraction takes place if electron distance from the metal exceeds the critical one: $r_{cr} = \sqrt{e/16\pi\varepsilon_0 E}$ when attraction to the surface is changed to repulsion. Thus, the work function can be calculated as the integral:

$$\phi \;=\; \int_a^{r_{cr}} F(r)dr \approx \frac{e^2}{16\pi\varepsilon_0\alpha} - \frac{1}{\sqrt{4\pi\varepsilon_0}} e^{3/2}\sqrt{E} \tag{2.19}$$

The **Schottky relation** above returns in the absence of electric field $E = 0$ to the previously mentioned expression $W = W_0$ for the work function. For practical calculation of the work function decrease in an external electric field, the Schottky relation can be rewritten in the following numerical way:

$$\phi, eV = \phi_o - 3.8 \cdot 10^{-4} \cdot \sqrt{E, V/cm} \tag{2.20}$$

The decrease of the work function is relatively small at reasonable values of electric field.However, the Schottky effect can result in a major change of the thermionic current because of it‘s strong exponential dependence on the work function in accordance with the Sommerfeld formula.

2.5 Thermionic emission

The **Richardson – Dushman equation**, dating from 1923, describes the current density emitted by a heated filament, as

$$J(T) = AT^2 exp(-\phi/kT) \tag{2.21}$$

so that a plot of $\log(J/T^2)$ versus $1/T$ yields a straight line whose negative slope gives the work function ϕ. This value of ϕ is referred to as the "Richardson" work function, since there is an intrinsic temperature dependence of the work function, whose value $\mathrm{d}\phi/\mathrm{d}T$ is of order 10^{-4} to 10^{-3} eV/K, with both positive and negative signs (Hölzl and Schulte 1979). When data is taken over a limited range of T, this temperature dependence will not show up on such a plot, but

will modify the pre-exponential constant. This constant, A, can be measured in principle, but is complicated in practice by the need to know the emitting area independently, since what is usually measured is the emission current I rather than the current density, J. The form of this equation can be derived readily from the free electron model, by considering the Fermi function, and integrating over all those electrons, moving towards the surface, whose "perpendicular energy " is enough to overcome the work function. In this calculation, ignoring reflection at the surface by low energy electrons, the value of A is $4\pi mk^2e/h^3 = 120A/cm^2/K^2$. Where absolute values of current densities have been measured, values of this order of magnitude have been found.

2.5.1 Comparison of the various measuring techniques

The measurement of surface work function means determination of the energy difference between the Fermi level and the top of the potential energy barrier. We expect to measure different apparent values of ϕ by various techniques due to changes in the barrier height, band structure effects, reflection problems and so forth. For example, the Schottky effect must be corrected for in thermionic emission measurements, and thermal effects must be considered in the field emission and photoemission measurements. Emission measurements on a polycrystalline surface will yield geometrically weighted average values.
For a single crystal surface, the capacitance methods of work function measurement should yield true values of contact potential difference between the sample under study and the reference surface. These methods do not depend upon detailed knowledge of electron emission mechanisms, nor are they affected by surface reflection of slow electrons or other similar properties. They simply measure the difference in surface potential between two electrodes whose Fermi energies are equalized. Because this type of measurement is usually made at room temperature, thermal effects are generally not serious. There is a major drawback, however, in these methods. The work function of the reference surface must be precisely known id absolute determination of the sample work function is to be made, Even when only relative changes are to be measured, as in adsorption experiments, the reference surface work function must be stable, either unaffected by adsorption or cleanable before each measurement.
The various emission techniques depend upon precise knowledge of the emission mechanism involved. The theories of thermionic emission, field emission and photoemission are based upon idealized models and do not take into account the detailed band structure in the region of the Fermi level (field emission) or near the top of the emission barrier (thermionic emission and photoemission). The emission may correspond exactly with the theory only in the free-electron limit. Deviation from the free-electron case, as observed to a greater or lesser extent in all metals, can result in an apparent work function greater than the true barrier heigh when measured by emission methods.
The retarding-potential methods have perhaps the broadest applicability of all. A variety of experimental arrangements may be used, including the scanning low-energy probe technique (SLEEP) which can be used to study work function variation over a non uniform surface. When the field emission retarding potential (FERP) technique is used, absolute work function values may be determined. IN general, the emission properties of the electron source may be checked independently to verify cleanliness, but , to first order, this is unnecessary in the FERP case.

2.6 Chemisorption and physisorption

A qualitative distinction is usually made between chemisorption and physisorption, in terms of the relative binding strengths and mechanisms. In **chemisorption**, a strong "chemical bond " is formed between the adsorbate atom or molecule and the substrate. In this case, the adsorption energy, E_a, of the adatom is likely to be a good fraction of the sublimation energy of the substrate, and it could be more. It was found that in a nearest neighbour pair bond model, $E_a = 2eV$ for an adatom on an FCC (100) surface when the sublimation energy $L_0 = 3eV$. In that case the atoms of the substrate and the "adsorbate" were the same, but the calculation of the adsorption stay time, τ_a, would have been valid if they had been different. Energies of 1 – 10 eV/atom are typical of chemisorption.

Physisorption is weaker, and no chemical interaction in the usual sense is present. But if there were no attractive interaction, then the atom would not stay on the surface for any measurable time – it would simply bounce back into the vapor. In physisorption, the energy of interaction is largely due to the (physical) van der Waals force. This force arises from fluctuating dipole (and higher order) moments on the interacting adsorbate and substrate, and is present between closed-shell systems. Typical systems are rare gases or small molecules on layer compounds or metals, with experiments performed below room temperature. Physisorption energies are 50 – 500 meV/atom; as they are small, they can be expressed in kelvin per atom, via $1eV \equiv 11604K$, omitting Boltzmann's constant in the corresponding equations. These energies are comparable to the sublimation energies of rare gas solids.

Adsorption of reactive molecules may proceed in two stages, acting either in series or as alternatives. A first, precursor, stage has all the characteristics of physisorption, but the resulting state is metastable. In this state the molecule may reevaporate, or it may stay on the surface long enough to transform irreversibly into a chemisorbed state. This second stage is rather dramatic, usually resulting in splitting the molecule and adsorbing the individual atoms: dissociative chemisorption. The adsorption energies for the precursor phase are similar to physisorption of rare gases, but may contain additional contributions from the dipole, quadrupole, and higher moments, and from the anisotropic shape and polarizability of the molecules. The dissociation stage can be explosive-literally. The heat of adsorption is given up suddenly, and can be imparted to the resulting adatoms.

The material in the adsorbed state is called **adsorbate**. The substance to be adsorbed (before it is on the surface) is called the **adsorpt** or **adsorptive**. The substance, onto which adsorption takes place, is the **adsorbent**.

Density of the molecules hitting the surface:

$$j = \frac{p}{\sqrt{2\pi kTm}}, \tag{2.22}$$

where p is gas pressure. At normal conditions (atmospheric pressure and room temperature) it falls 1 cm^2 at about 10^{24} molecules per second, at 10^{-4} Pa is in order 10^{15}, which is approximatively the number of atoms in the surface layer.An important question is how much of a material is adsorbed to an interface. This is described by the adsorption function $\Gamma = f(P,T)$, which is determined experimentally. It indicates the number of adsorbed moles per unit area. In general, it depends on the temperature. A graph of Γ versus P at constant temperature is called an adsorption isotherm.

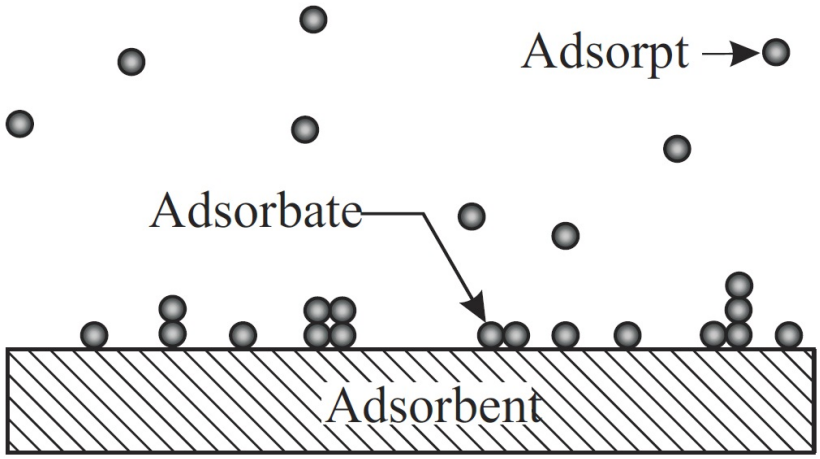

Figure 2.2: Schematics diagram - explanation of terms: adsorbate, adsorbent and adsorpt.

For a better understanding of adsorption and to predict the amount adsorbed, adsorption isotherm equations are derived. They depend on the specific theoretical model used. For some complicated models the equation might not even be an analytical expression.

Table 2.1: Adsorption coefficient for oxygen

material	(111)	(100)
Si	10^{-1}	10^{-2}
Ge	10^{-3}–10^{-4}	10^{-3}
InSb	10^{-5}	–

A useful parameter to characterize adsorption is the adsorption time. Let us first assume that no forces act between the surface and a gas molecule. Then, if a molecule hits the surface, it is reflected elastically with the same energy. An energy transfer between the surface and gas molecule does not take place. As a consequence "hot" molecules do not cool down even when they hit a cold surface. The residence time in proximity to the surface can be estimated by:

$$\tau = \frac{2\Delta x}{\bar{v}_x} \approx \frac{2\Delta x}{\sqrt{k_b T/m}}, \tag{2.23}$$

where Δx is the thickness of the surface region and $\bar{v}_x$ is the mean velocity normal to the surface.

An attractive force between the gas molecule and the surface increases the average residence time of the molecule at the surface to

$$\tau = \tau_0 \ \exp(E_\mathrm{a}/kT), \tag{2.24}$$

Where τ_0 is the bond vibration frequency and E_a is the heat of adsorption.

Another useful parameter is the accommodation coefficient α. The accommodation coefficient is defined by the temperature of the molecules before the impact T_1, the surface temperature T_2, and the temperature of the reflected molecules T_3

$$\alpha = \frac{T_3 - T_1}{T_2 - T_1} \tag{2.25}$$

For an elastic reflection, the mean velocity of the molecules before and after hitting the surface are identical and so are the temperatures: $T_1 = T_3$. Then $\alpha = 0$. If the molecules reside a long time on the surface they have the same temperature, after desorption, as the surface: $T_2 = T_3$ and $\alpha = 1$. Thus, the accommodation coefficient is a measure of how much energy is exchanged before a molecule leaves the adsorbent again.

2.7 Diffusion at surfaces

Diffusion phenomena at surfaces range from the random walk of single atoms to mass transport on macroscopic length scales which involves hundreds, even thousands of different individual processes with merely a few of them being rate determining. Their nature remains frequently unknown. A theoretical description of diffusive mass transport has to take the various length scales and the different levels of knowledge into account.

One of the most direct applications of the field emission microscopy is the study of adsorbate diffusion on clean metal surfaces as a function of surface coverage. The usual method relies on observing changes in the intensity of a well-defined temperature T. To minimize the possibility of the electric field affecting the measurement, diffusion is usually initiated at elevated temperatures in the absence of a field.

Gomer (1953) demonstrated that three distinct types of diffusion could occur for hydrogen and oxygen in tungsten. The particular type of diffusion depends on the morphology of the surface. If more than a monolayer of adsorbate was deposited, uniform diffusion with a sharp boundary was observed below 20 K for hydrogen and below 30 K for Oxygen. Gomer explained the observations by assuming that mobile physisorbed layer was diffusing on top of an immobile chemisorbed layer. When the molecules in the physisorbed layer reached the edge of the chemisorbed layer, they precipitated onto the clean surface, where they chemisorbed, thereby extending the sharp boundary. Gomer characterized this type of diffusion by an average diffusion constant

$$D = \frac{\bar{x}^2}{t} \tag{2.26}$$

where $\bar{x}$ is the average distance traversed by the boundary at the time t. He calculated an activation energy for diffusion by assuming a diffusion coefficient of the form

$$D = A^2 \nu \exp(-E_d/kT) \tag{2.27}$$

where $\nu \approx 10^{12} s^{-1}$ and $A \approx 0.3$.

2.8 Surface relaxation and reconstruction

An ideal crystal is characterized by a regular arrangement of its constituent atoms. Its microscopic structures possesses a three-dimensional translation invariance which mean that a crystal can be constructed by an infinite repetition or a unit cell along three independent directions, A surface eliminates this invariance along one of the directions. It retains a symmetry with respect to two-dimensional translation along the surface itself.
Upon crystal cleavage the surface atomic layer, as well a few adjacent layers, have a different local environment compared with the atomic layers deep inside the crystal. The forces from the atoms in the crystal interior acting on the surface atoms are no longer compensated by the removed part of the crystal. As a consequence, the net force applied to the surface atoms tends to rearrange their equilibrium positions. The possible types of surface rearrangements fall into two main classes. A modifications if the distances between the atomic planes near the surface is called **relaxation**. It is not accompanied by changes in the topmost surface layer structure compared with the structure in the bulk. Under a surface **reconstruction**, however, the surface atoms are shifted along the surface with respect to their positions in the bulk. As a result, the surface unit cell differs from the one which would exist if there were no displacements of the surface atoms.
Silicon, with a diamond-like FCC structure, usually cleaves along (111) and (100) planes. If the surface is (100), the as-cleaved surface without lateral relaxation has a 2×2 square unit cell, and each atom has two dangling bonds from diamond structures. After relaxation, two neighbouring Si atoms reunite with two dangling bonds to form a new bond. Hence, the number of dangling bonds is increased by a factor of 2, leading to a much lower surface energy. Due to the formation of the new bond, two Si atoms form a pair. They are closer to each other than the column of Si atoms on the left or the right side of the pair. Hence, the symmetry of the 2×2 unit cell in not longer held. Instead, the lower energy surface plane has reconstructed itself into a 2×1 symmetry with full and empty columns of atoms alternating with each other.

2.9 Preparation of Clean Surfaces

To prepare crystalline surfaces, usually the starting material is a suitable, pure, three-dimensional single crystal. From this crystal, a slice of the desired orientation is cut. Therefore the crystal must be oriented. Orientation is measured by X-ray diffraction. Hard materials are then grounded and polished. Soft materials are cleaned chemically or electrochemically. The surfaces are still mechanically stressed, contaminated, or chemically changed, e.g. oxidized. In principle, electrochemical processes in liquid can be used to generate clean crystalline surfaces. The problem is that an electrochemical setup is not compatible with an UHV environment. There are, however, combined ultrahigh vacuum/electrochemistry instruments (UHV-EC), where the transfer of electrochemically treated samples into the UHV chamber without contact to air, is possible. Still the sample surfaces may undergo structural or compositional changes during the transfer. Usually in situ methods of surface preparation are preferred that can be applied within the UHV chamber.

2.9.1 Thermal desorption

Heating of the material may cause desorption of weakly bound species from the surface and can therefore be used to clean surfaces. A positive side effect is that annealing reduces the number of surface defects since it increases the diffusion rates of surface and bulk atoms. There can also be some unwanted side effects: surface melting and other types of phase transitions may occur well below the bulk melting point, leading to other than the desired surface structure

$$v_{\mathrm{des}} = n_{\mathrm{s}} \frac{1}{\tau_0} exp(-\frac{Q_{\mathrm{ads}}}{kT}), \tag{2.28}$$

where n_{s} is the surface concentration of the adsorbed species,τ_0 is the oscillation, Q_{ads} is adsorption energy and T is the temperature. For each system is possible to determine the temperature necessary for a perfect cleaning of the surface from the adsorbed species. The thermal desorption can be done:

1. current flow
2. radiation
3. electron bombardment

There are also some advantages of this method: the simplicity and the efficiency.
Some disadvantage are:

- high temperature required ($\geq$ 1000 K),
- slow and prolonged heating can cause diffusion of impurities,
- sample stoichiometry can be altered,
- cannot remove particles (dirt).

2.9.2 Cleavage

Cleavage of bulk crystals to expose clean, defined lattice planes is possible for brittle substances. Some materials, like mica or highly oriented pyrolytic graphite (HOPG) that exhibit a layered structure, are readily cleaved by just peeling off some layers or using a razor blade. For other materials the so-called "double-wedge technique " can be used. Cleavage is a quick way to produce fresh surfaces from brittle or layered materials. There are, however, limitations: Cleavage may produce metastable surface configurations that are different from the equilibrium structure. Depending on the material, only certain cleavage planes can be realised. Crystals usually cleave along non-polar faces, so that positive and negative charges compensate within the surface. GaAs, for example, can only be cleaved along the non-polar 110 planes, whereas the polar 100 and 111 faces cannot be obtained.

2.9.3 Sputtering

A universal method for cleaning surfaces is sputtering. In sputtering the surface is bombarded with noble gas ions. Thereby contaminants – and in most cases the first few layers of the substrate as well – are removed. In sputtering, an inert gas (usually argon) at a pressure of typically 1 Pa is inserted into a vacuum chamber. A high electric field is applied. In any gas and at any given moment a certain number of atoms are ionized (although very few), for example by cosmic background radiation. The electrons which are set free in the ionization process are accelerated in the electric field. They hit and ionize further gas atoms. More electrons are liberated so that eventually a plasma is created. The ions are accelerated by the applied voltage of some kV towards the sample. After sputtering, annealing is often necessary to remove adsorbed or embedded noble gas atoms and to heal defects of the crystal surface created by the bombardment.
Sputtering is an excellent and versatile cleaning technique for elemental materials. Care has to be taken when applying it to composite materials like, e.g., alloys. Sputtering rates will depend on the component and lead to changes in surface stoichiometry. In these cases, cleavage may be the better choice. The necessary annealing process can also be critical and even induce surface contamination. A prominent example is iron, that will usually contain some sulphur that segregates at the surface during annealing. With such materials, consecutive cycles of annealing and sputtering may be required to obtain a clean crystalline surface.

2.9.4 Desorption in strong electric field

The metallic samples in the positive pole. If a strong electric field (10^8 V/cm) is applied, the valence electron level of the adsorbed atom is shifted just above the Fermi level. In this case, it is possible to tunnel electrons into the bulk of the metal. The atom becomes a positive ion, which is repelled by the electrostatic forces. In order to easily use this technique, the adsorbate should be electropositive. If greater electric fields are provided, electronegative atoms can be removed from the surface and also may as well pull out atoms from the sample.

2.9.5 Electron bombardment

If the surface is bombarded by low energy electrons (50-200 eV), the heating is negligible, but the probability that adsorbed species would be excited and thus resulting in a weakly surface bound is increased.

2.9.6 Laser beam

Irradiation with intense pulses of UV laser from an excimer laser can result in clean surfaces. The sample is inserted in a UHV chamber and the laser beam is directed through a window. In this case, the fast heating if the upper surface regions or the explosive evaporation of the uppermost layer, which has been penetrated by the laser, causes the cleaning.
Advantages:

- vacuum conditions, no foreign particles
- only surface heating

Disadvantages:

- ablation of material
- low area cleaned
- high cost

2.9.7 Surface reactions

The organic contaminants can be oxidized using oxygen, some impurities can be converted to volatile compounds by heating in hydrogen atmosphere.

Chapter 3

Interaction of Photons with Matter

3.1 Interaction of general radiation with matter

Interaction of radiation with the matter is necessary in order to characterize the microstructures:

- photons
- electrons
- neutrons
- protons
- ions/atoms

Penetration depth is a measure of how deep light or any electromagnetic radiation can penetrate into a material. It is defined as the depth at which the intensity of the radiation inside the material falls to $1/e$ of its original value at (or more properly, just beneath) the surface. The penetration depth or mean free path of the incident beam determines the depth and volume of material that will be sampled. In many cases, the material is irradiated with one type of radiation but a second type is detected. This occurs in X-ray photoelectron spectroscopy (XPS) where the incident probe is a beam of X-ray photons but emitted electrons are detected, whereas in energy dispersive X-ray (EDX) analysis it is reversed. Generally the particle or radiation which has the shortest mean free path in the material will determine the volume analyzed.

Whatever beam is selected we must be aware of

- its interaction with the material (*loss processes*), i. e. what radiation (photons, electrons etc.) is ejected or other particles are ejected and
- and how the internally ejected radiation interact with the material.

Only in this way we can use the emitted signals to gain an understanding of the material being examined.

Each radiation can cause a specific *material damage* and it has to be considered when selecting the analytical methods.

- **photons**
  Regarded in general as the least harmful, the photons will damage the target nevertheless. Damage can occur by heating the target, which depends on the radiant energy, photon flux and the depth of penetration. Moreover X-rays can induce surface oxidation and lasers can burn holes into material. In general the most photon radiation causes very little damage ⇒ it is used at the beginning of target characterization.

- **electrons**
  Although electrons have a dual nature, their weight leads to a relatively large transfer angular momentum if they are accelerated to several hundreds keVs. The resulted damage depends on the heat transferred and the thermal conductivity of the material. For metals and alloys the damage is minimum, but in polymers and oxides the damage is worse. It is possible to cover the surface with a conductive material (usually gold) but the disadvantage is that the composition can not longer be investigated.

- **ions and atoms**
  When atoms and ions penetrate the target, they can react with it or not cause any damage at all (e.g. Ion Scattering Spectroscopy, where ions interact elastically with the target) or they cause significant damage:

  – ejection of atoms form their normal lattice position

  – breaking the bonds (requires 10x more energy)

  For low ion fluxes the damage areas are isolated (the amorphous material is surrounded by intact one) but for high fluxes, the ions create an amorphous layer.

Mean free path determines the depth resolution, which has influence in the spatial one (defined as the perpendicular to the direction of the incident beam). Generally, the *spatial resolution* is influenced by the beam size and the wavelength. The image can be obtain by:

- illumination of the sample and use of lens for focusing the reflected or emitted radiation. The spatial resolution depends on the lens system used and the wavelength of emitted or reflected radiation. Optical, X-ray and some ion microscopes are using this method.

- a narrow beam is directed on the sample and absorbed or reflected radiation is detected. The sample surface is scanned by a narrow beam. In this case the spatial resolution depends in the wavelength, beam size and the scattered radiation in the sample. Most of the equipment are using electrons and ions.
  Nowadays, laser microscopes are used for sample characterization.

3.2 Introduction to photon interactions

Photons are discrete quanta of electromagnetic radiation. The photon is identified by the wavelength λ, energy E, and frequency ν as

$$h\nu = E = hc/\lambda \tag{3.1}$$

where h is the Planck constant and c the velocity if light.

The electromagnetic spectrum spans a vast range with wavelengths varying from 10^6 m down to 10^{-14} m (see Figure 3.1). If we are to use electromagnetic radiation for microstructural characterisation of materials a photon wavelength is needed that is of comparable size to the features being studied $\Rightarrow$ between 10^{-4}–10^{-10} m.

The long wavelength infrared radiation is used to characterise materials by determining how specific wavelengths are absorbed, visible light is used in a variety of instruments mainly to obtain a visual image of the surface while at the shorter wavelength ultraviolet radiation is often used to obtain information concerning the electron distribution in the surface atoms. After visible light, X-rays are probably the most utilized photon source for investigation of material microstructure.

When electromagnetic radiation is incident on the surface of a material, it may be (partly) reflected from that surface and there will be a field containing energy transmitted into the material. This electromagnetic field interacts with the atoms and electrons inside the material. Depending on the nature of the material, the electromagnetic field might travel very far into the material, or may die out very quickly. For a given material, penetration depth will generally be a function of wavelength.

- IR radiation: characterization of materials, which is depending of the absorbed wavelengths;
- VIS radiation: used often to see the surface. Some material are opaque while others are transparent. Even for high reflectivity opaque materials the penetration depth is in order of

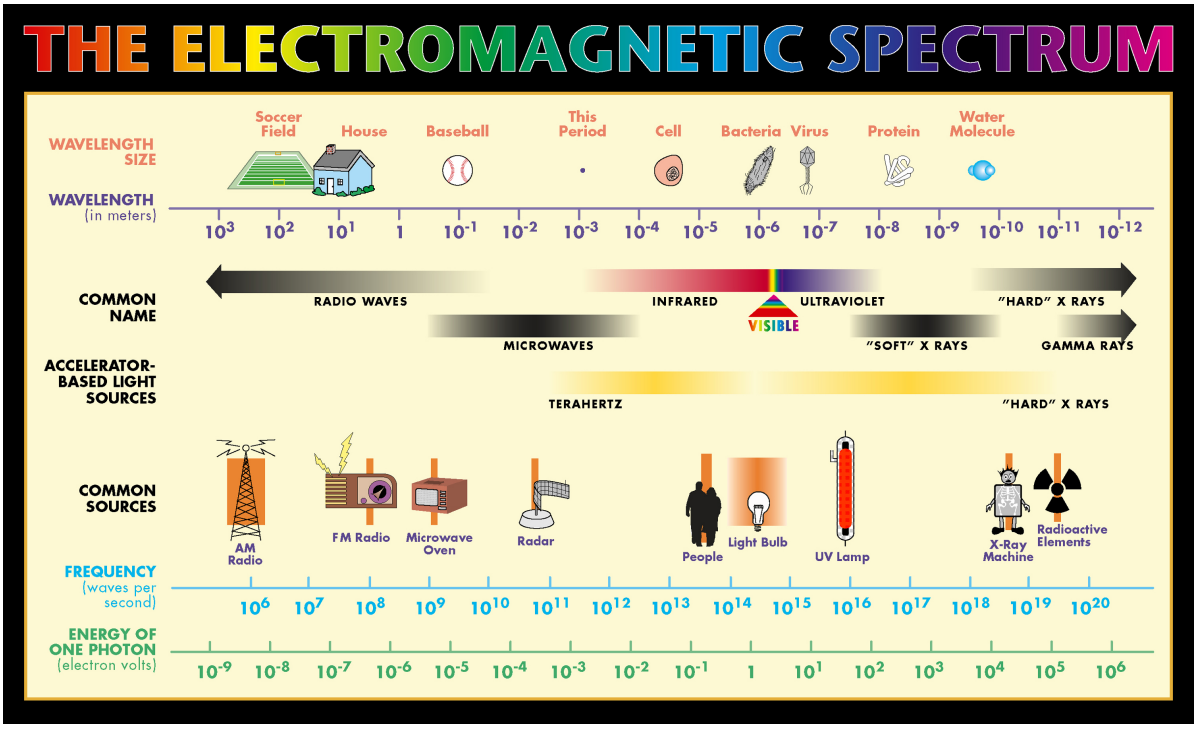

Figure 3.1: The electromagnetic spectrum illustrating the relationship between wavelength, frequency and energy of photons.

50–300 nm.

- UV radiation: reveals information about the electron distribution for surface atoms. Most substances absorb in this region.
- X-ray radiation: X-ray penetration is easier to predict than visible radiation. The penetration depth is typically μm. The intensity of radiation which is transmitted through sample thickness d is
$$I = I_0 \exp(-\alpha d), \tag{3.2}$$
where I_0 is the intensity of incident radiation and α, the **absorbance**, increases with the atomic number.
- Gamma (γ) radiation: has energy between 50 keV–50 MeV $\approx 10^{-2}$ nm. Absorbance is governed by the same relation for X-rays, but here α is inversely proportional with the atomic number. Gamma radiation penetrate almost all the laboratory samples.

3.3 Very short wavelengths ($< 10^{-12}$ m, γ-rays)

The method that uses γ-rays to characterize materials is called *Mössbauer spectroscopy*.

Key to the success of the technique is the discovery of recoilless γ-ray emission and absorption, now referred to as the *Mössbauer effect*, after its discoverer Rudolph Mössbauer, who first observed the effect in 1957 and received the Nobel Prize in Physics in 1961 for his work.

3.3.1 Mössbauer effect

Nuclei in atoms undergo a variety of energy level transitions, often associated with the emission or absorption of a gamma ray. These energy levels are influenced by their surrounding environment, both electronic and magnetic, which can change or split these energy levels. These changes in the energy levels can provide information about the atom's local environment within a system and ought to be observed using resonance-fluorescence. There are, however, two major obstacles in obtaining this information:

- the 'hyperfine' interactions between the nucleus and its environment are extremely smaller,
- the recoil of the nucleus as the gamma-ray is emitted or absorbed prevents resonance.

Just as a gun recoils when a bullet is fired, conservation of momentum requires a free nucleus (such as in a gas) to recoil during emission or absorption of a gamma ray.

- If a nucleus at rest emits a gamma ray, the energy of the gamma ray is slightly less than the natural energy of the transition (difference is equal to the recoil energy E_R),
- but in order for a nucleus at rest to absorb a gamma ray, the gamma ray's energy must be slightly greater than the natural energy.

This means that nuclear resonance (emission and absorption of the same gamma ray by identical nuclei) is unobservable with free nuclei, because the shift in energy is too great and the emission and absorption spectra have no significant overlap.

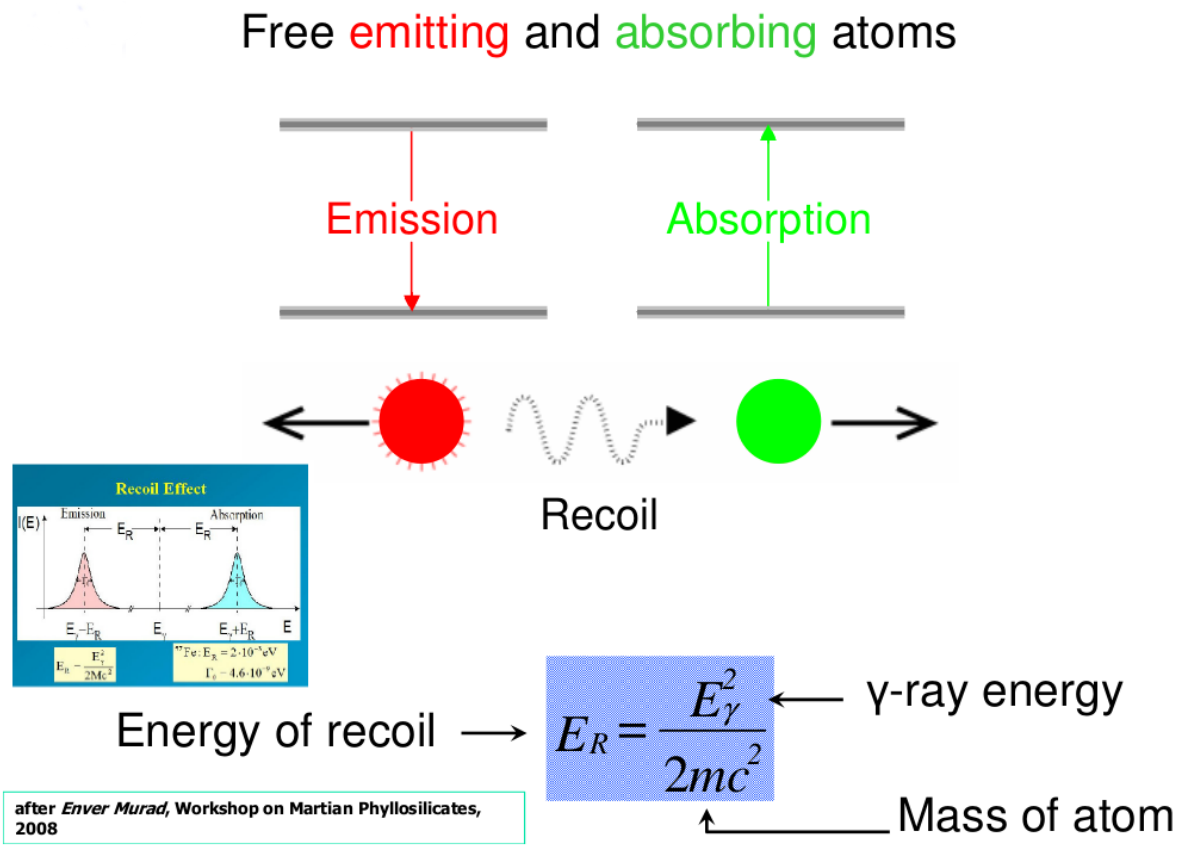

Figure 3.2: Recoil of free nuclei in emission or absorption of a gamma-rays

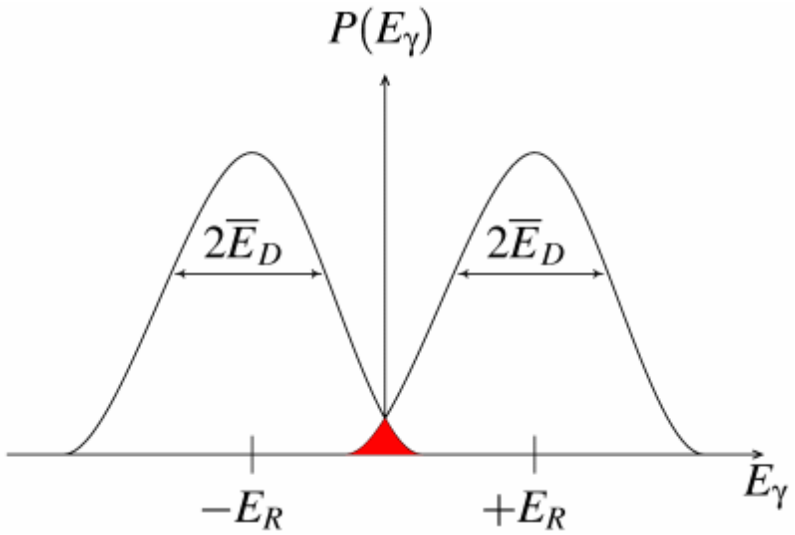

Figure 3.3: Resonant overlap in free atoms. The overlap shown shaded is greatly exaggerated.

In order to achieve resonance in emission and absorption the loss of the recoil energy must be overcome in some way.

Nuclei in a solid crystal are not free to recoil because they are bound in place in the crystal lattice. When a nucleus in a solid emits or absorbs a gamma ray, some energy can still be lost as recoil energy, but in this case it always occurs in discrete packets called phonons (quantized vibrations of the crystal lattice). Any whole number of phonons can be emitted, including zero, which is known as a "recoil-free" event. In this case conservation of momentum is satisfied by the momentum of the crystal as a whole, so practically no energy is lost.

Mössbauer found that a significant fraction of emission and absorption events will be recoil-free, which is quantified using the Lamb–Mössbauer factor. This fact is what makes Mössbauer spectroscopy possible, because it means gamma rays emitted by one nucleus can be resonantly absorbed by a sample containing nuclei of the same isotope, and this absorption can be measured.

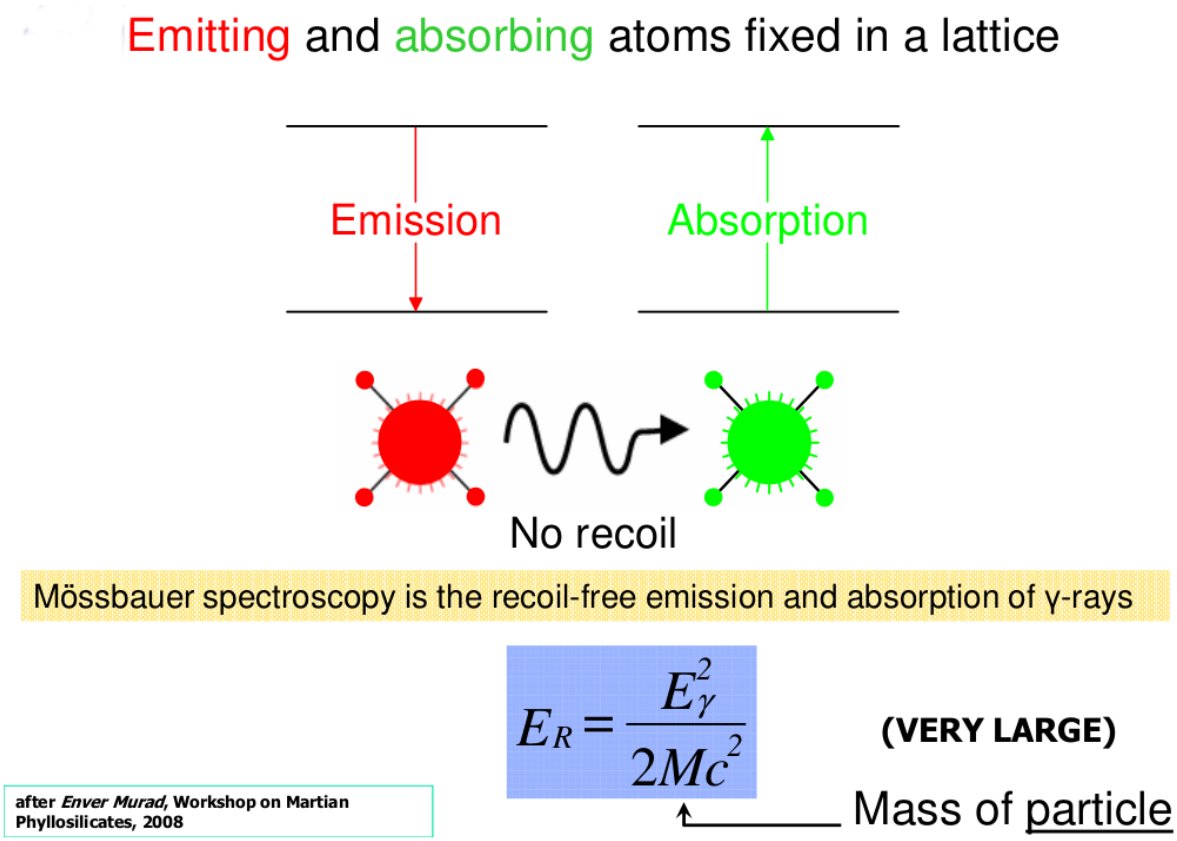

Figure 3.4: Atoms fixed in lattice.

In its most common form, Mössbauer absorption spectroscopy,

- a solid sample is exposed to a beam of gamma radiation,
- and a detector measures the intensity of the beam transmitted through the sample.

The atoms in the source emitting the gamma rays must be of the same isotope as the atoms in the sample absorbing them.

If the emitting and absorbing nuclei were in identical chemical environments, the nuclear transition energies would be exactly equal and resonant absorption would be observed with both materials at rest. *The difference in chemical environments, however, causes the nuclear energy levels to shift in a few different ways.* Although these energy shifts are tiny (often less than a micro-electronvolt), the extremely narrow spectral linewidths of gamma rays for some radionuclides make the small energy shifts correspond to large changes in absorbance. To bring the two nuclei back into resonance it is necessary *to change the energy of the gamma ray slightly*, and in practice this is always done using the *Doppler effect.*

During Mössbauer absorption spectroscopy, the source is accelerated through a range of velocities using a linear motor to produce a Doppler effect and scan the gamma ray energy through a given range. A typical range of velocities for 57Fe, for example, may be ±11 mm/s (1 mm/s = 48.075 neV).

In the resulting spectra, gamma ray intensity is plotted as a function of the source velocity. At velocities corresponding to the resonant energy levels of the sample, a fraction of the gamma rays are absorbed, resulting in a drop in the measured intensity and a corresponding dip in the spectrum. The number, positions, and intensities of the dips (also called peaks; dips in transmitted intensity are peaks in absorbance) provide information about the chemical environment of the absorbing nuclei and can be used to characterize the sample.

Mössbauer spectroscopy is limited by the need for a suitable gamma-ray source. Usually, this consists of a radioactive parent that decays to the desired isotope. For example,

- the source for 57Fe consists of 57Co, which decays by electron capture to an excited state of 57Fe,
- then subsequently decays to a ground state emitting the desired gamma-ray.
- The radioactive cobalt is prepared on a foil, often of rhodium.

Ideally the parent isotope will have a sufficiently long half-life to remain useful, but will also have a sufficient decay rate to supply the required intensity of radiation.

Mössbauer spectroscopy has an extremely fine energy resolution and can detect even subtle changes in the nuclear environment of the relevant atoms. Typically, there are three types of nuclear interactions that are observed

- isomer shift (or chemical shift) - is a relative measure describing a shift in the resonance energy of a nucleus due to the transition of electrons within its s orbital. The whole spectrum is shifted in either a positive or negative direction depending upon the s electron charge density. This change arises due to alterations in the electrostatic response between the non-zero probability s orbital electrons and the non-zero volume nucleus they orbit.

- quadrupole splitting - reflects the interaction between the nuclear energy levels and surrounding electric field gradient (EFG). Nuclei in states with non-spherical charge distributions, i.e. all those with angular quantum number (I) greater than 1/2, produce an asymmetrical electric field which splits the nuclear energy levels. This produces a nuclear quadrupole moment.

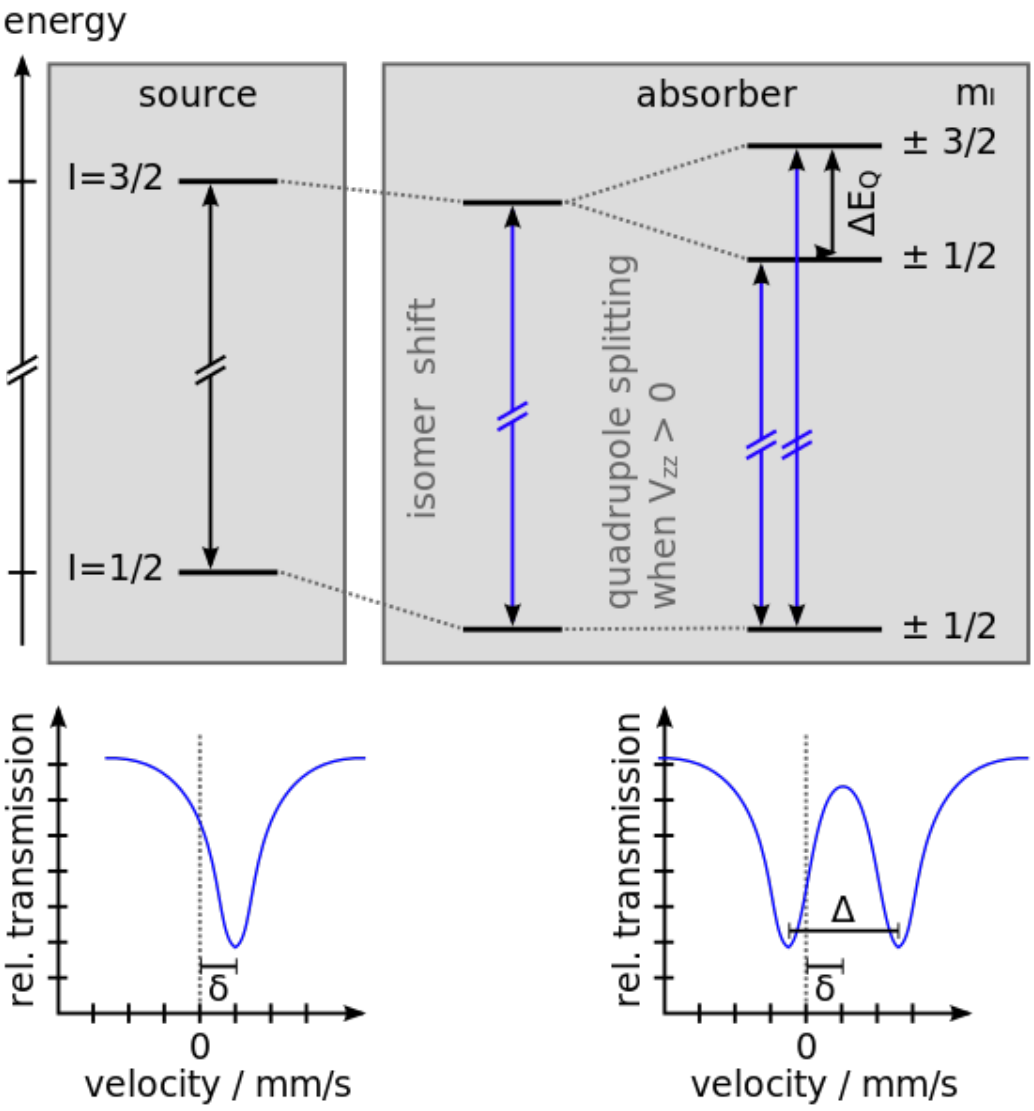

Figure 3.5: Chemical shift and quadrupole splitting of the nuclear energy levels and corresponding Mössbauer spectra

- hyperfine splitting (or Zeeman splitting) - is a result of the interaction between the nucleus any surrounding magnetic field. A nucleus with spin, I, splits into 2I + 1 sub-energy levels in the presence of magnetic field. For example, a nucleus with spin state I= 3/2 will split into 4 non-degenerate sub-states with mI values of +3/2, +1/2, -1/2 and −3/2. Each split is hyperfine, being in the order of 10^{-7}eV. The restriction rule of magnetic dipoles means that transitions between the excited state and ground state can only occur where mI changes by 0 or 1. This gives six possible transitions for a 3/2 to 1/2 transition.

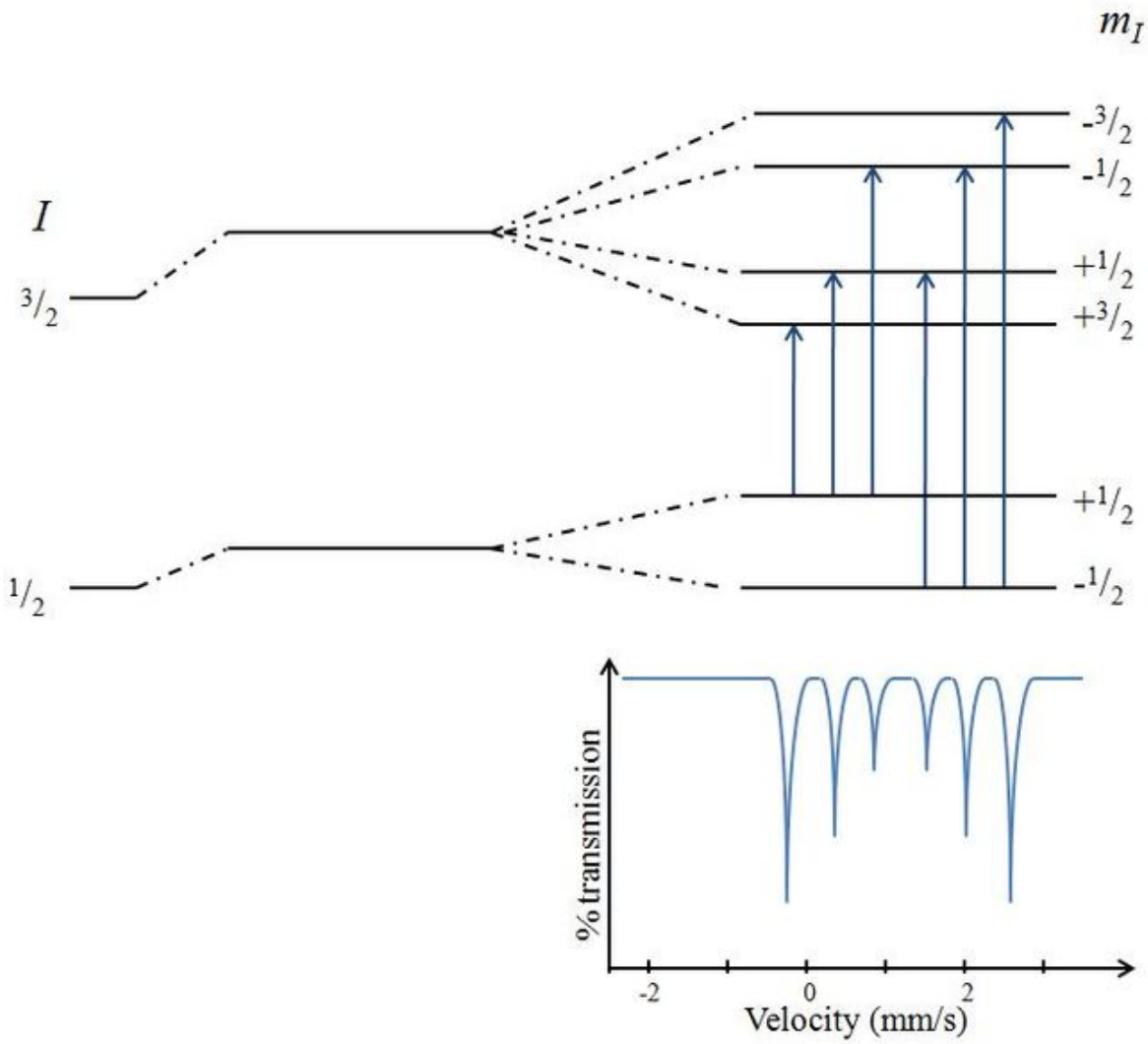

Figure 3.6: Magnetic splitting of the nuclear energy levels and the corresponding Mössbauer spectrum

3.4 Short wavelengths (10^{-12} to 10^{-9} m, including X-rays and ultraviolet)

If photon has enough energy to excite electron to high energy levels, two effects can occur:

- **internal photoeffect** (e.g. photoconductivity)
- **external photoeffect** or the photoemission.

The kinetic energy is:

$$\frac{1}{2}mv^2 = E_{\mathrm{F}} \pm \delta E - E_{\mathrm{af}} + h\nu - \Delta E. \tag{3.3}$$

At 0 K the kinetic energy is maximum

$$(\frac{1}{2}mv^2)_{\max} = h\nu - (E_{\mathrm{af}} - E_{\mathrm{F}}) = h\nu - \chi = h(\nu - \nu_0), \tag{3.4}$$

where ν_0 is the frequency of photoelectric effect.

In the case of photoemission induced absorption (**X-ray**), the photon has enough energy to excite an electron from some inner layers of solid.

$$\frac{1}{2}mv^2 = h\nu - \chi - E_{\mathrm{B}}, \tag{3.5}$$

where E_{B} is the binding energy of the inner layers. The binding energy is characteristic for each substance, so the kinetic electrons emitted bear information related to the electronic structure and thus, the type of material.

3.4.1 Fowler‘s theory for metal/vacuum interfaces

Fowler proposed a theory in 1931 which showed that the photoelectric current variation with the light frequency could be accounted for by the effect of temperature in the number of electrons available for emission, in accordance with the distribution law of Sommerfeld‘s theory for metals. Sommerfeld‘s theory had resolved some of the problems surrounding the original models for electron in metals. In classical Drude theory, a metal had been envisaged as a three-dimensional potential well (box) containing a gas of freely mobile electrons. This adequately explained their high electrical and thermal conductivities. However, because experimentally it was found that metallic electrons do not show a gas-like heat capacity, the Boltzman distribution law is inappropriate. A Fermi-Dirac distribution function is required, consistent with the need that the electrons obey the Pauli exclusion principle and this distribution function has the form

$$P(E) = \frac{1}{1 + exp[(E - E_F)/kT]} \tag{3.6}$$

At ordinary temperatures, the Fermi energy $E_F \gg kT$. Fowler‘s law, referred to above as the "square law", is readily tested in practice since it predicts at T=0 K

$$i \propto (\nu - \nu_0)^2 \tag{3.7}$$

where ν_0 is the photoelectric threshold frequency and ν refers to a range of energies from threshold to a few kT above threshold. To a good approximation, the photoelectric yield per unit light intensity near ν_0 is proportional simply to the number of electrons incident per unit time. The energy condition can be written

$$(1/2m)p^2 + h\nu > \phi \tag{3.8}$$

where p is the initial momentum of the electron normal to the surface. The escaping electrons have been termed the "available electrons".
Fowler‘s derivation for the single photon does not explicitly involve the quantum mechanical form of current; instead, a semi-classical flux of electrons arriving at the metal surface is used. The electron gas in the metal will obey Fermi-Dirac statistics, and the number of electrons per unit volume having velocity components in the ranges $u, u+du, \nu, \nu+d\nu$ and $w+dw$ is given by the formula

$$n(u,\nu,w)dud\nu dw = 2(\frac{m}{h})^2 \frac{dud\nu dw}{1+exp[\frac{1}{2}m(u^2+\nu^2+w^2)-E_F]/kT} \tag{3.9}$$

where u is the velocity normal to the surface and m is the electron mass. The number of electrons per volume, $n(u)du$, with their velocity component normal to the surface in the range $u, u+du$ is given by:

$$n(u)du = \frac{4\pi kT}{m}(\frac{m}{h})^3 \log[1+\exp(E_F - \frac{1}{2}mu^2)/kT]du \tag{3.10}$$

The solution for the photoelectric current resulted in the form

$$i \propto \frac{(h\nu-\phi)^{3/2}}{(\phi_0-h\nu)^{1/2}}. \tag{3.11}$$

A method for determining the threshold frequency of the illuminated surface ν_0 is that which makes use of the complete photoelectric emission. When a metal surface is exposed to the total thermal radiation from a black body with a temperature T, the total photoelectric current is given by:

$$i = A‘T^2 e^{-\frac{h\nu_0}{kT}} \tag{3.12}$$

were $A‘$ is a constant.

3.4.2 Measurement of the photoelectric work function

- Fowler isotherm: measurement of the photocurrent depending on the frequency of incident radiation at constant temperature, the $\ln i_\mathrm{f}/T^2$ is expressed as $h\nu/kT$ and compared with the theoretical curve

$$\ln\frac{i_\mathrm{f}}{T^2} = \ln(\alpha A_0) + \ln f(x) = B + \Phi[\frac{h}{kT}(\nu-\nu_0)]. \tag{3.13}$$

  From the Fowler equation, giving the relation between temperature and photoelectric emission, ν_0 can be determinate by plotting the $\ln f(\Delta)$ as a function of Δ. A universal curve is obtained. Then $\ln\frac{i}{T^2}$ is plotted against $\frac{h\nu}{kT}$. A curve us obtained of the same shape as the universal curve, which can be made to coincide with it by a parallel shift. The vertical shift is measure of B, the horizontal is equal to $\frac{h\nu_0}{kT}$.

- duBridge isochromatic method: measurements at one frequency ν but different temperatures. For this purpose $\ln f(\Delta)$ is plotted against $\ln|\Delta|$, and again a universal curve is obtained. From the experimental data $\ln i_\mathrm{f}/T^2$ is plotted against $\ln 1/T$. For different frequencies the temperature dependence of the photoemission differs
- for $\nu = \nu_0$ is $i_\mathrm{f} = \alpha A_0 = \pi^2/12T^2$
- for $x \gg 1$; $\nu > \nu_0$, is $f(x) = \pi^2/6 + x^2/2$ and

$$i_\mathrm{f} = \frac{\alpha A_0}{2}\left[\frac{h^2(\nu-\nu_0)^2}{k^2} + \frac{\pi^2}{3}\right], \tag{3.14}$$

  where the parabolic dependence is applied obly when the first term in the brackets is sufficiently small.

- for $x \ll 1$, $\nu < \nu_0$, is $f(x) = e^x$ and

$$i_\mathrm{f} = \alpha A_0 T^2 \exp(-\frac{h(\nu_0-\nu)}{kT}). \tag{3.15}$$

3.4.3 Interaction of excited electrons with matter

The **hot-electron** problem represents the study of the deviations from the linear response regime due to heating of charge carriers above the thermal equilibrium. Studies have been carried out in 1930s, mainly by Russian physicist Landau and Davidov. This means that electron temperature T_e which , in the presence of an external high electric field, is higher that the lattice temperature T.
Nonlinear transport deals with problems that arise when a sufficiently strong electric field is applied to a semiconductor sample, so that the current deviates from the linear response. This effect is typical of semiconductors and cannot be seen on metals since, owing to their large conductivities, Joule heating would destroy the material before deviations from the linearity could be observed.

Considering

$$v^{(i)}(t) = v_0^{(i)} + a\Delta t^{(i)} \tag{3.16}$$

where $v^{(i)}(t)$ is the instantaneous velocity if the i-th electron at time t, $\Delta t^{(i)}$ is the same time elapsed after its last scattering event, and $a = eE/m$ is the electron acceleration, due to a constant and uniform applied electric field E. The region of field strengths where transport starts to deviate from linearity is called **warm-electron region**.

3.4.4 Photoemission from semiconductors

There are some differences when we speak about the photoemission from metals and semiconductors. All high quantum yield photocathodes are semiconductor ones. The absorption of light is affected by:

- internal absorption due to their band gap

- external absorption from the external layer

The Fermi level is influenced by the surface layers and the type of semiconductor used. Electron coming from different depths have different space charge and work function ⇒ as they would have different work function for different photoelectrons excited at different wavelengths.
The density of stated around Fermi level increases strongly and we cannot assume that photon absorption is independent from electron‘s energy state. The quantum yield increases with the temperature faster than in metals.

3.4.5 Photocathode

- IR region: Ag-O-Cs, also called S-1. This was the first compound photocathode material, developed in 1929. Sensitivity from 300 nm to 1200 nm. Since Ag-O-Cs has a higher dark current than more modern materials photomultiplier tubes with this photocathode material are nowadays used only in the infrared region with cooling.

- visible region: Sb-Cs has a spectral response from UV to visible and is mainly used in reflection-mode photocathodes. and also bi-alkali (antimony-rubidium-caesium Sb-Rb-Cs, antimony-potassium-caesium Sb-K-Cs). Spectral response range similar to the Sb-Cs photocathode, but with higher sensitivity and lower dark current than Sb-Cs. They have sensitivity well matched to the most common scintillator materials and so are frequently used for ionizing radiation measurement in scintillation counters.

- UV region: metals and Cs-Te (Cs-I). These materials are sensitive to vacuum UV and UV rays but not to visible light and are therefore referred to as solar blind. Cs-Te is insensitive to wavelengths longer than 320 nm, and Cs-I to those longer than 200 nm.

3.5 Intermediate wavelengths (including visible and ultraviolet light)

- Absorption/emission by isolated atoms - spectroscopy of gaseous samples (ICP used for solid materials)

- Raman and Rayleigh scattering

3.6 Long wavelengths (infrared)

3.7 Very long wavelengths photons ($\geq 1mm$) - including radio and microwaves

All nucleons, that is neutrons and protons, composing any atomic nucleus, have the intrinsic quantum property of spin. The overall spin of the nucleus is determined by the spin quantum

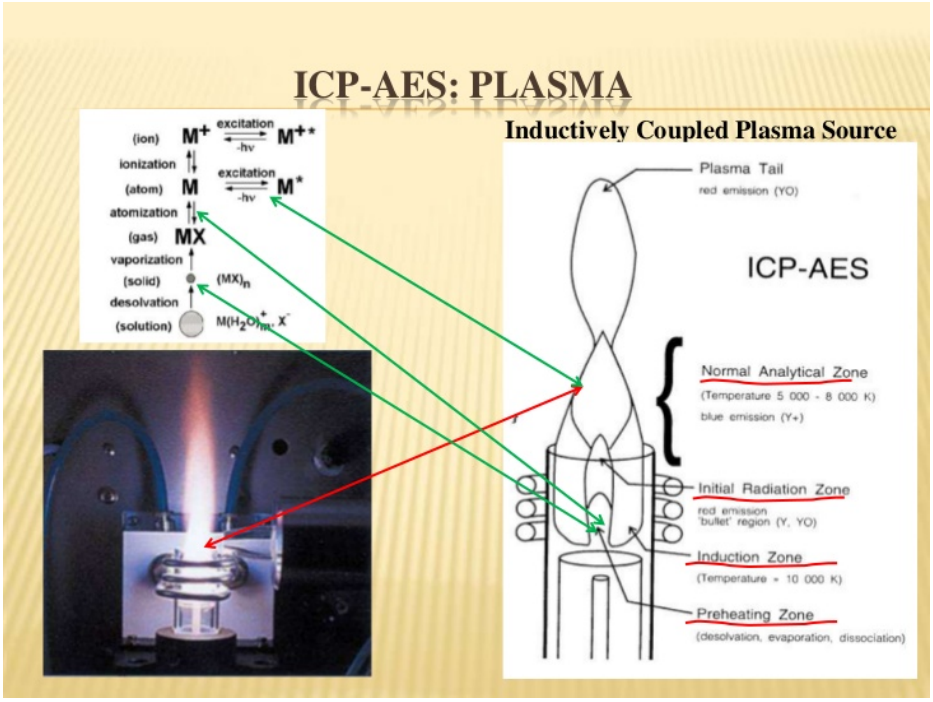

Figure 3.7: Atomic emission spectroscopy in inductively coupled discharge

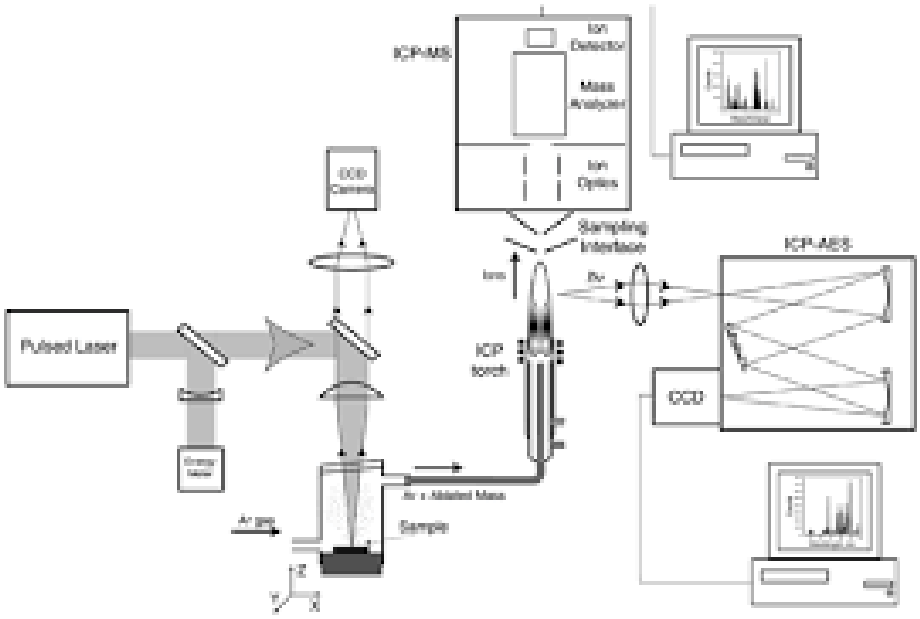

Figure 3.8: AES-ICP with laser ablation

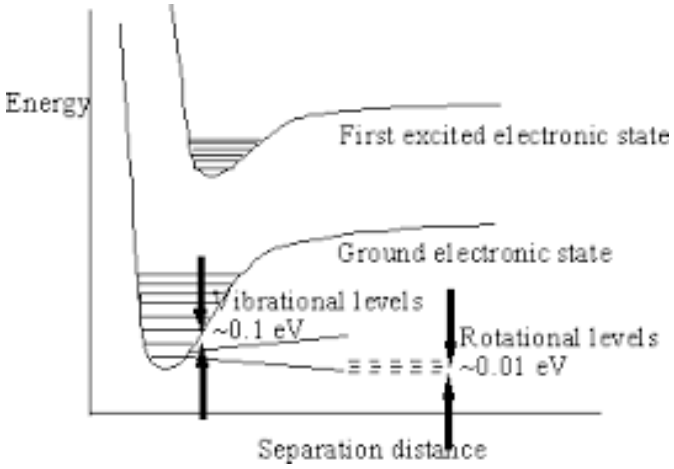

Figure 3.9: Demonstration of different energy levels in molecules.

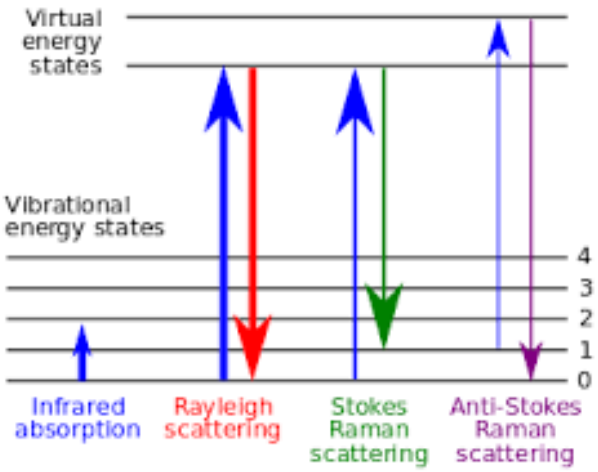

Figure 3.10: Different spectroscopies involving vibrational(-rotational) states.

number I. Some nuclei have integral spins (e. g. $I = 1, 2, 3 \ldots$), some have fractional spins (e.g. $I = 1/2, 3/2, 5/2....$), and a few have no spin, $I = 0$ (e.g. 12C, 16O, 32S, ...). Isotopes of particular interest and use to organic chemists are 1H, 13C, 19F and 31P, all of which have I = 1/2.

A non-zero spin is always associated with a non-zero magnetic moment μ

$$\mu = \gamma S \tag{3.17}$$

where γ is the gyromagnetic ratio.

It is this magnetic moment that allows the observation of nuclear magnetic resonance (NMR) absorption spectra caused by transitions between nuclear spin levels in the presence of external magnetic field (spin states splitting).

`http://www2.chemistry.msu.edu/faculty/reusch/VirtTxtJml/Spectrpy/nmr/nmr1.htm`

Electron spin resonance (ESR) or *electron paramagnetic resonance (EPR)* is a related technique in which transitions between electronic spin levels are detected rather than nuclear ones. The basic principles are similar but the instrumentation, data analysis, and detailed theory are significantly different. Moreover, there is a much smaller number of molecules and materials with unpaired electron spins that exhibit ESR absorption than those that have NMR absorption spectra. ESR has much higher sensitivity than NMR does.

`http://www.uottawa.ca/publications/interscientia/inter.2/spin.html`

`https://en.wikipedia.org/wiki/Electron_paramagnetic_resonance`

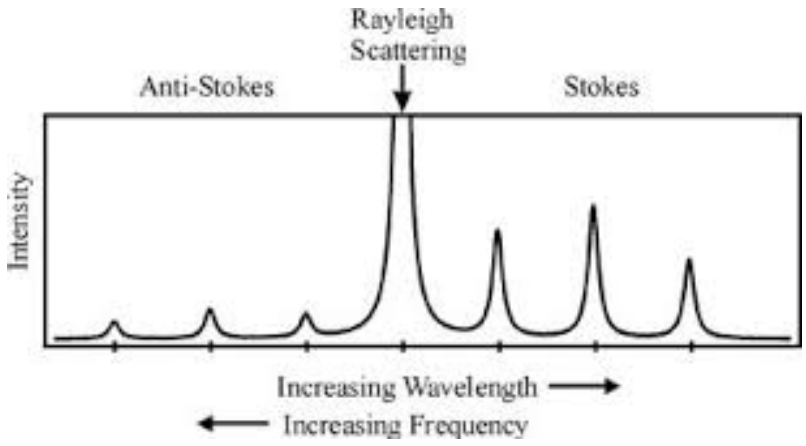

Figure 3.11: Position of peaks in Raman scattering.

Chapter 4

Interaction of Electrons with Matter

4.1 Electron interactions

- desorption of neutral particles
- excitation of photons (x-ray, chatodoluminescence)
- reality of material: cleaning, activation energy for chemical and physical processes, electron lithography
- change of material
- emission of electrons: (a) without interaction, (b) elastic scattering (diffraction on passage), (c) elastic reflection (diffraction on reflection), (d) inelastic reflection (characteristic energy loss), (e) backscatter electron, (f) electron transmission with the possibility to emit others and (g) electron transmission with secondary electron emission.
  When a sample is bombarded with charged particles, the strongest region of the electron energy spectrum is due to secondary electrons. The secondary electron yield depends on many factors, and is generally higher for high atomic number targets, and at higher angles of incidence. There is a lot of information in this secondary electron "background", but, unlike Auger and other electron spectroscopies, it is not directly chemical or surface specific in general.
  Total electron current from a substance is the **current of secondary electrons** on reflection or transmission.

4.2 Penetration depth of electrons

Penetration depth changes significantly with the electron energy and the atomic number of the material:

- for stainless steel: around one tenth of a μm for energy 10 keV and 2 μm for 30 keV,

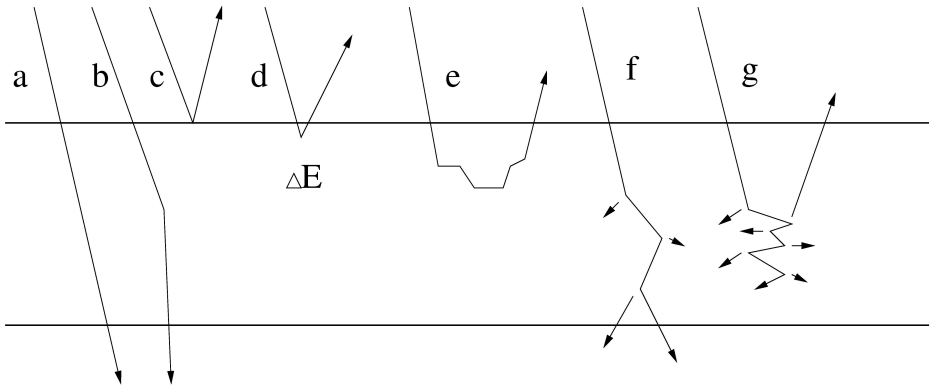

Figure 4.1: Electron interaction with the solid state.

- for energies higher than 10 keV: elements with atomic number under 20 have a penetration depth up to 10 μm while the elements with Z higher than 40 below 2 μm
- for energies between 0–2 keV: the penetration depth is reduces to 0.4–300 nm

4.2.1 Electron emission

The ration between this current I_s and primary I_p is called **secondary emission coefficient** $\sigma = I_\mathrm{s}/I_\mathrm{p}$. By selecting the secondary electrons by their energies we can identify individual interactions:

- the highest maximum of primary energy level $\Rightarrow$ elastic reflection of e^-
  interaction with the atom like a whole, there is no change in energy but, the electron momentum can be changed dramatically. For electron energy higher than ($\geq$ 5 keV)the effect is called Rutherford Backscattering (RBS)

$$\frac{dQ(\theta)}{d\Omega} = \frac{1}{4}\left(\frac{e^2\ (Z - F(\theta))}{4\pi\epsilon_0\ m_\mathrm{red}\ g^2}\right)^2 \frac{1}{\sin^4(\theta/2)}, \tag{4.1}$$

  where $F(\theta)$ is the screening effect of electrons. $F(\theta)$ is insignificant at high angles θ and strong scattering can occur only in heavy atoms (used for TEM contrast). When the target is a crystalline material **diffraction** and **channelling** occurs. When electron scattering from crystal lattice is coherent, amplification in those direction occurs, which is represents **Bragg law**:

$$n\lambda = 2d_\mathrm{hkl}\sin\theta, \tag{4.2}$$

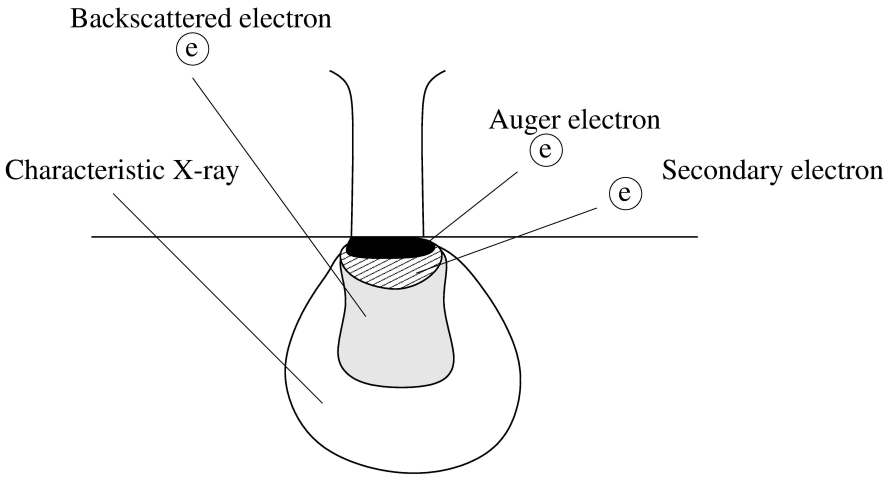

Figure 4.2: Penetration depth for different particles.

where n is a integer d_{hkl} is is the spacing between the planes in the atomic lattice expressed with Miller indexes. This method is used to examine the bulk crystalline structure ($E \approx$ 10 keV) or the surface structure using low-energy electron diffraction (LEED) or very small angle relection in reflection high-energy electron diffraction (RHEED).

- the smaller peaks to the left show the shift in maximum elastic reflection of e^- $\Rightarrow$ electrons which suffer energy losses.
  Electrons undergo a variety of interactions:
- adsorbed molecules are excited on vibrational state $\Delta E \approx$ 50–500 meV;
- individual interaction with valence e^-, $\Delta E \approx$ 3–20 eV but without a sharp peak because the valence band has a width of several eV;
- multiple interactions with the valence e^-which is bombarded by an electron, vibrating with frequency

$$\omega_{\mathrm{p}} = \frac{1}{\epsilon_0} \frac{n_0 e^2}{m} \tag{4.3}$$

for plasmon in volume, or

$$\omega_{\mathrm{s}} = \frac{\omega_{\mathrm{p}}}{\sqrt{1+\epsilon_r}} = \frac{\omega}{\sqrt{2}} \tag{4.4}$$

for excitation of the surface plasmon. ΔE is between 5 and 60 eV.

Inelastic interactions include phonon excitations, inter and intra band transitions, plasmon excitations, inner shell ionizations are studied by **electron energy loss spectroscopy** (EELS).

- smaller peaks which are not shifted by energy ⇒ **Auger** e^- which have for each substance a characteristic position.

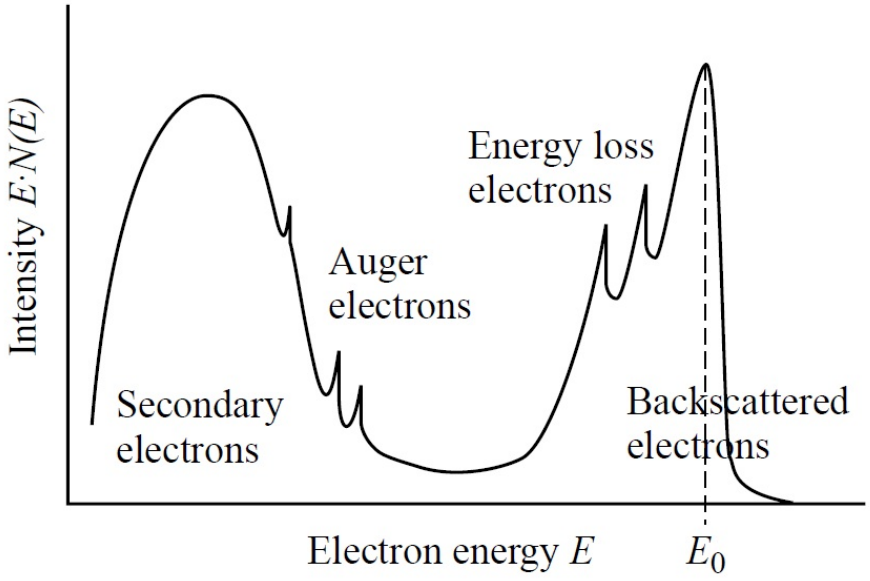

Figure 4.3: Electron energy distribution.

Primary e^- removes a core e^- (e.g. from K shell). The core state electron is removed leaving behind a hole. As this is an unstable state, the core hole can be filled by an outer shell electron, whereby the electron moving to the lower energy level loses an amount of energy equal to the difference in orbital energies. The transition energy can be coupled to a second outer shell electron which will be emitted from the atom if the transferred energy is greater than the orbital binding energy. The Auger energy released

$$E_\mathrm{k} = E_\mathrm{K} - E_\mathrm{L} - E'_\mathrm{V} - E_\mathrm{af}. \tag{4.5}$$

The E'_V is not equal with the original level energy E_V, because the e^- on the level V moves in a potential and the e^- on the level L is missing. The Auger requires the existence of at least two energy levels to three electrons. That is why it can not measure H and He. The elements with atomic number between 3 and 14 have KLL line, elements between 14 and 40 have LMM line, between 40 and 79 are MNN line and for heavier elements NOO line exists.

4.3 Electron spectroscopies

- UPS - Ultraviolet Photoelectron Spectroscopy, VUV radiation, especially using synchrotron radiation;
- XPS - X-ray Photoelectron Spectroscopy (ESCA - Electron Spectroscopy for Chemical Analysis), soft X-rays;

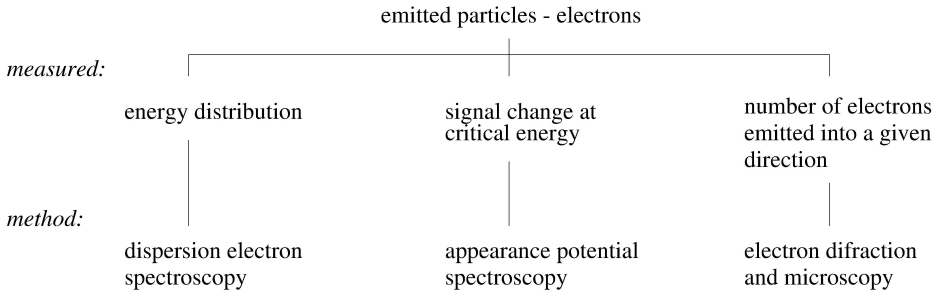

Figure 4.4: Overwiev of measuring methods using emitted electrons.

- AES - Auger Electron Spectroscopy
- ELS or EELS - Electron Energy Loss Spectroscopy, used in the case of internal excitation of electron levels, also known as IS - Ionization Spectroscopy;
- INS - Ion Neutralization Spectroscopy
- FES - Field Electron Spectroscopy, energy distribution measurements of field-emitted electrons

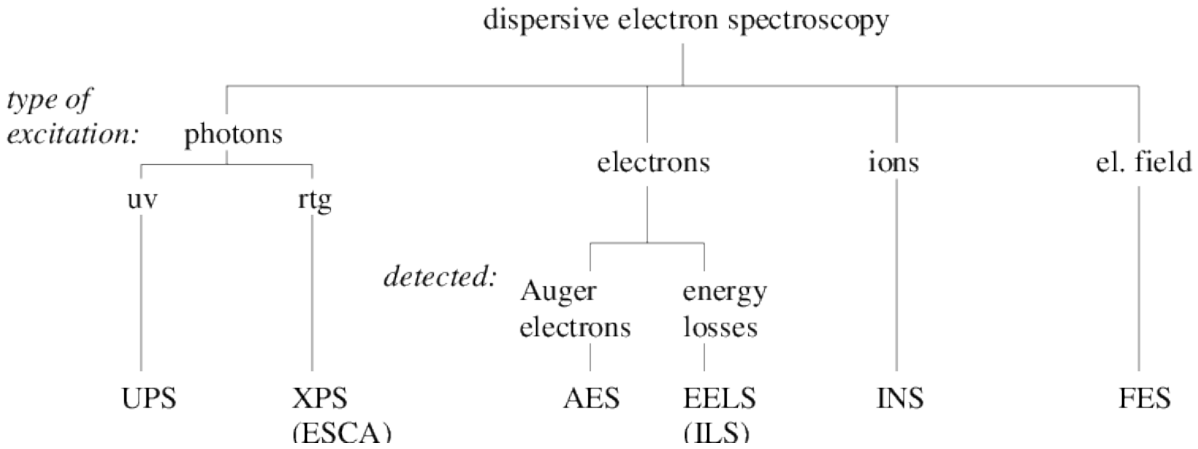

Figure 4.5: Overwiev of different dispersive electron spectroscopy methods

- XXAPS, XEAPS - X-ray X-ray Appearance Potential Spectroscopy, X-ray Electron Appearance Potential Spectroscopy. Methods in which X-rays are generated from the sample. They are practically not used since electron generation is much easier.
- SXAPS - Soft X-ray APS, electrons impact the sample and emitted X-rays are detected.
- DAPS - Disappearance Potential Spectroscopy, used to measure the surface electrons current.
- AEAPS - Auger Electron APS, records the secondary electrons current.

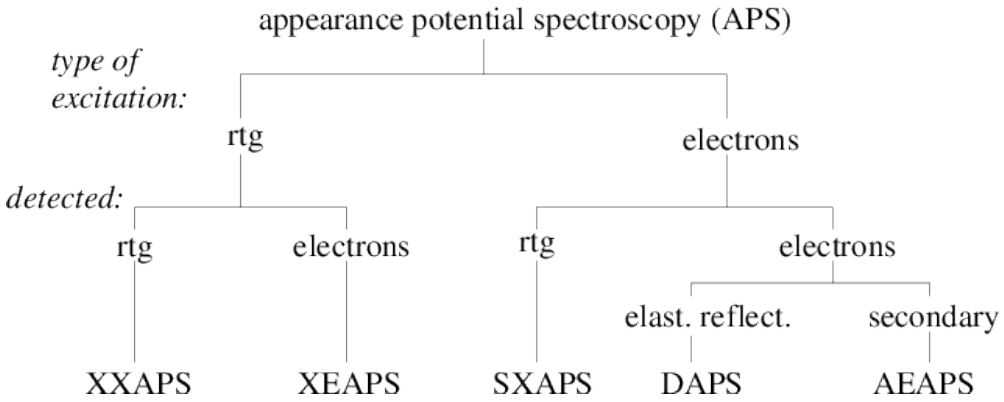

Figure 4.6: Overwiev of different APS methods

4.4 Electron spectroscopy conditions

All methods except FES require a **monochromatic source** - more or less focused, a **analyser** and a **detector** (electron multiplier). All this system must be kept under high vacuum conditions ($\leq 10^{-7}$ Pa). The surface sensitivity is greater so the depth profile is small. The most stringent conditions for surface are for UPS and not so for XPS. The device is equipped with a surface cleaning systems (Ar^+ sputtering and baking) or for preparation of clean surfaces in situ (cleaving or applying of layers).

4.5 Sources of primary particles

X-rays: soft X-rays are generated by bombardment of a suitable material (Al,Mg, Mo, Co, W) with sufficient e^- energy $\Rightarrow$ characteristic X-rays.

- when beam width may limit the resolution ($E_k = h\nu - E_B - e\phi$). The best e^-energy is ≈ 1.0 eV $\Rightarrow$ characteristic X-ray width s narrower.
- The energy must be high enough in order to obtain emission of photoelectrons from the bulk of material.

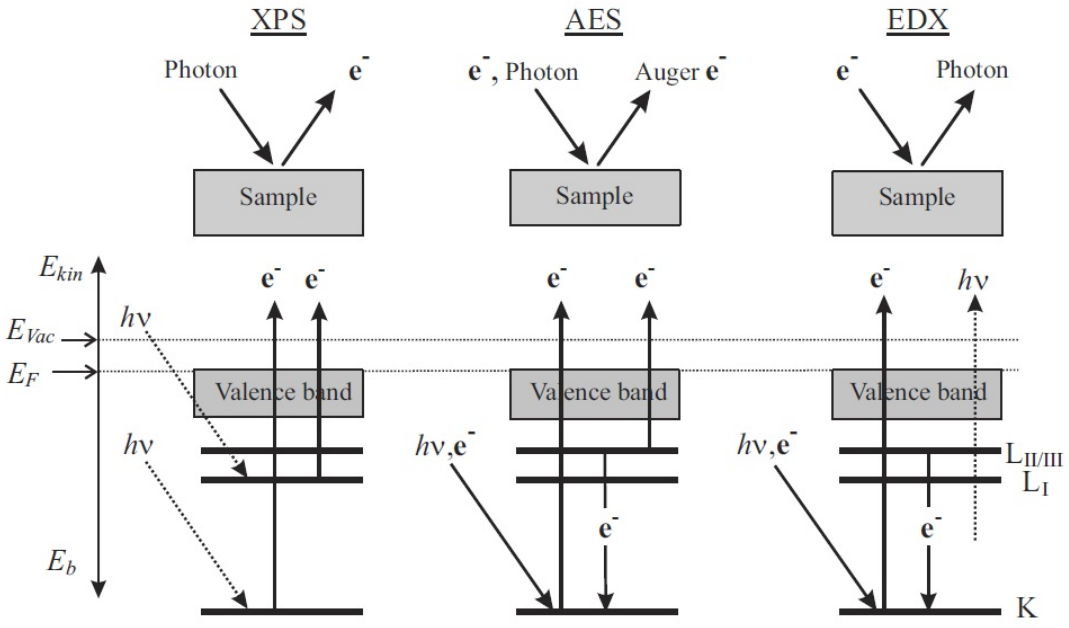

Figure 4.7: Schematic drawing of method's differences.

- In addition, the anode material needs to be capable of working even under e^-bombardment.

$\Rightarrow$ Mg Kα ($E = 1253.6$ eV, $\delta E = 0.7$ eV), Al Kα ($E = 1486.6$ eV, $\delta E = 0.85$ eV).
Photoemission starts at e^-energies equal with electron ionization threshold for the inner shell and growing rapidly with increasing energy. Therefore, devices allow e^- acceleration up to 15 keV.

The e^- source is the closest to the anode, which is often composed of two anodes. For continuous operation at 1–8 kW, a rotating anode is required. Beside the characteristic lines (Kα for Mg and Al), satellite, Kβ and continuous spectrum (Bremsstrahlung) lines exists $\Rightarrow$ sometime monochromatic radiation is used: Bragg diffraction from crystal.Rowland focusing is approximated by aligning the platform of the multi-crystal segmented analyser at a tangent to the Rowland circle (0.5 m).
Synchrotron radiation if the charged particles are accelerated, they radiate energy which covers an area of electromagnetic radiation from hard X-rays up to IR. The synchrotron is a particular type of cyclic particle accelerator in which the magnetic field (to turn the particles so they circulate) and the electric field (to accelerate the particles) are carefully synchronised with the travelling particle beam. Synchrotron radiation has many advantages: a broad spectrum, natural collimation, high intensity, coherence, the source is under vacuum. Maximum intensity is at the critical wavelength (0,1–0,4 nm), which is the curving path of the e^-. The intensity decreases rapidly for lower wavelengths.

Sources of electrons thermionic or field-emission guns. AES monochromatic e^- source. Only the electrons with sufficient energy are able to ionize the inner layer. Beam size is important for EELS max. 0,3–0,5 eV, which is to large for HREELS which requires special monochromatic

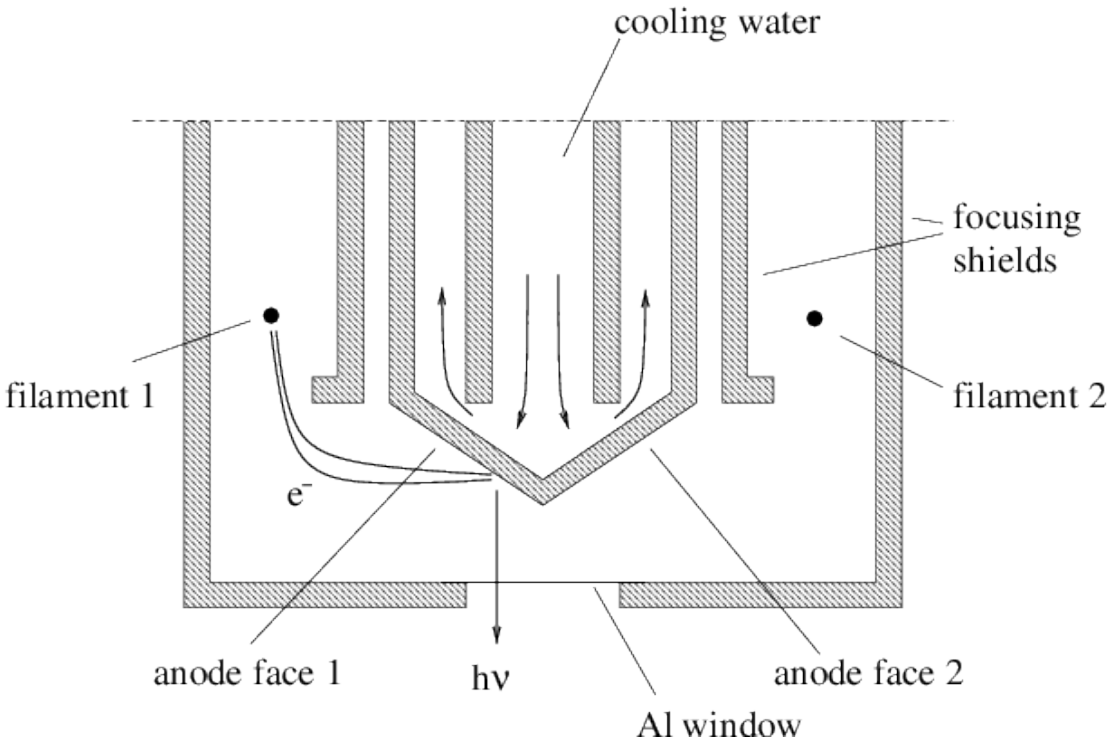

Figure 4.8: Scheme of X - ray source.

electron sources.

4.6 Electron energy analysers

The electron spectroscopy uses electrostatic analysers. The measured values can be divided into

- analysers with retarding field - recording of the total current of particles,
- dispersion analysers - select only certain e^-energies by changing the trajectories.

When choosing the analyser some parameters are assessed:

- resolution $R = E/\Delta E$ - indicates the energy;
- intensity (brightness) -affects the intensity of the output signal;
- analyser size - needs to be under vacuum;
- complexity - economic factor

The final solution is a compromise because the individual requirements have a contradictory character.

4.6.1 Analysers with retarding field

The operation principle is based on potential barrier high V_b. The flow of particles over the barrier is devided in fast and slow components. Only the faster ones are usually recorded:

$$J(E) = \int_E^\infty N(E')dE', \tag{4.6}$$

where $N(E')$ is the energy distribution of particles, $E = eV_\mathrm{b}$ is the lower energy limit and the symbol ∞ upper limit (maximum energy of particles). The energy distribution function can be obtained from the derivative of the above equation.

Planar analyser
The analysed beam, which is crucial for the accuracy of measurement is usually selected by modifying the slit. Around the threshold energy $E = eV_\mathrm{b}$, the resolution is:

$$R_{\mathrm{r}_0} = \frac{16d^2}{r_0^2}. \tag{4.7}$$

The basic parameter is the diameter of the solid angle Ω, under which the beam enters the detector (effective area). Impute increases with the slit and Ω.

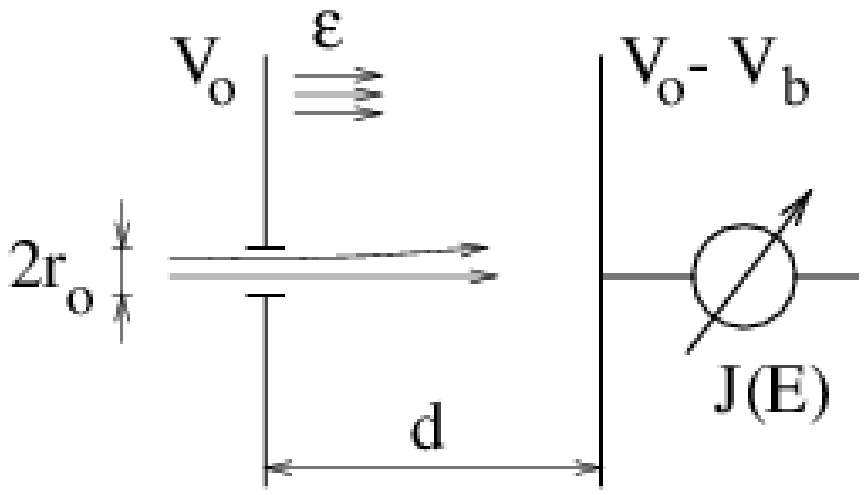

Figure 4.9: Scheme of planar analyser

Spherical analysers

Compact electrode system often use a system of 3 or 4 grids (collectors). Total energy analysis is carried out in a radial trajectory of the particles. It can be used for LEED if the system in equipped with a fluorescent screen or a small movable detector. Retarding fields are generated between the 1st and 2nd (or 3rd and 4th) grids. The resolution is given by the field inhomogeneity(mesh size, number of grids). Analyser throughput is high because it can detect

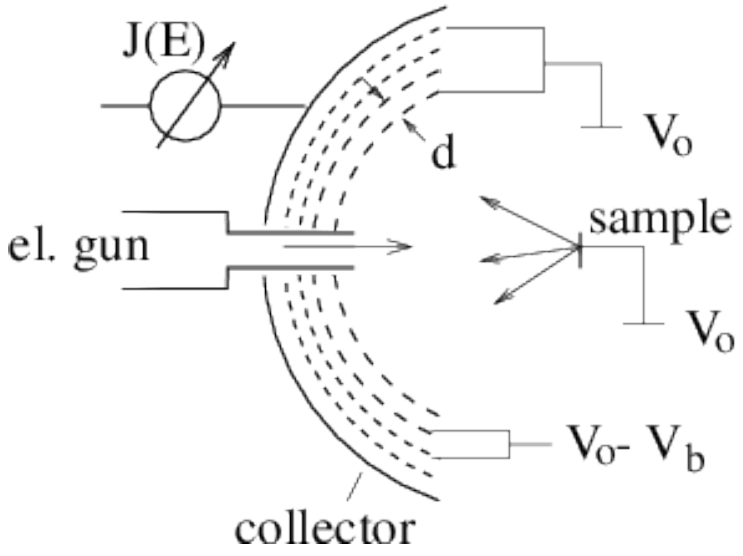

Figure 4.10: Scheme of spherical analyser

particles from a large solid angles (120° or 180°).

Dispersion analyser (deflectors)

In this case are detected either the coordinates of the particle impact or the energy E_0. Analysed properties reveal the dispersion $D(E) = E\ \partial x/\partial E$, which along the field focus properties determines the resolution.In all cases of analyser type, the energy determination is inaccurate due to overlapping trajectories of different energy E_0 and incorrect angle input. It is used the following approximation:

$$R \doteq \frac{2D}{Ms_1 + s_2 + \Sigma}\ , \tag{4.8}$$

where s_1 and s_2 are the slit sizes for input and output, M is the magnification ($\sim$1) and Σ is the blur due to the input divergence. From this expression is observed the decrease of R with the increase of slit size directly ($Ms_1 + s_2$), and indirectly with Σ. Dispersion analysers are divided into:

- mirror analyser: the beam enters through field lines at an different angle than $\pi/2$; the velocity component perpendicular to the field direction is maintained, $v_{\|}$ is gradually changed to the opposite direction $\Rightarrow$ symmetrical axis trajectory $\|$ to the field. The input and output slits are places in the positive potential electrode. The entrance angle is chosen with regard to the position of the source and the detector.
  - planar - two parallel electrodes focusing only the deflection plane a. Two arrangements (a) $\phi_0 = \pi/4$, source and detector in the entrance and exit slits, (b) $\phi_0 = 30°$, source and detector tangent to field.
  - cylindrical (CMA) - it is frequently used because allows the construction of high resolution systems. It consists of to concentric cylinders, with a positive potential between.

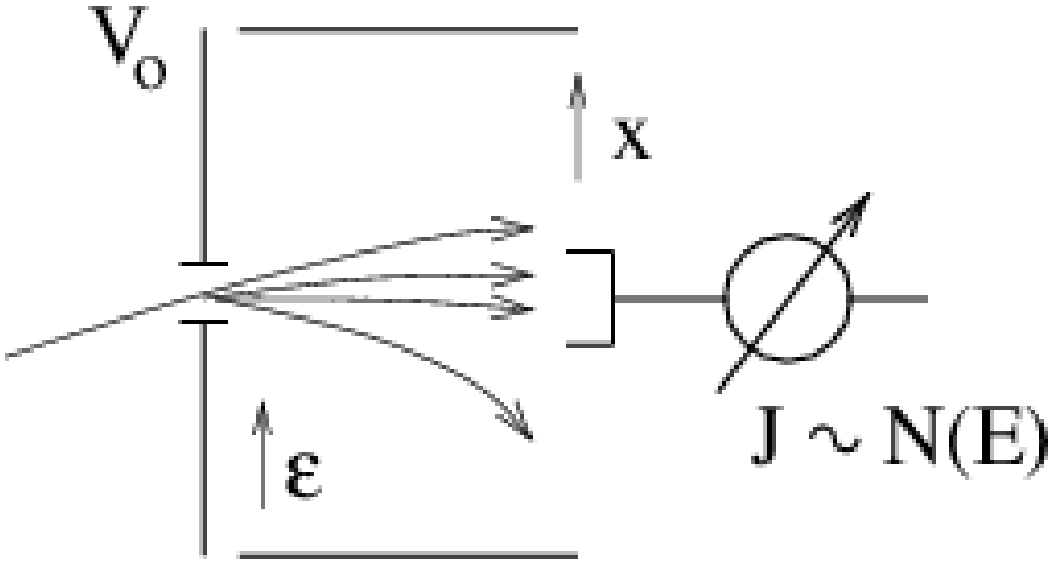

Figure 4.11: Scheme of dispersion analyser

- sectors: the beam enters $\perp$ to the field. The main trajectory is a circle, where the centrifugal force associated with the kinetic energy compensates the centripetal force. The incident and reflected angles is determined by the focus and position of the source and detector. It is mainly used in the differentiated angular spectroscopy:

  - cylindrical - two cylindrical sector analyser and to pairs of planar electrodes (in front and lateral); in the frontal one are located the slits. Deflection potential $V_1 - V_2$ is inserted between the cylinders (inner potential is positive), both planar electrodes are isolated and maintained on the potential $V_0 = (V_1 + V_2)/2$. The analyser is focusing only in one direction. Sector angle is $\Phi = \pi/\sqrt{2} = 127,3^\circ$ therefore $\Rightarrow$ the name of 127° analyser.

  - spherical (CHA - concentric hemispherical analyser) - two concentric spherical segments; input and output electrodes are radial slices are maintained at median surface potential V_0. The spherical deflector is capable of spatial focusing. Angle or the sector is usually $\Phi = 180^\circ$.

Conclusion
Analysing the energy of electrons has some other associated phenomena such as reflection and secondary emission. It is advantageous to use electron optics in order to increase the input angle, to obtain the image in a suitable place in the optimal regime area of the analyser, finely tune the input angle for slow electrons. The relative resolution of the analyser is constant $\Rightarrow$ absolute intensity will decrease with the decrease of energy.

4.7 Ultraviolet photoelectron spectroscopy

- if the photon energy is < 3 eV (VIS radiation), photoemission can occur only for substances with very low ϕ and the energy spectrum is narrow because e^- are emitted only from the highest occupied level $\Rightarrow$ information only about ϕ.
- if the photon energy is higher (UV radiation) electrons from the valence band can be emitted (UPS) $\Rightarrow$ distribution of densities of states in valence band can be obtained.
- in addition to energy distribution is possible to measure the angular distribution (ARUPS). In an isolated atom, the electrons occupy certain energy levels. In a solid, the levels involved in bonding 'the valence states', become blurred, and electrons can occupy a range of energies called bands. The energy of an electron in the solid depends on its momentum. Hence, by detecting photoelectrons emitted from a surface at different emission angles, the energy of the electrons as a function of the momentum vector may be determined. This process is known as "band mapping" and is a powerful probe of the electronic structure of crystalline materials.
- The mean free path in the case of UPS is only 0,5–2 nm $\Rightarrow$ surface characterization method.

Several modes exist for the evaluation of the emitted electrons:

- for a fixed position of source, surface elementary cell and the photos energy is measured by the kinetic energy of electrons EDC (energy distribution curve)by integrating or differentiating the angle.
- for constant photon energy and the electrons change the position in the detector ADC (angle distribution curve).
- for fixed geometries and fine tuned energies of photons - the kinetic energy detected is constant CIS (constant-initial-state spectra).
- for fixed geometries and constant kinetic energy CFS (constant-final-state spectra).

Photoemission
The first paper of Burglund and Spicer (1964) worked out what is called the three-step model for photoemission, and the second applied it to new data on Cu and Ag. The three-step model uses this picture in considerable detail to predict the spectrum of photoelectrons from a given band structure. This spectrum sometimes resembles the density of occupied electronic states weighted by a function that varies smoothly with energy. This model assumes the photoemission process can be described by three sequential processes:

- photoexcitation of an electron (photoabsorbtion) - general theory based on Fermi's golden rule, which determines the transition probability between two electron states of the same Hamiltonian H^N, if the disturbance Δ is small.

$$w = \frac{2\pi}{\hbar} | < \psi_{\mathrm{f}}^N | \Delta | \psi_{\mathrm{i}}^N >^2 \ \ \delta(E_{\mathrm{f}}^N - E_{\mathrm{i}}^N - \hbar\omega) \tag{4.9}$$

- transport of that electron to the surface without inelastic scattering
- scape of the electron into the vacuum

The law of energy conservation must be applied ($E_{\text{kin}} = E_{\text{f}}^{\text{u}} - e\Phi = E_{\text{i}}^{\text{u}} + \hbar\omega - e\Phi$) and the wavelength vector. Overall, the wave-vector is not maintained because the emitted electron escapes into vacuum, and the system achieve three-dimensional symmetry. The surface has only two-dimensional translation symmetry of the surface reciprocal lattice vector $\vec{G}_{\text{S}}$:

$$\vec{k}_{\parallel}^{\text{vn}} = \vec{k}_{\text{f}\parallel}^{\text{u}} + \vec{G}_{\text{S}} \tag{4.10}$$

Inside the crystal the wave-vector is preserved:

$$\vec{k}_{\text{f}}^{\text{u}} = \vec{k}_{\text{i}}^{\text{u}} + \vec{G}_{\text{B}}, \tag{4.11}$$

where $\vec{G}_{\text{B}}$ is the reciprocal lattice volume vector. Dispersion relation for free e^-:

$$E_{\text{kin}} = \frac{\hbar^2}{2m}(k_{\parallel}^2 + k_{\perp}^2). \tag{4.12}$$

If we don't know the dispersion relation within the crystal we are able to directly measure the band structure, but if we know the initial dispersion or the final states, we can limit the dispersion or the initial conditions. For surface conditions these restrictions do not apply ⇒ layered materials with two-dimensions periodicity exists: TaS_2, GeS or graphite, where the bulk band structure $E(k_{\parallel})$ will be explored.

$$k_{\parallel} = \sqrt{\frac{2m}{\hbar^2}\ E_{\text{kin}}}\sin\theta, \tag{4.13}$$

where θ is the angle between the surface normal and the axis of the detector. The UPS method can be applied to absorb on substrate system like CO on Ni

EDC

The spectrum actually measured in a photoemission experiment involves not only the electron excitation out of the atom but also the probability that this electron can escape from the solid. This conversion from the energy distribution of electrons inside the solid produced by the optical excitation to the experimental distribution of electrons measured outside the solid, termed the *energy distribution curve*. The EDC measured experimentally are directly proportional to the rate of photo-excitation and hence the density of states. Since the density of states can be determined analytically from the atomic wave-function and the band theory and the response of the experimental system can be factored out, one can use the spectral feature measured versus calculated to measure a wide range of features.

In the case of EDC that results from exciting an arbitrary initial density of states (DOS) with the photon $h\nu$, the photo-excitation creates a replica of the density of occupies states distributed in energy below the vacuum level, shifted up by the photon energy. Electrons that scatter inelastically are termed secondary electrons and form a continuum with the lowest density at the highest EDC energy and highest density at near-zero kinetic energy, corresponding to the vacuum level cutoff.

CFS

CFS spectroscopy uses the tunability of synchrotron radiation to measure the density of empty

states above the vacuum level into which electrons are photoexcited. First, one selects a photon energy range from slightly below to slightly above the energy difference between a relatively narrow core level energy E_{core} and an empty surface state at or below the conduction band edge E_c. Second sets the electron analyser energy to an energy E_k several eV above the cutoff energy for photoemission. Finally, one scans $h\nu$ across the range to obtain partial yield spectra. These spectra exhibit peaks in the emission of secondary electrons when electrons are photoexcited from the core level to an empty state either in the conduction band or within the bandgap. The energy gained by refilling the core hole indirectly increases the emission of secondary electrons.
The electron emission versus photon energy curves at a constant final kinetic energy reveal changes with surface condition that can be attributed to the formation of new surface state. Even though complicated by the lattice relaxation energy correction factor, the CFS or partial yield spectroscopy demonstrates the creation of new gap states as new atoms absorb.

CIS
The converse of CFS is CIS spectroscopy. In this technique, the incident photon energy is again scanned, but E_g is scanned in energies to match. In other words, $E_{final} - h\nu = E_i$ (initial) energy. Densities of final states are useful in determining filled state densities since the former must be known to determine the latter acording to Fermi‘s golden rule. It is also known as inverse photoemission spectroscopy and provides useful empty state information for semiconductors and organic electronic materials.

4.8 Spectroscopic photoemission of electronic states

Molecules can possess several types of angular momentum. Electrons possess orbital and spin angular momenta, rotation of the molecule generates angular momentum, degenerate vibrations may give rise to vibrational angular momentum, and nuclei may also have spin angular momentum. Interactions (coupling) between these various types of angular momentum can have important implications for interpreting spectra, particularly high resolution spectra, and so it is important to be familiar with some basic results from the quantum theory of angular momentum.

The angular momentum is a vector quantity and a simple vector model provides a useful visual recipe for assessing how different angular momenta interact. There are more powerful and rigorous mathematical approaches to angular momentum coupling than that described here. These more comprehensive treatments deal explicitly with the angular momenta as mathematical operators, and the coupling behaviour then follows from the properties of these operators when added vectorially. The simple vector picture is use to emphasize the physical principles underlying the coupling of angular momenta, focussing on electronic angular momentum.

The magnitude of the orbital angular momentum for a single electron in an atom is given by the expression $\hbar\sqrt{l(l+l)}$ where l is the orbital angular momentum quantum number with allowed values 0, 1, 2, . . . Similarly, the magnitude of the spin angular momentum vector is given by $\hbar\sqrt{s(s+l)}$ where s is the spin quantum number which, for a single electron, can only take the value $1/2$. For an electron with both orbital and spin angular momenta, the total angular momentum vector j will be the sum of the two constituent vectors $j = l + s$. The magnitude of this vector is $\hbar\sqrt{j(j+l)}$, where j is the corresponding quantum number, and according to the quantum theory of angular momentum this can only take on the values $j = l+s, l+s-1, ..., |l-s|$. Series such as this are called Clebsch – Gordan series and arise when the total angular momentum results from a system composed of any two sources of quantized angular momentum. In the general case, if two angular momenta, say j_1 and j_2, can interact then the allowed values for the angular momentum quantum number for the resultant total angular momentum will be given by the Clebsch – Gordan series $j = j_1 + j_2, j_1 + j_2 - 1, ..., |j_1 - j_2|$

4.8.1 L-S (Russell-Saunders) coupling

In the Russell – Saunders limit the coupling between the orbital angular momenta is strong. The source of the coupling is the electrostatic interaction between two electrons. Electron spins can also couple together, although spin is a magnetic phenomenon and therefore the coupling is via magnetic fields,which tends to be a weaker effect than electric field coupling. In Russell – Saunders coupling the interaction between the orbital and spin angular momenta of a given electron is assumed to be small compared with the coupling between orbital angular momenta. In this limit the principal torque causes the orbital angular momenta to precess about a common direction, the axis of the total orbital angular momentum of all electrons. The spin angular momenta also couple together through the magnetic interaction of electron spins.

The vector model described above can be employed to see the effect of coupling on atoms.

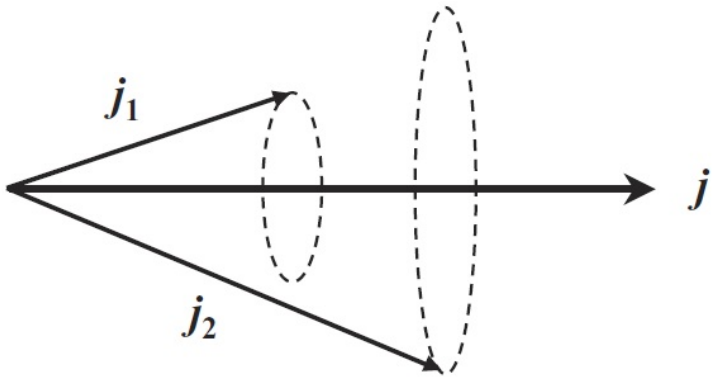

Figure 4.12: Forming the total angular momentum.

For illustration, consider an atom with two electrons outside its closed shell. The orbital angular momenta of these electrons are represented by l_1 and l_2, and the corresponding spin momenta by s_1 and s_2. The coupling of orbital angular momenta dominates and they form a resultant total orbital angular momentum $L = l_1 + l_2$. In the same way, the spin momenta also couple to form $S = s_1 + s_2$. When this coupling case is valid, the individual orbital angular momenta l_1 and l_2 precess rapidly around L, and s_1 and s_2 precess rapidly around S. L and S can themselves couple with each other, but this coupling, known as spin – orbit coupling, is assumed to be relatively weak. As a result, L and S precess slowly around the resultant total angular momentum $J = (L + S)$.

4.8.2 jj coupling

The Russell–Saunders scheme describes the electronic states of light atoms rather well but breaks down for heavier atoms, particularly for the lanthanides and actinides. This is due to increasing coupling between the orbital and spin angular momenta of individual electrons to the point where it is no longer negligible, as was assumed in the Russell – Saunders case. In the limit of very strong coupling between orbital and spin angular momenta, the appropriate coupling scheme is known as *jjcoupling*. A dominant spin – orbit torque will first couple the spin and orbital momenta of each electron to form resultants, $j_1 = l_1 + s_1$ and $j_2 = l_2 + s_2$. The vectors j_1 and j_2 interact more weakly, forming the total angular momentum $J = j_1 + j_2$. In jj coupling, $l_1(l_2)$ and $s_1(s_2)$ precess rapidly around $j_1(j_2)$, while jj_1 and j_2 precess slowly around their resultant J. As a result, only j_1, j_2, J and the projection of $J(M_J)$ are good quantum numbers, i.e. the quantum numbers L and S in the Russell – Saunders scheme have no significance in jj coupling. Of course it is also possible that the spin–orbit coupling is neither weak enough for Russell–Saunders to be applicable, nor strong enough for true jj coupling.

4.9 Auger electron spectroscopy

4.9.1 Auger effect

Auger electrons were named after Pierre Auger who, together with Lise Meitner, discovered Auger electron emission in 1920s. When a high-energy electron (or X-ray photon) strikes an inner shell electron of an atom, the energy of the incident particle can be high enough to knock out the inner shell electron. Thus, the atom becomes ionized and in an excited state. The atom will quickly return to its normal state after refilling the inner electron vacancy with an outer shell electron. In the meantime, the energy difference between the outer shell electron and the inner shell may cause emission of either an Auger electron from an electron shell or a characteristic X-ray photon. The kinetic energy of an Auger electron is approximately equal to the energy difference between binding energies in the electron shells involved in the Auger process. For example, the kinetic energy of an Auger electron is approximated by the following equation:

$$E_{KL1L2,3} = E_K - E_{L1} - E^*_{L2,3}, \tag{4.14}$$

where E_i is the binding energy and $E^*_{L2,3}$ is mark with asterisk because the energy levels $L^*_{2,3}$ differs slight from the energy levels of $L_{2,3}$.
The notation for kinetic energy of Auger electron describes its origin, but the nomenclature is rather complicated. For example, the kinetic energy of an Auger electron is from a following process: an incident electron knocks out a K shell electron, a L_1 shell electron refills the K shell vacancy, and a $L_{2,3}$ shell electron is ejected as the Auger electron. Auger electron spectroscopy (AES) identifies chemical elements by measuring the kinetic energies of Auger electrons. In an AES spectrum, an individual kinetic energy peak from an Auger electron is marked with an elemental symbol and subscripts indicating the electron shells or sub shells involved, for example, in aluminium oxide case, Al_{KLL}, O_{KLL}. . .

A typical AES spectrum is a plot of intensity versus kinetic energy; most commonly,it is a plot of the first derivative of intensity versus the kinetic energy. The primary electrons ejected from a solid surface by inelastic scattering comprise the background of an AES spectrum in the region of high kinetic energies while the secondary electrons comprise the background in the region of low kinetic energies. The number of Auger electrons ejected from a sample is much less than that of scattered primary electrons and secondary electrons. Thus, the direct-mode spectrum is not favoured except for quantitative analysis.

4.9.2 Fine Auger structure

A recent interest is concerned with the fine structures in the neighbourhood of Auger lines, denoted by EXAFS (extended X-ray absorption fine structure). It is a powerful nondestructive technique that provides structural information on metal or metal oxide phases highly dispersed on inorganic supports under reaction conditions. Bond lengths and coordination numbers of X-ray absorbing material can be determined. When single crystals are employed as supports, characterization of metal sites on them can be achieved separately in two different bonds parallel

and normal to the surface by polarized X-ray radiation.

In transmission mode, the EXAFS signal of surface species on solid substrates can not be detected because of the large adsorption by the substrate. To determine surface structures, it is possible to measure EXAFS spectra by detecting the reflected X-rays from sample, but usually the sensitivity is worse.

4.9.3 Quantitative analysis

Quantitative elemental analysis in electron spectroscopy is similar to that in X-ray spectroscopy. Analysis quantifies the concentrations of chemical elements on a sample surface from the peak intensities of the spectra. In theory, the quantitative relationship between the intensities of electron signals and atomic fractions of elements can be calculated. In practice, for quantification in both XPS and AES, most parameters for calculations are not available.

Sensitivity factor method: the Auger current is described by

$$I_{\alpha,\mathrm{XYZ}} = I_\mathrm{p}\gamma_{\alpha,\mathrm{XYZ}}\, T(E_{\alpha,\mathrm{XYZ}})D(E_{\alpha,\mathrm{XYZ}}) \int_{E_{\alpha,\mathrm{X}}}^{E_\mathrm{p}} \sigma_{\alpha,\mathrm{X}}^{\mathrm{total}}(E)dE \int_0^\infty n_\alpha(z)e^{\left(-\frac{z}{\lambda^\mathrm{M}(E_\alpha)\cos\theta}\right)}dz \qquad (4.15)$$

where I_p is the excitation current, $\gamma_{\alpha,\mathrm{XYZ}}$ is the Auger efficiency, $\sigma_{\alpha,\mathrm{X}}^{\mathrm{total}}(E)$ is the ionization cross section X the element α, E_p is the energy of the primary electron $n_\alpha(z)$ is the density of element α at depth z. The transmittance of the spectrometer is $T(E_{\alpha,\mathrm{XYZ}})$ and the sensitivity of the detector is $D(E_{\alpha,\mathrm{XYZ}})$.

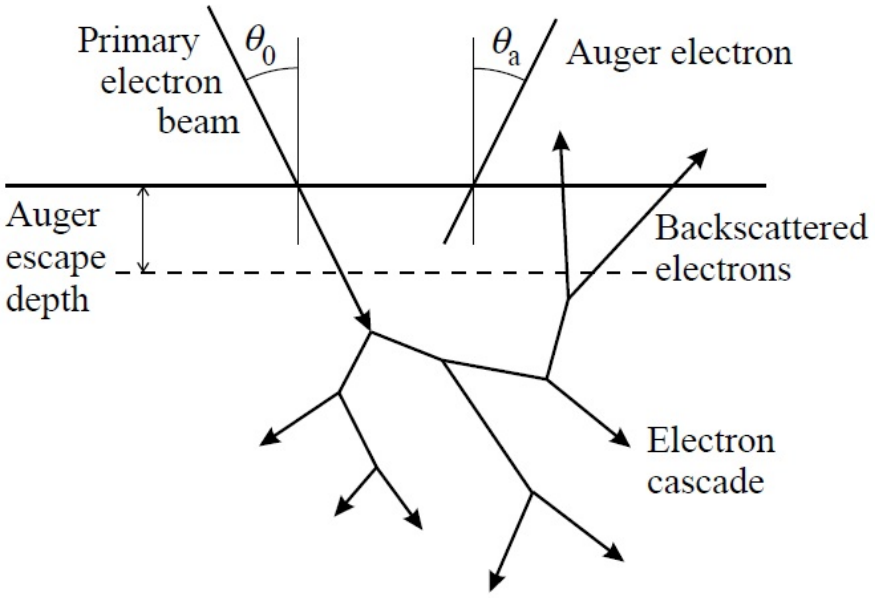

Figure 4.13: The physical processes occuring when an electron strikes a solid surface.

Ionization is caused not only by the electrons but also by the backscattered energy which has the distribution $n(E)$

$$\sigma_{\alpha,\mathrm{X}}^{\mathrm{total}} = \sigma_{\alpha,\mathrm{X}}(E_{\mathrm{p}}) + \int_{E_{\alpha,\mathrm{X}}}^{E_{\mathrm{p}}} \sigma_{\alpha,\mathrm{X}}(E) n(E) dE \tag{4.16}$$

This relation can be approximated as:

$$\sigma_{\alpha,\mathrm{X}}^{\mathrm{total}} = \sigma_{\alpha,\mathrm{X}}(E)[1 + r^{\mathrm{M}}(E_{\alpha,\mathrm{XYZ}}, \psi] \tag{4.17}$$

which can be simplified for homogeneous material

$$I_{\alpha,\mathrm{XYZ}} = I_{\mathrm{p}} \gamma_{\alpha,\mathrm{XYZ}}\ T(E_{\alpha,\mathrm{XYZ}}) D(E_{\alpha,\mathrm{XYZ}}) \sigma_{\alpha,\mathrm{X}}(E)[1 + r^{\mathrm{M}}(E_{\alpha,\mathrm{XYZ}}, \psi] n_{\alpha} \lambda^{\mathrm{M}}(E_{\alpha}) \cos\theta \tag{4.18}$$

The sensitivity factor $S_{\alpha,\mathrm{XYZ}}$ is defined as:

$$I_{\alpha,\mathrm{XYZ}} = I_{\mathrm{p}} n_{\alpha} \cos\theta\ S_{\alpha,\mathrm{XYZ}} \tag{4.19}$$

and the atomic concentration α in the M matrix

$$c_{\alpha} = \frac{n_{\alpha}}{\sum\limits_{\alpha'} n_{\alpha'}} = \frac{I_{\alpha,\mathrm{XYZ}}}{S_{\alpha,\mathrm{XYZ}}} \sum_{\alpha'} \frac{I_{\alpha',\mathrm{XYZ}}}{S_{\alpha',\mathrm{XYZ}}} \tag{4.20}$$

The sensitivity factor must be determined either theoretically or directly experimentally. Common practice is to use the sensitivity factors from published handbooks with certain corrections according to the instrument characteristics, because it is not feasible to compile a set of in-house sensitivity factors.

Standard method: For simplicity, a binary alloy $\alpha\beta$ is selected. No contamination on the surface or segregation phenomena exists:

$$\frac{I_{\alpha}}{I_{\alpha}^{\mathrm{s}}} \frac{I_{\beta}^{\mathrm{s}}}{I_{\beta}} = \frac{n_{\alpha}}{n_{\beta}} \left(\frac{n_{\alpha}^{\mathrm{s}}}{n_{\beta}^{\mathrm{s}}} \frac{\lambda_{\alpha} \lambda_{\beta}^{\mathrm{s}}}{\lambda_{\beta} \lambda_{\alpha}^{\mathrm{s}}} \frac{(1 + r_{\alpha})(1 + r_{\beta}^{\mathrm{s}})}{(1 + r_{\beta})(1 + r_{\alpha}^{\mathrm{s}})} \right) = \frac{n_{\alpha}}{n_{\beta}}\ K \tag{4.21}$$

and the elemental concentration α is

$$c_{\alpha} = \left(1 + \frac{I_{\beta} I_{\alpha}^{\mathrm{s}}}{I_{\alpha} I_{\beta}^{\mathrm{s}}} \frac{1}{K} \right)^{-1}. \tag{4.22}$$

The matrix correction factor K describes the influence of the $\alpha\beta$ alloy. When $K = 1$, we assume that the influence on matrix is negligible.

4.10 X-ray photoelectron spectroscopy

The X-ray photoelectron is an electron ejected from an electron shell of an atom when the atom absorbs an X-ray photon. An incident X-ray photon can have sufficient energy (a value of $h\nu$) to knock out an inner shell electron, for example from the atom's K shell. In such a case, the K-shell electron would be ejected from the surface as a photoelectron with kinetic energy E_K. Knowing the kinetic energy E_K, we can calculate the binding energy of the atom's photoelectron (E_B) based on the following relationship:

$$E_{\mathrm{B}} = h\nu - E_{\mathrm{K}} - \phi \tag{4.23}$$

The value of ϕ depends on both the sample material and the spectrometer. The binding energies (E_B) of atomic electrons have characteristic values, and these values are used to identify elements, similar to the way that characteristic X-ray energy is used in X-ray spectroscopy. X-ray photoelectron spectroscopy (XPS) identifies chemical elements from the binding energy spectra of X-ray photoelectrons.

Inner shell

- depending on how deep is, we obtain atomic number and the energy of X-rays
- doublet separations in photoelectron lines $\Leftarrow$ spin-orbital coupling jj. Splitting distance is directly proportional with $< 1/r^3 >$ for a given orbit, so it increases for higher Z or lower l (at constant n).

subshell	value of j	area ratio
s	$\frac{1}{2}$	–
p	$\frac{1}{2},\frac{3}{2}$	1:2
d	$\frac{3}{2},\frac{5}{2}$	2:3
f	$\frac{5}{2},\frac{7}{2}$	4:4

- Relative intensities are given by the photoemission cross section, analyser transmission and very little by the X-ray energy
- peak width (FWHM) is determined by

$$\Delta E = (\Delta E_{\mathrm{n}}^2 + \Delta E_{\mathrm{p}}^2 + \Delta E_{\mathrm{a}}^2)^{1/2}, \tag{4.24}$$

  where ΔE_{n} is the natural width of the inner surface, ΔE_{p} is the width of the X-rays ΔE_{a} is the analyser resolution (in all cases Gaussian distribution).

  – ΔE_{n} associated with the lifetime τ

$$\Gamma = \frac{h}{\tau}. \tag{4.25}$$

    where τ is related with the photoemission of X-rays, emission of Auger electrons or special type Auger electron (Coster-Kronig transition), which prefers l and is very fast. Width for light elements ($1s$, $2p$) increases with the atomic number.

– ΔE_a is constant for all peaks in "constant analyser energy" (CAE) mode, but changes in "constant retard ratio" (CRR), because $\Delta E/E$ ratio remains constant.

Valence shell
Electrons with low binding energy (0–20 eV). They are very close to each other ⇒ band structure. At high resolution spectrum scanning can show the band structure and a sharp decrease of intensity for E_F.

Auger series
Kinetic e^- energy from Coster-Kronig transition is very low; four basic series exists:

- KLL - from boron to magnesium(with Mg Kα) or aluminium (with Al Kα),
- LMM - from sulphur to germanium (with Mg Kα) or selenium (with Al Kα),
- $M_{4,5}N_{4,5}N_{4,5}$ - from molybdenum to neodymium (with Mg Kα),
- $M_{4,5}N_{6,7}N_{6,7}$ - only for high energy X-rays (e.g. Ag Lα, 2984 eV).

4.10.1 Energy scale calibration

For meaningful measurements it is important to ensure the instrument is calibrated. For example, to identify chemical constituents from the peak energy correctly, the energy scale needs to be calibrated. To provide quantitative information, use sensitivity factors and compare with other instruments, while the intensity scale needs to be linear and also corrected for the intensity response function. The intensity response function (IRF) includes the angular acceptance of the analyser to electrons, the transmission efficiency of electrons and the detection efficiency.

- for metals is possible to observe directly the Fermi level in the valence lines;
- the semiconductors are sufficiently conductive in order to offset the E_F. It is yet difficult to determine the exact location of line since the Fermi level depends on doping, surface states and defects;
- in the analysis of dielectrics the surface charge and energy shift occurs. The most commonly used method is called internal standard - a reference line from photoemission with a known binding energy from other measurements. It is based on the fact that often the sample is contaminated with hydrocarbons (C1s = 284,6–285,2 eV).

Cu and Au samples set with their angle of emission $\leq 56°$ are sputtered clean, and the measured energies of the peaks are compared with the energy values given in the table. As for AES, the peak energy for the calibration is evaluated from the top of the peak without background subtraction. For gold line $4f_{7/2}$ the energy is 83.95 eV. The lineshapes and energies of the $K_{\alpha 1}$ and $K_{\alpha 2}$ X-rays that characterize $h\nu$ appear to be the same in all unmonochromated instruments. However, the lineshapes and energies of the K_α X-rays, when monochromated vary significantly and depend on the set-up of the monochromator and its thermal stability. By

altering the monochromator settings, the measured energies of the peak may be moved over a kinetic energy range of 0.4 eV without too much loss of intensity.

Use of the standard with a modern, well-maintained spectrometer should result in calibration within tolerance limits of ±0.2 eV over four months or ±0.1 eV over one month before recalibration is required. For many purposes ±0.2 eV is satisfactory.

4.10.2 Primary structure information

Inner shell line
The binding energy is influenced by interactions with other electrons → chemical shift. The exact calculation of the binding energy is very difficult and limited to small molecules → approximate methods, such as electrostatic model - the model potentials(charge Potential model)

$$E_{\mathrm{B}} = E_{\mathrm{B}}^{0} + kq_i + \sum_{i \neq j} \frac{q_j}{4\pi\epsilon_0 r_{ij}}, \tag{4.26}$$

where E_{B}^{0} has significant calibration factor , k s a constant indicating an average repulsion between inner shell and valence e^-, q_i is the atom i charge and sum of potentials of neighbouring atoms j, also called Madelung potential, where r_{ij} are the internuclear distances.

Valence band peak
The valence electrons are directly involved in bond formation and molecular interactions, so the intensity and energy of the valence band peaks depend on their bonding environment. Thus, quantitative interpretation of the valence band spectrum for most materials requires a full molecular orbital calculation. For multi-component materials or those containing a large number of atoms per structural unit (e.g. polymers) this requires computer calculations.

Valence band analysis is worth pursuing because it can provide electronic structure information that cannot be obtained from typical core level analysis. Also, it is sometimes possible to extract useful structural information from valence band spectra.
In metals the information about the valence band and the Fermi energy give the opportunity to observe the transformation of the material from dielectric to metal (VO_2 non-conductor x metal at 65°, Na_xWO_3 non-conductor x metal when changing x).

Auger chemical shift
To identify the oxidation state of an element is often preferable to use the Auger parameter:

$$\alpha = E_{\mathrm{K}}(jkl) - E_{\mathrm{K}}(i) = E_{\mathrm{K}}(jkl) + E_{\mathrm{B}}(i) - h\nu, \tag{4.27}$$

where $E_{\mathrm{K}}(jkl)$ and $E_{\mathrm{K}}(i)$ is the kinetic Auger energy. α does not depends on the reference surface or the sample charge. The Auger parameter is modified

$$\alpha' = \alpha + h\nu = E_{\mathrm{K}}(jkl) + E_{\mathrm{B}}(i). \tag{4.28}$$

Auger line shapes
Auger lines can be readily distinguished from photoemission lines by changing X-ray sources (e.g.

using a Mg K_α source instead of an Al K_α source). If the Auger process causes the formation of at least one hole, then the distribution of Auger lines intensities strongly depends on the type of molecule.

4.10.3 Final state effects

X-ray satellites and ghost peaks
Satellites appear together with the less intensive X-ray characteristic peaks. The main peak $K\alpha_{1,2}$ corresponding to the $2p_{3/2,1/2} \rightarrow 1s$transition, satellites are $K\beta$, valence bands $\rightarrow 1s$ or multi ionized atoms.
Ghosts appear due to excitation of surface contaminants. Often, Al $K\alpha_{1,2}$ from the Mg $K\alpha$ (due to the aluminium window), followed by Cu $L\alpha$ and O $K\alpha$.

Multiplet splitting
A requirement for this splitting of the s photoemission peak into a doublet is that there be unpaired orbitals in the valence shells. Complex peak splitting can be observed in transition metal ions and rare earth ions when multiplet splitting occurs in p and d levels.

$$\Delta E = (2S^{\mathrm{v}} + 1)K_{\mathrm{sd}} \qquad \text{a} \qquad \frac{I(S^{\mathrm{v}} + 1/2)}{I(S^{\mathrm{v}} - 1/2)} = \frac{S^{\mathrm{v}} + 1}{S^{\mathrm{v}}}, \tag{4.29}$$

where S^{v} is the total spin of a unpaired valence electron and K_{sd} is the s-d exchange integral.

Shake-up satellites
It represents photoelectrons that have lost energy through promotion of valence electrons from an occupied energy level (e.g. a π level) to an unoccupied higher level (e.g. a pi^* level). Shake-up peaks (also called "loss peaks" because intensity is lost from the primary photoemission peak) are most apparent for systems with aromatic structures, unsaturated bonds or transition metal ions. In contrast to the continuum of reduced energies seen in the inelastic scattering tail, shake-up peaks have discrete energies ($\sim$ 6.6eV higher binding energy than the primary peak in C_{1s} spectra of aromatic-containing molecules) because the energy loss is equivalent to a specific quantized energy transition (i.e., the $\pi \rightarrow \pi^*$ transition).

Asymmetric metal lines
The metal lines may change with the degree of surface charging during data acquisition. With asymmetric metal lines as encountered with many transition metals, this effect may mimic the presence of metal ions, The line broadening is , most likely, due to varying degree of differential charging, since it is paralleled in the widths of the support elements.

Asymmetric non-metal lines
Appears only at high resolution. The asymmetry occurs due to fine vibrational structure of molecules. After ionization there is a change in interatomic distances and narrowing the potential curves of the molecule.

Shake-off satellites
If the departing photoelectron transfers sufficient energy into the valence electron to ionize it into the continuum, the photoemission loss peak is called a "shake-off" peak. The shake-off satellite peaks of the photoemission peak can have a wide range of possible energies (of course, always with a lower KE than the photoemission peak). This energetically broad feature is typically hidden within the background signal and is usually not detected or used analytically.

4.10.4 Quantitative analysis

The intensity of the photoemission line i

$$I^i_{\mathrm{A}} \sim Q\mathcal{A}\; c_{\mathrm{A}}\sigma^i_{\mathrm{A}}\lambda^i T^i L^i_{\mathrm{A}} f(\phi,\theta), \tag{4.30}$$

where Q is the photon flux [$\mathrm{cm}^{-1}\mathrm{s}^{-1}$], $\mathcal{A}$ effective are of the sample, c_{A} concentration of A, σ^i_{A} is the partial ionization cross section, λ^i mean free path, T^i the transmission, L^i_{A} angular asymmetry coefficient and $f(\phi,\theta)$ function, depending on the geometry of the experiment. The above equation does not detect the absolute concentration of elements. The intensities of the lines for individual measured elements under the same conditions can determine the relative atomic composition. When a solid is homogeneous within the analysed depth for all elements of interest (A and B for example), the uncertainties can be partially cancelled by considering relative atomic values. We obtain:

$$\frac{I^i_{\mathrm{A}}}{I^j_{\mathrm{B}}} = \frac{c_{\mathrm{A}}\sigma^i_{\mathrm{A}}\lambda^i T^i L^i_{\mathrm{A}}}{c_{\mathrm{B}}\sigma^j_{\mathrm{B}}\lambda^j T^j L^j_{\mathrm{B}}} = \frac{c_{\mathrm{A}}\sigma^i_{\mathrm{A}}L^i_{\mathrm{A}}}{c_{\mathrm{B}}\sigma^j_{\mathrm{B}}L^j_{\mathrm{B}}}R. \tag{4.31}$$

If the kinetic energy differs by more than ~ 400 eV, correction of T and λ should be performed. the correction used for transmission:

$$T \sim 1/E_{\mathrm{k}} \qquad \text{for constant energy (CAE)} \tag{4.32}$$

and

$$T \sim E_{\mathrm{k}} \qquad \text{for constant resolution (CRR).} \tag{4.33}$$

To calculate the mean free path, the typically used equation is

$$\lambda = aE_{\mathrm{k}}^{-2} + bE_{\mathrm{k}}^{1/2}. \tag{4.34}$$

One of the major problem in quantitative analysis is the integral of photoemission intensity lines. When using the theoretical values σ we have determine the overall intensity of lines including the contributions of all satellites and inelastic electron scattering. For practical purposes we can use the equation:

$$\frac{I^i_{\mathrm{A}}}{I^j_{\mathrm{B}}} = \frac{c_{\mathrm{A}}S^i_{\mathrm{A}}}{c_{\mathrm{B}}S^j_{\mathrm{B}}}. \tag{4.35}$$

4.10.5 Angular effects

1. **Enhancement of system sensitivity and depth profile**
   Almost all electrons (95 %) come on a path equal with 3λ. If $e^-$are detected at angle θ different from normal, the thickness of the analysed layer is:

$$d = 3\lambda \sin\theta \tag{4.36}$$

   For the substrate (s) with homogeneous layer (v), the change of intensity in the ideal case is:

$$I^{\mathrm{s}}(d) = I_0^{\mathrm{s}}\ e^{-d/\lambda \sin\theta} \qquad \text{and} \qquad I^{\mathrm{v}}(d) = I_0^{\mathrm{v}}\ (1 - e^{-d/\lambda \sin\theta}). \tag{4.37}$$

   In practice, however, the geometry of the system also exhibits a angular response dependence function $\Rightarrow$ measured values for $I^{\mathrm{v}}/I^{\mathrm{s}}$

2. **Single-crystal studies**
   Measuring the absolute core electron intensity from a single-crystal surface, depending on the angle θ gives modulated intensity. Similar modulation is observed for fixed θ and rotation of surface plane. $\Rightarrow$ **X-ray photoelectron diffraction XPD**

4.10.6 Numerical data analysis

Simple operation with data:
(a) integration and determination of area, (b) noise removal, (c) satellites removal, (d) background subtraction, (e) addition and subtraction of spectra, (f) search for lines maxima, (g) conversion to the binding energy after calibration.

background subtraction

- linear background: straight line between the first and last point of the spectrum
- integral background: the integral is calculated over the hole line area and a calibrated curve thus obtained is subtracted from the peak area
- background based on the elastic and inelastic processes

Signal to noise ratio
The noise is characterised in three different ways: peak-to-peak (p.t.p.), root-mean-square (r.m.s.), standard deviation. If the spectrometer is limited to statistical noise, the signal to noise ratio (S/N) can be defined like:

$$S/N = \sqrt{\frac{S+B}{F}}, \tag{4.38}$$

where S is the height of the line above background B, is the background B and F is the intensity factor

$$F = \frac{(S/B+1)(S/B+2)}{(S/B)^2}. \tag{4.39}$$

If we desire S/N constant

$$t_2/t_1 = F_2/F_1. \tag{4.40}$$

Smoothing

- fitting the data with a suitable smooth function (polynomial, fractional polynomial, exponential, Fourier and splines)
- convolution data using a suitable algorithm, which leads to a smoothing

$$y_r^{\mathrm{sm}} = \sum_{r=-m}^{m} \frac{C_r y_r}{\mathrm{NORM}}, \tag{4.41}$$

  where C_r is the convolution number and NORM is the normalizing factor. Savitsky-Golay convolution is recursive. the convolution function represented by lest squares fitting of an polynomial(cubic-quadratic) to m points on either side of each data point.

- frequency filter for Fourier transformation (mathematical equivalent of convolution algorithm).

Analysis of overlapping spectral lined

- spectra derivation (background removal, separation of overlapping lines), negative lines in the second derivative correspond to approximately the position of overlapping lines ⇒ noise problems ⇒ smoothing with derivation
- deconvolution, mostly for the shape of the line

$$y_j^{\mathrm{m}} = \sum_{i=1}^{N} y_i^{\mathrm{t}} g_{j-1} \ + \ n_j, \tag{4.42}$$

  where n_j is the noise. The instrument function g can be determined by line measurement of Ag 4 eV from the Fermi level with a monochromatic X-ray source.

- fitting with Gaussian or Lorentz function. It can either be used the Voigt convolution or a mix Gauss-Lorentz function

$$f(E) = \frac{A}{[1 + M(E - E_0)^2/\beta^2] \exp([1 - M][\ln 2(E - E_0)^2]/\beta^2)}, \tag{4.43}$$

  wheree M is mixing ration (1 for pure Lorentz shape) and β is a parameter, which is nearly 0.5 FWHM.

4.11 Electron energy loss spectroscopy

The EELS experiment was developed from gas-phase electron scattering experiments, which probed electronic states within molecules. For the analysis of surface vibrations, the technique utilizes the interaction of very low energy electrons (1 – 10 eV) with the surface electric fields produced by adsorbate molecules and substrate atoms.
Two types of scattering of electrons may be considered, "elastic" and "inelastic" (a third mechanism in which the incoming electron is trapped for a finite time within the surface forming a so called "negative ion resonance" is not treated here). Electron scattering is directly analogous to neutron diffraction. This analogy with a diffraction experiment is a useful one, since it illustrates why the best energy resolution in EELS, as measured by the full width at half maximum height (FWHM) of the elastically scattered electron peak, is obtained when using a single crystal substrate. Both elastic and inelastic scattering are broadened in energy terms when the scattering potential of the surface is poorly defined, e.g. a polycrystalline sample.
The laws of energy and impulse conservation forms

$$E'(\vec{k}') = E_0(\vec{k}) - \hbar\omega, \tag{4.44}$$

$$\vec{k}'_{\parallel} = \vec{k}_{\parallel} - \vec{q}_{\parallel} \pm \vec{g}_{\parallel}, \tag{4.45}$$

where $E_0(\vec{k})$ is the incident e$^-$energy with momentum $\hbar\vec{k}$, $E'(\vec{k}')$ is the backscattered e$^-$energy with momentum $\hbar\vec{k}'$, $\hbar\omega$ is e$^-$energy loss in the transmission, $\vec{q}$ is the transferred momentum $\vec{g}$ is the lattice reciprocal vector. EELS modifications: AREELS - Angle Resolved EELS, HREELS - High Resolution EELS.

Experimental
If we consider the experimental requirements for EELS or HREELS, low energy electrons, single crystal substrates (usually), then it is clear that this is a high vacuum technique. In practice the working pressure limit for most EELS instruments is 10^{-6} mbar due to a gas-phase scattering processes.
Usually at least one unit, the monochromator or analyzer, has some ability to rotate about an axis perpendicular to the plane of the experiment while the sample may also rotate. In this way it is possible to vary the angle of incidence over a wide angular range and still maintain the ability to detect at angles away from the specular position. The monochromators and analysers are electrostatic selection units based upon either 127-degree cylindrical capacitors or hemispherical capacitors. The potentials applied to these capacitors are such that only electrons having specific pass energies may reach first the sample surface and second the detector. The working surfaces of the spectrometer are coated with an inert material such as graphite in order to minimize changes in spectrometer work function that may occur upon exposure to various gases.
The design of an EEL spectrometer is such that the energy spread of the incident low-energy electron beam is minimized while maintaining a reasonable electron flux. This primary consideration means that the area of surface sampled by the beam is of secondary importance.
Three independent ways for measuring spectra can be used:

1. measurements at constant angle θ, θ' and constant energy loss value $\hbar\omega$ depending on the incident energy loss profile

2. measurement of the loss energy $\hbar\omega$ at constant $\vec{k}$ in accordance with the scattering angle θ'.
3. measurements at constant $\vec{k}'$ electron dispersion direction depending on the energy loss spectrum.

The basic problem of the measurements is the assignment scattering mechanism for measured energy loss. First the plasma loss should be determined and then distinguish between the remaining peak volume and the surface processes. They are often represented as the corresponding maximum ionization of deeper levels.

4.12 Threshold techniques

An alternative form of core level spectroscopy is based on the detection of the onset on ionization as the exciting beam energy passes through such a threshold (equal to the binding energy of the core level relative to the Fermi level of the solid). A technique of this kind involves sweeping the exciting energy beam and detecting the onset of emission of photons or Auger electrons associated with the refilling of the core hole thus created. These different modes of detection form a group under the general heading of APS (Appearance Potential Spectroscopy). In principle, either incident electrons or photons could be used but the photon calls for a tunable light source in the 50–2000 eV range, only possible using synchrotron radiation.
All three modes of the incident electron technique have been used, however, the thresholds either being detected by fall in the elastically scattered electron flux (Disappearance Potential Spectroscopy - DAPS), by the onset of photons emission (Soft X-ray Appearance Potential Spectroscopy - SXAPS) or by the onset of the new Auger electron emission channel (Auger Electron Appearance Potential Spectroscopy - AEAPS). Note that in all of these techniques the surface sensitivity is guaranteed by inelastic scattering of the incident electron beam.
Primary energy E_p is determined by:

$$E_\mathrm{p} = eV_\mathrm{p} + \phi + kT. \tag{4.46}$$

By applying the conservation of energy

$$E_\mathrm{p} - E_1 = E_\mathrm{B} + E_2, \tag{4.47}$$

where E_1 is the primary electron energy level, E_B is the binding energy of the electron on the surface E_2. At the threshold energy can be captures just above the Fermi level i.e.$E_1 = E_2 = 0$ and E_p=E_B. If instead of thermionic cathode we have tunnel cathode, the $eV_\mathrm{p} = E_\mathrm{B}$. The probability of excitation of the inner layers is:

$$W(E_\mathrm{p}) \approx \int_0^{E_\mathrm{p}} \psi(E' - E_\mathrm{B}) \int_0^{E_\mathrm{p}+E'} \tag{4.48}$$

Chapter 5

Interaction of Ions with Matter

5.1 Ion interactions and penetration depth

Differences exists in the interaction of ions and electrons with matter. Ions are much heavier, have bigger dimensions and they can have higher charges. At ion impact may occur the emission of:

- secondary electrons (secondary ion-electron emission),
- ions (ion scattering, ion-ion secondary emission),
- neutral particles (cathode sputtering),
- photons (characteristic x-rays and visible radiation - ionoluminescence).

Also, changes in the electronic shell may occur and also ion implantation in material.

Penetration depth of protons: Protons interactions are similar to electron ones, but some peculiarities can be observed. Being 1836 times the mass of electron, has a higher angular momentum and loses only a small portion of eat at each collision $\Rightarrow$ penetration depth is greater than for electrons. For 2.5 MeV proton, the penetration depth is around 55 μm for carbon and 28 μm for silver; it decreases with the the proton energy and Z of the material.

Penetration depth depends on the number of protons in the ion, its energy and the target. For low energies (several eVs) it is reflected from the target and part of its energy is transferred to the surface atom, causing ejection of atoms, ions or clusters. It can also create cascade collisions.
The range R - the total distance that the ion (projectile) travels in coming to rest, is longer than the penetration depth x. The **projected range** R_p is defined as the total path length of the projectile with energies $0.002 \leq \epsilon \leq 0.1$ keV measured along the direction of incidence.

$$R_\mathrm{p} = C_1(\mu) M_2 \left[\left(\frac{Z_1^{2/3} + Z_2^{2/3}}{Z_1 Z_2} \right) E \right]^{2/3}, \tag{5.1}$$

where M_2 is the atomic mass of the target , Z is the atomic number while $C_1(\mu)$ is experimentally determined. for projectiles with energies $0.5 \leq \epsilon \leq 10$ keV is

$$R_\mathrm{p} = C_1(\mu) M_2 \left[\left(\frac{(Z_1^{2/3} + Z_2^{2/3})^{1/2}}{Z_1 Z_2} \right) E \right]^{2/3}. \tag{5.2}$$

Ion channelling is possible along crystallographic axes with small critical angles. In this case the penetration depth is substantially increased.

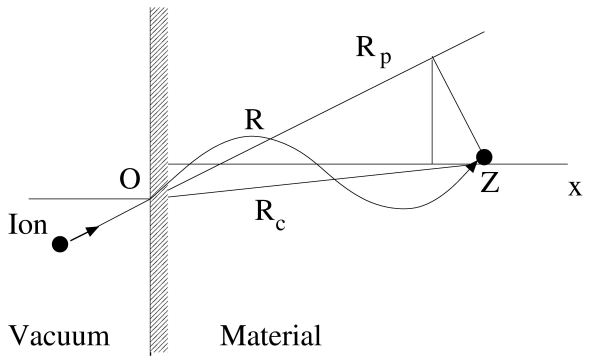

Figure 5.1: Calculation of total distance of ion.

5.1.1 Basic ion penetration concepts and the energy transfer mechanism

Because $m_{\text{ion}} \sim m_{\text{target}}$, it leads to considerable energy loss due to elastic collisions. The energy loss is defined like $\Delta E/\Delta x \to dE/dx$, where $\Delta x \to 0$. Often

$$S \equiv \frac{dE}{dx} \tag{5.3}$$

is called **stopping power** or **specific energy loss**. The **stopping cross section** can be defined as:

$$\epsilon = \frac{1}{N}\,\frac{dE}{dx} \qquad \text{or} \qquad \epsilon = \frac{1}{\rho}\,\frac{dE}{dx}, \tag{5.4}$$

where N represent [atoms/m^3] and ρ is the density [kg/m^3]. Sometimes ϵ also represents stopping power.
The relative importance of interactions between ions and matter depends on the ion speed, their charge and the atoms of the target

- for $v_{\text{ion}} \ll v_0$, where v_0 is the Bohr velocity of electrons in the atom. Ions will carry their electrons which tend to be neutralized by electron capture. At these speeds, the elastic collisions dominates and the losses are called **nuclear energy losses**.
- for higher velocities, the importance of nuclear energy losses decreases with a factor of $1/E$ and the inelastic collisions with electrons because important. Above 200 keV/amu, the contribution of nuclear energy losses is typically less than 1 % than electronic one. Between $0.1v_0 \leq v_{\text{ion}} \geq Z_1^{2/3}v_0$ electron collisions are proportional with the velocity ($E^{1/2}$).

- for $v \gg v_0$ the ion charge increases till it completely losses all electrons. The Bethe-Bloch Formula for the electron energy is

$$\frac{dE}{dx} = NZ_2(Z_1e^2)^2 f(E/M_1), \tag{5.5}$$

where Z_1 is the ion atomic number.

5.1.2 Secondary ion-electron emission

According to the adiabatic principle, heavy ions are not efficient for transferring energy to light electrons to provide ionization. This general statement can be referred to the direct electron emission from solid surfaces induced by ion impact.
The secondary electron emission coefficient γ (electron yield per ion) becomes relatively high only at very high ion energies exceeding 1 keV, when the Massey parameter becomes low. Although the secondary electron emission coefficient γ is low at lower ion energies, it is not negligible and remains almost constant at ion energies below the kilovolt range.

$$\gamma = \frac{i_\mathrm{e}}{i_\mathrm{i}}. \tag{5.6}$$

Total γ coefficient is the sum of

$$\gamma = \gamma_\mathrm{p} + \gamma_\mathrm{k}, \tag{5.7}$$

where γ_p is the potential emission and γ_k for the kinetic one. The **Penning mechanism of secondary ion-electron emission**, also called the potential mechanism defines the ion approaching the surface which extracts an electron from there because the ionization potential Φ exceeds the work function ϕ. The defect of energy $\Phi - \phi$ is usually large enough ($\Phi - \phi > \phi$) to enable the escape of more than one electron from the surface. Such a process is non-adiabatic and its probability is not negligible. The **secondary ion-electron emission coefficient** γ can be estimated using the empirical formula:

$$\Phi \geq 2\phi, \tag{5.8}$$

$\Rightarrow$ potential emissions are observed especially when bombing the surface with ions of inert gases that have high Φ. γ_p is higher for higher ion charge.

Ion-neutralization spectroscopy (INS) is an emission electron spectroscopy. In INS the externally applied agent is a slowly moving positive ion, such as He^+, presented to the solid surface. Near the surface a non radiative, Auger type electronic transition process occurs which simultaneously neutralizes the ion to the ground state of the parent atom and excites a second electron, which may be ejected into vacuum. The kinetic-energy distribution of these ejected electrons contains spectroscopic information concerning the electronic structure in the surface region of the solid.

- When the incoming ions is just outside the metal surface, two electrons in the filled valence band of the metal interact, exchanging energy and momentum.

- One electron, the neutralizing electron, tunnels through the potential barrier into the potential well presented by the ion, and drops to the vacant atomic ground level.

- The energy released in this transition is taken up by the second interacting election which now may have sufficient energy to escape from the metal
- These Auger type transition can take place anywhere within the filled valence band so that the ejected electrons have a range of energies rather than one specific energy. Outside the metal surface the electron energy distribution can be measured quite straightforwardly.

5.2 Ion sources

In case of surface and thin films analysis can ion sources can be used. Suitable sources provide proper ion beams for surface cleaning and for surface layer sputtering in order obtain a depth profile (such as XPS or AES), primary beam for static and dynamic SIMS. Another sources are represented by the particles accelerators used for energetic ion analysis (such as RBS, PIXE, NRA, ERDA etc.)

The ionization methods can be classified according to:

- electron impact
- fast atom bombardment
- electro-spray ionization
- gas discharge ion sources
- solid state surface atom ionisation sources
- high electric field desorption

Ion beam focus:

- wide ion beam sources
- narrow focused ion beam sources

5.2.1 Electron impact ionisation sources

The principle of ionization source is similar as a ionisation gauge. The only modification include a geometry of gauge and ion collector must be replaced by the system which is able to extract the produced ions. Ionisation space is inside the cylinder - screened by anode with the ion trap at the end. Electrons are accelerated from a thermionic emission cathode by high voltage (100 - 500 V). The electrons travel through the ionisation space and ionize gas molecules around them. The resulting ions are collected at a negative trap electrode - thus resulting in an ion beam. The operating pressure is lower 0.01 Pa and the source provides high focused ion beam with beam current to 10 μA. Due to its properties it is possible another manipulation in ion optics.

Another source modification - double anode source. Two parallel bars - anodes - are placed along the cylindrical cathode (voltage up to 10 kV). Electrostatic field with a saddle point is form on anode axis. Electrons oscillate around this point and they are effectively ionise the gas. The

produced ions are accelerated along the plane symmetry to cathode with the outlet. Operation pressure is tenths of Pa, ion current is tens of μA. Electrons are ejected in the form of diverging beam with wide energy distribution $\rightarrow$ they are inappropriate to another manipulation in ion optics. It causes a high chromaticism. In consequence, it is use to surface sputtering.

5.2.2 Plasma sources

Plasma sources generate plasma - excitation of the gas requires ionization of neutral atoms and molecules. High intensity electric field extracts ions from the plasma surface (negative charged electrode). The dependency of extracts ion current I and electrode surface voltage U_{ex} on the thickness d is described by Child-Langmuir law

$$I \approx U_{\text{ex}}^{3/2}/d^2. \tag{5.9}$$

Two types of plasma sources are most often use to surface and thin films analyses. In van der Graff accelerators, high frequency discharge are the ion sources generally use to analysis with ion energy in order MeV. The duoplasmatron is a type of ion source compresses the plasma by a magnetic field in front of the extraction system. The plasma is so dense that matching to the extraction field strength requires an expansion cup to lower the current density. Most often is used as a source of Ar and O ions.

High frequency ion source

Ions can be created in an inductively or capacitively coupled plasma. The electric field has a frequency in order tenth of MHz, the power is tenth to hundreds of W, the pressure is units of Pa, current is from tenth of μA to tenth of mA. The ionization efficiency can be enhanced by magnetic field.
Two types of inductively coupled RF structures are most common. In one type, the induction coil is placed outside a glass or quartz cylindrical tube in which the plasma is generated. The other type has a metallic discharge chamber with an RF antenna inside the discharge plasma.
Although capacitively coupled RF sources are widely used in plasma etching processes, they are seldom employed for the production of ion beams. Capacitively coupled discharges form a very high positive plasma potential. As a result, material is sputtered from the chamber wall to form impurity ions in the extracted beam.

Duoplasmatron

The duoplasmatron operates as follows: a cathode filament emits electrons into a vacuum chamber, then the gas is introduced in very small quantities into the chamber, where it becomes charged or ionized through interactions with the free electrons from the cathode, forming a plasma. The plasma is then accelerated through a series of at least two highly charged grids, and becomes an ion beam, moving at fairly high speed from the aperture of the device. Duoplasmatrons are characterized by high efficiency - usually above 90 %.

The duoplasmatron components are:

- cathode (K)- generally the heated cathode (thermionic emission), sometimes (for oxygen ions) is use the hollow cold cathode
- intermediate electrode (IE),
- anode (A).

The intermediate electrode and anodes are ferromagnetic and create the part of magnetic circuit. Demirkhanov installed a ferromagnetic anticathode electrode to ensure oscillation of electrons in the anode region of the duoplasmatron. The anticathode was located behind a copper anode and had a potential close to the cathode potential. Electrons oscillating in the magnetic field (1500 G) efficiently ionize the gas at a low pressure of ~ 5–$10^{\breve{}3}$ Torr. When the anticathode negative bias relative to the anode was increased from 0 to 100 V, the ion current increased by a factor of five. The source, which had an outlet aperture 6 mm in diameter and an expansion cup 50 mm in diameter, provided a pulsed hydrogen ion current of up to 1.5 A at a discharge current of 20 A.

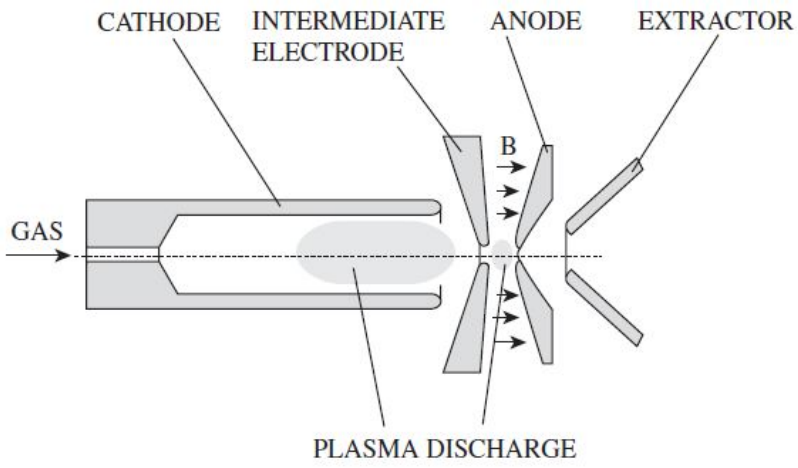

Figure 5.2: Duoplasmatron scheme.

Duoplasmotrons can have different ion sources:

- Penning-type electrode system (PIG) to maintain a high current discharge by electrons supplied through a double electric layer from a plasma cathode, has been embodied most completely in the DuoPIGatron type ion source. The magnetic field diverges toward the ion optics, ensuring oscillation of primary electrons between the intermediate and screen electrodes and formation of a large, uniform plasma surface. To increase the cathode lifetime, an inert gas (argon) is fed into the cathode stage and oxygen into the anode stage of the source. An ion optics system with 13 holes of diameter 5 mm provided an ion beam current up to 170 mA at an accelerating voltage of up to 50 kV. After mass separation of the beam and acceleration of ions to energy of 200 keV, a beam of O^+ ions with current 100 mA was obtained. The filament cathode lifetime is over 25 hours.

- periplasmatron-type ion source has a unique electrode system design, which decreases heating of the screen electrode by thermal radiation of the cathode, reduces the effect of secondary electron back flow from the accelerating gap, and ensures a high uniformity of plasma flow to the screen grid. A rectangular variant of this source provided a hydrogen ion current of 96 A from an extractor 40 x 16 cm in size.

- magnetic-field-free source for use in neutral beam injectors has been developed in which the plasma is generated by a diffuse low-pressure high-current discharge, with a distributed thermionically emitting cathode. Twenty hairpin filaments, 0.5 mm in diameter, are installed around the periphery of the discharge chamber, 14 cm in diameter, near the cylindrical wall, which serves as the anode. The peripheral placement of the cathode provides generation of uniform ($\pm$ 6 %), oscillation-free plasma of 12 cm diameter. For a discharge current of 1000 A the deuterium ion beam current density is 0.5 A cm$^{\breve{}2}$ and the beam current 15 A at an extraction voltage of 15 kV.

5.2.3 Surface ionization sources

Surface ionization sources are commonly used for producing a Cs^+ ion beam. The surface ionization source emits ions from a hot plate. This configuration is ideal for designing beam optics with minimum aberration because the emitting surface is a solid boundary. In fact, the surface ionization source can be designed to produce a beam with very large aperture (and therefore high current per beam) because of the rigid emitting surface. The ion temperature from a surface ionization source is typically low, of the order of a fraction of an eV; therefore the beam emittance is kept low, even when the source diameter is large. The two main types of surface ionization sources are contact ionizers and aluminosilicate sources.

The ration of density of emitted positive ions flux j_+ to density of emitted atoms flux j_a is defined

$$j_+/j_\mathrm{a} = \frac{g_+}{g_\mathrm{a}} e^{-\frac{V_i-\phi}{kT}}, \tag{5.10}$$

where g_+ a g_a are statistical weight of ionized and atomic state of adsorbed atom, V_i is ionization energy of adsorbed atom, ϕ represents work function of solid, T is the temperature of solid and k is Boltzmann constant.

5.2.4 Field ionization

Field emission from sharp needle points at which very intense electric fields are created can be used to extract either electrons or ions from the solid (or liquid) state:

- liquid metal ion sources (LMIS) - is used in liquid metal ion sources to produce beams of species of low melting point metals such as Ga, In, Bi, Al, Sn, ... with extraordinarily high brightness

- gas field ion source (GFIS)

In both types the electric field with intensity 10 V/nm is use.

5.3 Ion scattering spectroscopy - ISS

Sometimes called Low Energy Ion Scattering Spectroscopy (LEIS) is a surface sensitive analytical technique used to characterize the chemical and structural properties of materials. The range of ion energies is from hundreds of eV to units keV. When a beam of ions hits a solid surface part of the projectiles will be scattered back into the vacuum after one or more collisions with target atoms of the layer. Measurement of the energy of the backscattered particles is use to identify chemical structure of solid. primary ion energies of 0.5 – 5 keV are used with noble gas ions (He, Ne, Ar) and also alkali ions (Li, Na, K). With this method, information is obtained from the topmost atomic layer, under certain circumstances also from the second or third layer.

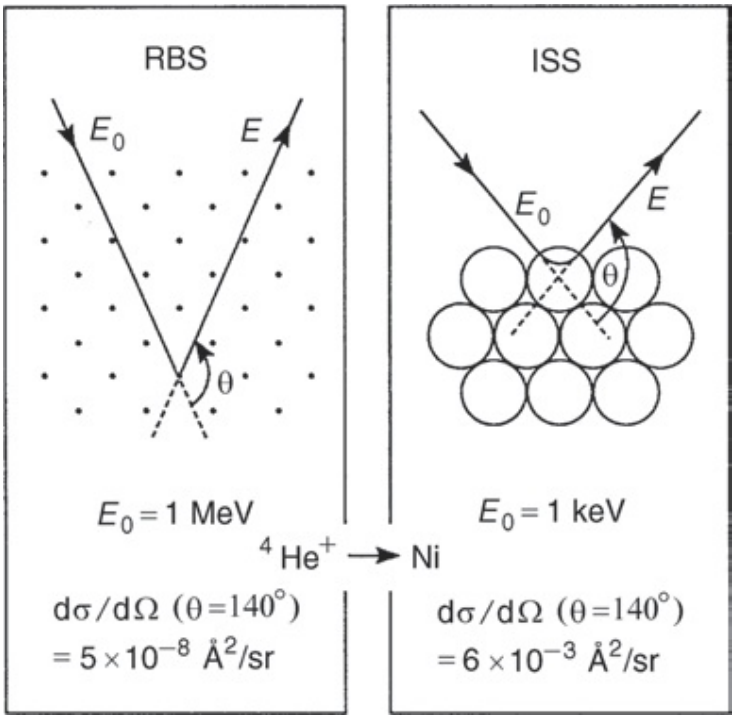

Figure 5.3: Comparison of RBS and ISS techniques.

5.3.1 Qualitative analysis

From the applied conservation and momentum laws in the case of two-body collisions it is possible to calculate the ion kinetic energy after a collision with a surface atom without knowing the interaction potential.

If the incident ion has energy E_0, the mass M_1 and the surface atom M_2, we obtain the energy and mass conservation relation for the backscatter energy E_1:

$$\frac{E_1}{E_0} = \left[\frac{\cos\theta \pm [(M_2/M_1)^2 - \sin^2\theta]^{1/2}}{M_2/M_1 + 1}\right]^2, \tag{5.11}$$

When this relation is derived, the kinetic energy of atom should be neglected

For 90° and 180°: backscattering angles the relation is simplified:

$$\frac{E_1}{E_0} = \frac{M_2 - M_1}{M_2 + M_1} \quad \text{for} \quad \theta = 90^\circ \tag{5.12}$$

$$\frac{E_1}{E_0} = \frac{(M_2 - M_1)^2}{(M_2 + M_1)^2} \quad \text{for} \quad \theta = 180^\circ \tag{5.13}$$

The ration $K = E_1/E_0$ is named kinematic factor. The above relations show that the energy of ion after collision is given by the projectile and the target atom weight and the backscattered angle (for constant E_0) $\Longrightarrow$ determination of target atom mass M_2. The corresponding expression for the recoiling target atom is:

$$\frac{E_2}{E_0} = \frac{4A}{(1+A)^2} cos^2\theta_2 \tag{5.14}$$

Scattered-ion energy spectra are transformed into mass spectra by the backscattered relation for $\theta = 180^\circ$. Consequently, the mass resolution also can be calculated from this equation for the special case of $\theta = 90^\circ$:

$$\frac{M_2}{\Delta M_2} = \frac{E}{\Delta E} \frac{2A}{A^2 - 1} \tag{5.15}$$

Assuming a constant relative energy resolution of the detector of $E/\Delta E = 100$ the mass resolution is better for large scattering angles and about equal ion and target atom masses. So the primary projectile mass has to be selected accordingly if mass resolution is important.

5.4 Rutherford backscattering spectroscopy - RBS

In Rutherford Backscattering Spectroscopy (RBS) the primary ion energy ranges from about 100 keV (for H^+) to several MeV (for He^+ and heavier ions). The ion-target atom interaction can be described using the Coulomb potential from which the Rutherford scattering cross-section is derived,which allows absolute quantification of the results. Information in principle arises from a thickness of the order of 100nm (10^{-5} cm), but analysis of surface layers is also possible by using channelling/blocking techniques. Scattering of H^+ with energies around 100 keV is sometimes referred to as MEIS (Medium Energy Ion Scattering), probably because it only needs a smaller type of accelerator, but physically it is within the RBS regime.

The physical principles are the same for both techniques (ISS and RBS): an ion beam is directed onto a solid surface, a part of the primary projectiles is backscattered from the sample and the energy distribution of these ions is measured. Since the ion–target atom interaction can be described by two-body collisions, the energy spectra can be easily converted intomass spectra. The difference between ISS and RBS arises from the difference in the cross-sections and the influence of electronic excitations and charge exchange processes, which result indifferent information depths. In both cases, structural information is obtained from crystalline samples by varying the angles between beam and sample. Deduction of structural information from the data is straightforward, since both techniques are "real space" methods which are based on fairly simple concepts. With ion scattering only the individual atoms of an element can be detected and no information on compounds or molecules can be gained.

In terms of analytical characteristics, is important the variable cross section for elastic scattering, which integrates a number of dispersed particles with the number of atoms in the substance to be examined. Differential scattering cross section at the angle θ in the laboratory system is then:

$$\frac{d\sigma_R}{d\Omega} = \left(\frac{Z_1 Z_2 e^2}{2E_0}\right)^2 \frac{\left[(M_2^2 - M_1^2 \sin^2\theta)^{1/2} + M_2 \cos\theta\right]^2}{M_2 \sin^4\theta (M_2^2 - M_1^2 \sin^2\theta)^{1/2}}, \tag{5.16}$$

where Z_1 and Z_2 are the atomic numbers of the ion and the target.

Analysis using heavier particles and lower energies can play a significant role in electron screening. In such cases the first correct approximation of the cross section is multiply by the correction factor F in the form:

$$F = \frac{\sigma}{\sigma_R} = 1 - \frac{0,049 Z_1 Z_2^{4/3}}{E_{\mathrm{CM}}}, \tag{5.17}$$

where E_{CM} is the energy of particles expressed in keV. In a conventional design RBS the correction is below 5 %. Significant deviation of the cross section appear when the energy of the particles is increased , or particles with lower atomic number are used. The effect of nuclear forces appears when the scattered are scattered at large angles and energies $E_0 > E_{\mathrm{critical}}$

$$E_{\mathrm{critical}} = 10^3 Z_1 Z_2 M_2^{-1/3}. \tag{5.18}$$

For example, nuclear effects occur when the α particles ($Z_1 = 2$, $M_1 = 4$)on Si atoms ($Z_2 = 14$, $M_2 = 28$) sat energies$E_{\mathrm{krit}} > 9$ MeV are scattered.

5.4.1 Elemental composition determination

The basic relationship is

$$Y = QN \int_{\Delta\omega} \frac{d\sigma}{d\Omega} d\Omega, \tag{5.19}$$

where Y is the number of the dispersed particles registered, Q is the number of incident particles, N is the area density in the layer (atoms/cm^2) and $\Delta\omega$ is the interval of the solid angle from which is detected the scattered particle. The equation can be applied in a layer containing multi-elements or a thin layer on a stronger substrate.

5.4.2 Energy loss

Only a small fraction of the primary ions come close enough to a target nucleus (impact parameters of the order of 10^{-12} cm) to undergo an elastic nuclear collision which is described by the kinematics given in the previous section. If such an ion is backscattered, its final energy is determined by the *elastic* nuclear collision in a certain depth of the sample and the additional *inelastic* energy loss to electrons on its way in and out of the target.

The relation for energy loss per unit length, $--dE/dx$ given in eV/Åand commonly called **stopping power**:

$$S = -\frac{dE}{dx} \qquad (\mathrm{keV.cm^{-1}}), \tag{5.20}$$

The stopping cross section ϵ (eV/(atoms/cm^2)) relates this quantity to the atomic density N and is therefore more specific for a

$$\epsilon = \frac{1}{N} S \qquad (\text{keV.cm}^2), \tag{5.21}$$

The stopping power curve exhibits a broad maximum around 1 MeV and that is the operational regime of RBS: here, the stopping power does not depend very much on the ion energy and hence can be assumed to be constant as a sufficient approximation in many cases; the stopping power there has its maximum value and therefore RBS its best depth resolution and in this energy range the nuclear interaction is exactly given by the Coulomb potential, giving RBS the advantage of an absolute analytical method. Stopping cross section for a particle with energy E and a mixture of $A_m B_n$ elements is

$$\epsilon^{A_m B_n} = m\epsilon^A(E) + n\epsilon^B(E), \tag{5.22}$$

where $\epsilon^A(E)$ ans $\epsilon^B(E)$ are the stopping cross sections for the elements A and B.

5.5 Detection of ejected atoms - ERDA

Detection of light elements by RBS is difficult due to the low effective elastic scattering cross-sections and often because the signal lies on a high background originated by scattering on heavier elements. Therefore, the method used is ERDA (Elastic recoil detection analysis).
In this method, atoms or ions are detected which are removed from the surface by one single collision with an incoming projectile. They can therefore be identified by their kinetic energy. Directly recoiling particles are therefore different from those secondary particles that originate from a collision cascade in a sputtering process and have a broad energy distribution around one to two eV. They are used in secondary ion or neutral mass spectroscopy.Recoil cross-sections are generally of the same order as scattering cross-sections. They are largest towards $\theta_2 = 90°$, but then the recoil energy approaches zero. A useful energy range is obtained between 30° and 60°.
ERDA is also often done using a relatively low energy (2 MeV) He beam specifically to depth profile hydrogen. In this technique multiple detectors are used, at backscattering angles to detect heavier elements by RBS and a forward (recoil) detector to simultaneously detect the recoiled hydrogen (the cross-section for which reaction is strongly non-Rutherford at these energies). The recoil detector has to have a *range foil*: a thin film (typically 6 micrometres of PET film) to preferentially stop the incident He beam scattered into the forward direction.

5.6 Secondary ion mass spectrometry - SIMS

Secondary Ion Mass Spectrometry (SIMS) is a relatively new technique for surface chemical analysis compared with Auger enectron spectroscopy (AES) and X - ray photoelectron spectroscopy (XPS). SIMS examines the mass of ions escaped from a solid surface to obtain information on surface chemistry.

SIMS uses energized primary particles, usually ions such as Ar^+, Ga^+ and Cs^+, to bombard a solid surface in order to induce sputtering of secondary particles from an area. The interactions

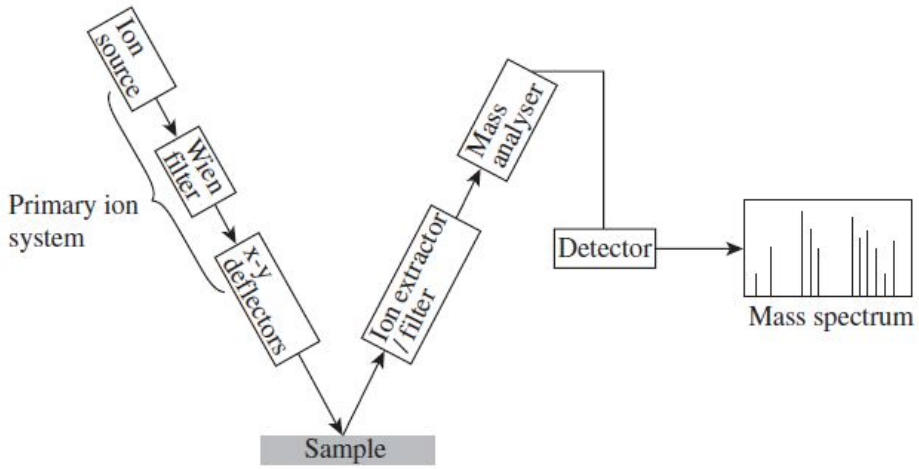

Figure 5.4: SIMS instumentation.

between primary ions and the solid are rather complicated. First, the secondary particles include electrons, neutral species of atoms or molecules, and ions. The majority of the secondary particles are neutral and not useful in SIMS. Only the secondary ions generated by the bombarding process carry chemical information. Second, the interactions are often more than a simply one-to-one knock-out of a surface ion by a primary ion. Commonly, the primary ions induce a series of collisions (collision cascade) in a solid because the energy of a primary ion is transferred by collisions between atoms in a solid before secondary ions on the surface are emitted.
The ionization probability is strongly affected by the electronic properties of the sample matrix. Ionization directly affects the signal intensity of secondary ions as shown in the basic equation of secondary ion yield.

$$J_{\mathrm{s}}^{\pm} = J_{\mathrm{p}} c Y \beta^{\pm} f, \tag{5.23}$$

where J_{p} is the primary ion flux, Y is the sputter yield, c is concentration of species m in the surface layer, $\beta^{\pm}$ represents the probability for positive ions and f is the transmission of the detection system. The transmission is defined as the ratio of the ions detected to ions emitted, and it varies from 0 to 1 depending on the analyser. The yield of elemental secondary ions can vary by several orders of magnitude across the periodic table.

5.6.1 Ion sputtering

Emission of secondary particles can result from collision sputtering or from other processes such as thermal sputtering. Collision sputtering includes direct collision sputtering and slow collision sputtering. The former can be considered as a direct impact between a primary ion and a surface atom. Direct collision sputtering is extremely fast, and occurs in the range of 10^{-15} to 10^{-14} seconds after the primary ion strikes a surface. Slow collision sputtering, represents the case that a primary ion never has chance to collide with a surface atom; instead, atoms in the solid transfer the impact energy to surface atoms after a series of collisions. The time scale of slow collision sputtering is in the range of 10^{-14} to 10^{-12} seconds.

Only a small portion of secondary particles ($\sim 1\%$ of total secondary particles) are ionized and become the secondary ions that are analysed in SIMS. A sputtered particle faces competition between ionization and neutralization processes when it escapes a sample surface. Ionization probability represents the chance of a sputtered particle being an ion.

5.6.2 Ion sources

The commonly used primary ions include argon (Ar^+), xenon (Xe^+), oxygen (O^{2+}), gallium (Ga^+) and caesium (Cs^+) ions. Heavier metal ions such as bismuth (Bi^+) are also available in modern static SIMS instruments. The ions of elements normally occurring in gaseous phases, such as oxygen and argon, are produced by electron bombardment sources or plasma ion sources. Electron bombardment sources use a circular filament cathode surrounding a cylindrical grid anode. The gas to be ionized is injected into the open space of the grid, and the gas molecules are bombarded by the electrons emitted from the cathode. The electrons travel in orbit inside the grid in order to increase their chances of striking gas molecules. An extraction field inducted in the grid will draw the gas ion beam through an opening in the center of the extractor. The electron bombardment sources provide moderate brightness of primary ions ($\sim 10^5$ Am^{-2} per solid angle).

5.6.3 Mass analysis system

The mass analysis system collects and analyses the ion masses to produce mass spectra with the assistance of a computer. The extractor filter extracts secondary ions from the surface, selects a mass range of ions to analyse, and eliminates scattered primary ions from a mass spectrum. The mass analyser, the critical component for secondary ion mass analysis, can be one of the following types:

- magnetic sector analyser,

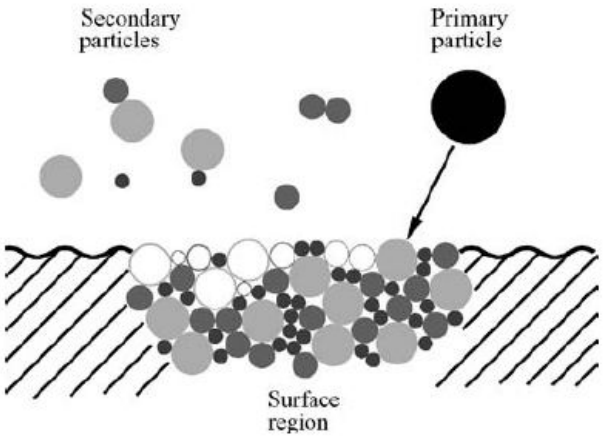

Figure 5.5: Secondary particle generation by an energetic primary particle.

- quadrupole analyser,
- time-of-flight analyser.

Magnetic sector analyser

This analyser was the oldest type used for mass spectroscopy. Secondary ions are accelerated by an extraction potential of 4 kV before entering a magnetic field. The magnetic field in the magnetic sector will impose a field force in a direction orthogonal to the direction in which the ions travel. The ions with a given kinetic energy will change their travel path to a circular trajectory. The radius of path curvature R has the following relationship with the ion mass.

$$R = \frac{(2V)^{1/2}}{B}\left(\frac{m}{z}\right)^{1/2} \tag{5.24}$$

where the extraction potential (V) is constant. We can adjust the magnetic field strength B, to select ions with a certain mass-to-charge ratio (m/z) with a fixed radius of magnetic sector R.

Quadrupole mass analyser

The quadrupole mass analyser selects ions with a certain mz^{-1} by generating unstable oscillation

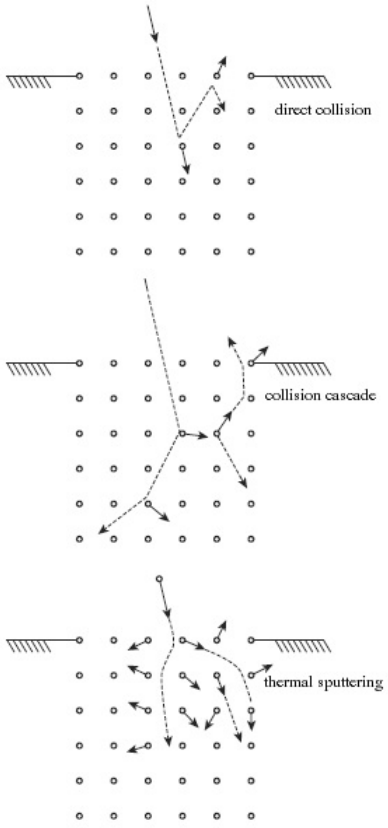

Figure 5.6: The sputtering proces: (a) direct collision sputtering;(b) collision cascade; and (c) thermal sputtering.

travels for the non-selected ions. Oscillations of ion trajectories are created by an electric field combining a constant direct current (DC) and alternating current with a radio frequency (RF). The secondary ions are accelerated by an extraction field, and then the ions travel through the center of four circular rod electrodes. Combined DC and RF voltages are applied to one pair of rods and equal but opposite combined voltages are applied to another pair of rods. Such an arrangement of electric fields generates ion oscillation. The oscillation can be so severe that ion trajectories become unstable and ions strike the rods. Ions with unstable trajectories cannot travel through the exit slit of the analyser to reach the mass detector. Only the ions with a certain mz^{-1} have stable trajectories and can pass through the exit slit under a given ratio of DC:AC voltages. The analyser is a sequential type that only allows the ions with single mz^{-1} values to reach the detector. Thus, the quadrupole analyser is a device with low transmission, as less than 1% of ions can reach the detector at any time. To obtain a whole mz^{-1} spectrum, the analyser increases the voltages but keeps the ratio of DC:AC voltages constant.

Time-of-Flight analyzer

The time-of-flight (ToF) analyser is the most widely used analyser in static SIMS. As its name indicates, for this analyser the flight time of an ion is the parameter for measurement. When ions are obtained with a constant kinetic energy from an acceleration potential (V) of 3 – 8 kV, the flight time of ions through a distance (L) of flight tube to reach a detector is calculated.

$$t = L(2V)^{-1/2}\left(\frac{m}{z}\right)^{1/2} \tag{5.25}$$

Thus, the mz^{-1} of ions is analysed by measuring their flight time in the analyser. Heavier ions will have longer flight times in the tube. To measure the time of flight, precisely pulsed primary ions should be used. The pulse is controlled by a highly accurate clock. The pulse periods are typically in the order of 10 ns. The flight time of ions to the detector is electronically measured and converted to mz^{-1}. In a pulse period, all the ions can be measured and a whole mass spectrum can be obtained almost simultaneously. Again, the initial kinetic energy of secondary ions will affect the resolution of mass analysis, because the velocity could be different when ions with the same mz^{-1} enter the flight tube.